RMZ – MATERIALS AND GEOENVIRONMENT

PERIODICAL FOR MINING, METALLURGY AND GEOLOGY

RMZ – MATERIALI IN GEOOKOLJE

REVIJA ZA RUDARSTVO, METALURGIJO IN GEOLOGIJO

Historical Review

More than 80 years have passed since in 1919 the University Ljubljana in Slovenia was founded. Technical fields were joint in the School of Engineering that included the Geologic and Mining Division while the Metallurgy Division was established in 1939 only. Today the Departments of Geology, Mining and Geotechnology, Materials and Metallurgy are part of the Faculty of Natural Sciences and Engineering, University of Ljubljana.

Before War II the members of the Mining Section together with the Association of Yugoslav Mining and Metallurgy Engineers began to publish the summaries of their research and studies in their technical periodical Rudarski zbornik (Mining Proceedings). Three volumes of Rudarski zbornik (1937, 1938 and 1939) were published. The War interrupted the publication and not until 1952 the first number of the new journal Rudarsko-metalurški zbornik - RMZ (Mining and Metallurgy Quarterly) has been published by the Division of Mining and Metallurgy, University of Ljubljana. Later the journal has been regularly published quarterly by the Departments of Geology, Mining and Geotechnology, Materials and Metallurgy, and the Institute for Mining, Geotechnology and Environment.

On the meeting of the Advisory and the Editorial Board on May 22nd 1998 Rudarsko-metalurški zbornik has been renamed into "RMZ - Materials and Geoenvironment (RMZ -Materiali in Geookolje)" or shortly RMZ - M&G.

RMZ - M&G is managed by an international advisory and editorial board and is exchanged with other world-known periodicals. All the papers are reviewed by the corresponding professionals and experts.

RMZ - M&G is the only scientific and professional periodical in Slovenia, which is published in the same form nearly 50 years. It incorporates the scientific and professional topics in geology, mining, and geotechnology, in materials and in metallurgy.

The wide range of topics inside the geosciences are welcome to be published in the RMZ -Materials and Geoenvironment. Research results in geology, hydrogeology, mining, geotechnology, materials, metallurgy, natural and antropogenic pollution of environment, biogeochemistry are proposed fields of work which the journal will handle. RMZ - M&G is co-issued and co-financed by the Faculty of Natural Sciences and Engineering Ljubljana, and the Institute for Mining, Geotechnology and Environment Ljubljana. In addition it is financially supported also by the Ministry of Higher Education, Science and Technology of Republic of Slovenia.

<div align="right">Editor in chief</div>

Table of Contents – Kazalo

Dissolution of iron in aluminium alloys

Raztapljanje železa v aluminijevih zlitinah

Stanislav Kores[1], Maja Vončina[1], Primož Mrvar[1], Jožef Medved[1]

[1]University of Ljubljana, Faculty of Natural Sciences and Engineering,
Department of Materials and Metallurgy, Aškerčeva cesta 12, SI-1000 Ljubljana, Slovenia;
E-mail: stanislav.kores@ntf.uni-lj.si, maja.voncina@ntf.uni-lj.si, primoz.mrvar@ntf.uni-lj.si,
jozef.medved@ntf.uni-lj.si

Abstract: Iron presents in Al-alloys the main impurity, but in some alloys iron presents an alloying element, which increases the hardness of the alloys, but also increases brittleness. In this work the dissolution of iron in electrolytic aluminium and AlSi12Cu(Fe) alloy has been investigated. In experiments iron wire was dissolved in the investigated alloys at temperature 750 °C for 0, 15 and 30 minutes. These specimens were characterized using scanning electron microscope (SEM) and EDS analyzer, in order to determine concentration of iron in the aluminium and to identify iron phases. With the simultaneous thermal analysis (STA) the characteristic temperatures and the solidification, melting and precipitation heats of investigated alloys with dissolved iron were determined. Using the Thermo-Calc simulation program the equilibrium phases were calculated, special emphasis was given to iron phases that form during solidification.

Izvleček: Železo predstavlja v aluminijevih zlitinah glavno nečistočo, pri nekaterih zlitinah pa predstavlja zlitinski element, ki povečuje trdoto zlitine in krhkost zlitine. V tem delu se je preiskovalo raztapljanje železa v elektroliznem aluminiju in zlitini AlSi12Cu(Fe). Eksperimentalno je bilo raztapljanje železa opazovano z raztapljanjem železove žičke pri temperaturi 750 °C in času 0, 15 in 30 minut. Vzorci so bili preiskani z vrstičnim elektronskim mikroskopom (SEM) in EDS analizatorjem za določitev koncentracije železa v aluminiju in za definiranje železovih faz. Z uporabo simultane termične analize (STA) so bile definirane karakteristične temperature strjevanja in taljenja ter latentne toplote izločanja preiskovanih zlitin z raztopljenim železom. Z računalniško simulacijo Thermo-Calc so bile izračunane ravnotežne faze, predvsem železove faze, ki se tvorijo pri strjevanju.

Key words: Al-alloys, iron dissolution, thermal analysis, thermodynamic equilibrium
Ključne besede: aluminijeve zlitine, raztapljanje železa, termična analiza, termodinamično ravnotežje

Scientific paper

Introduction

Iron presents in Al-alloys the main impurity that aggravates ductility and corrosion behaviour. Iron in aluminium is gained from ore, from master alloy or from tools that are used during melting and aluminium casting. Another source of iron in aluminium can be scrap of metallurgical aluminium. In some alloys iron is added as an alloying element to increase hardness; however it also increases the brittleness of the alloys as a side effect. The aim of this work was to determine the dissolution of iron in electrolytic aluminium and AlSi12Cu(Fe) alloy with 0.8 wt.% of Fe. Experiments were carried out in an electrical-resistance furnace at 750 °C. The iron wire was placed into the melt and stayed in it at this temperature over different times. After the preset time the furnace was

turned off and samples were cooled down to the room temperature. Samples were investigated using a scanning electron microscope (SEM), an EDS analyzer and simultaneous thermal analysis (STA). Equilibrium solidification was calculated by the Thermo-Calc simulation program.

Influence of iron concentration in Al-alloys on solidification process

For the study of aluminium alloys, where iron is the main alloying element the equilibrium phase diagram Al-Fe, which is presented in Figure 1 was used[1]. Solubility of iron in solid aluminium is very low and amounts 0.04 wt.% at 625 °C [1].

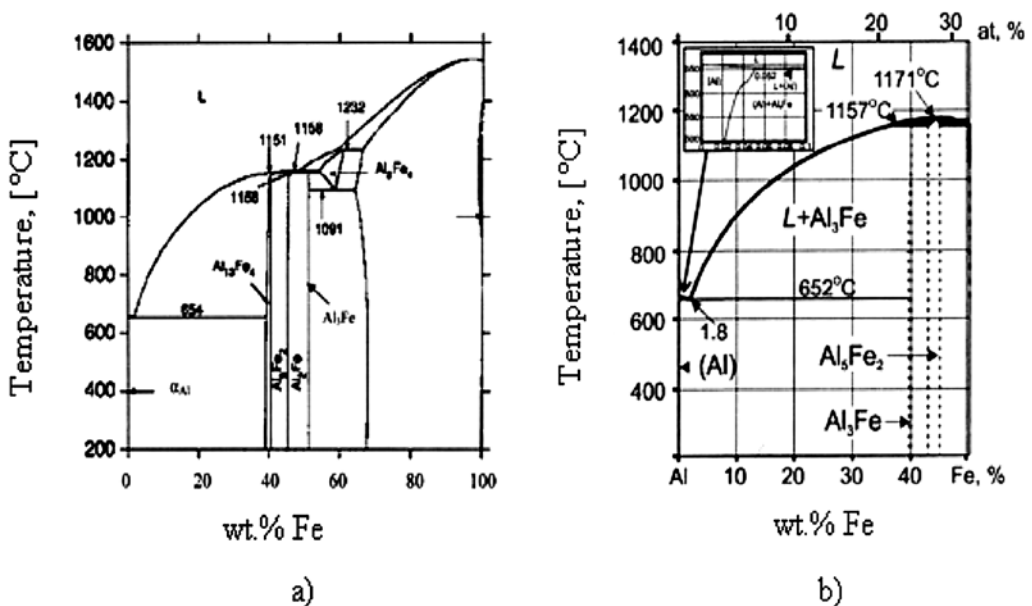When concentration of iron exceeds 10 wt.% in the system Al-Fe, a peritectic

Figure 1. Equilibrium phase diagram Al-Fe (a) and the aluminium-rich corner (b)[1]
Slika 1. Ravnotežni fazni diagram Al-Fe (a) in njegov aluminijev kot (b)[1]

reaction $L + Al_5Fe_2 \rightarrow Al_3Fe$ takes places at temperature 1158 °C, which causes formation of Al_3Fe phase, which contain 40.7 wt.% Fe (Figure 1). This phase appears in microstructure in the form of needlelike crystals and is fragile and unwished[1].

In Al-Si casting alloys in addition to β-Al_5FeSi phase numerous other phases can be present[2]. In Figure 2 the aluminium corner of ternary phase system Al-Fe-Si is presented[3].

Depending on chemical composition and solidification conditions in microstructure of Al-Si casting alloys the following intermetallic phases could be observed: α-Al_8Fe_2Si, β-Al_5FeSi and δ-Al_9FeSi_2 as
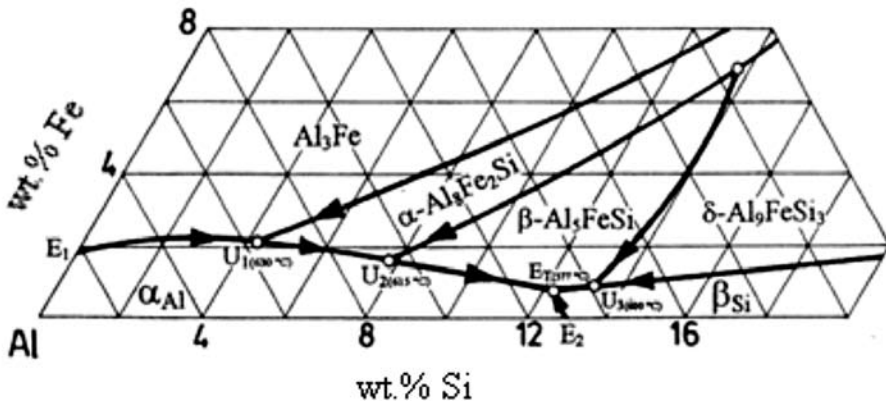

Figure 2. The aluminium corner of the ternary system Al-Fe-Si [3]
Slika 2. Aluminijev kot ternarnega sistema Al-Fe-Si [3]

Table 1. Binary and multi-component phases containing iron in Al-Si cast alloys[2]
Tabela 1. Binarne in večkomponentne spojine z železom v Al-Si zlitinah[2]

Phase	Chemical composition (wt.%)
$Al_{13}Fe_4$ (Al_3Fe)	Fe: 33.9-37.8; Si: 0.8-2.9
Al_6Fe	Fe: 25.6-28.0
β-Al_5FeSi	Fe: 23.5-30.0; Si 12.0-18.9
β-$Al_{4.5}FeSi$ ($Al_9Fe_2Si_2$)	Fe: 27.0-28.0; Si 14.0-15.0
γ-Al_3FeSi	Fe: 33.0-38.0, Si: 13.0-18.5
δ-Al_9FeSi_3	Fe: 15.0-25.4; Si: 20.0-25.5
α-Al_8Fe_2Si	Fe: 28.2-31.6; Si: 7.9-10.5
$Al_9Fe_{0,84}Mn_{2'16}Si$	Fe: 10.7; Si: 6.44; Mn: 27.2
π-$Al_8Si_6Mg_3Fe$	Fe: 8.0; Si: 25.0-33.8; Mg:13.0-16.0
α-$Al_{12-15}(Fe,Mn,Me)_3Si_{1-2}$, Me=(Cr,Cu)	Fe: 8.6-30.7; Si: 4.5-12.5; Mn: 0.52-14.0; Cu: from 7.5, Cr: to 14.4
α-$Al_{12-25}(Fe,Me)_{2-3}Si_{2-4}$, Me=(Mn,Cr,Cu,Co,Ni)	Fe: 6.3-25.2; Si: 4.6-10.0; Mn: to 13.1; Cu: to 13.0, Cr: to 14.4; Co: to 20.1; Ni: to 26.8
$Al_{19}Fe_4MnSi_2$	Fe: 19.2; Si: 8.3; Mn: 7.8; Cu:2.5; Cr: 0.2

primary crystallized phases. Most often precipitated phase in Al-Si casting alloys is β-Al$_5$FeSi phase. Table 1 shows typical binary and multi-component phases with iron and other alloying elements in Al-Si castings alloys.

Experimental work

Iron dissolution was investigated in molten electrolytic aluminium and AlSi12Cu(Fe) alloy. Chemical compositions of investigated alloys are shown in Table 2.

Samples were melted in an electrical-resistance furnace in a graphite crucible. When the temperature of the melt reached 750 °C, iron wire was placed into the melt in the middle of the crucible (Figure 3). Dissolution of iron wire was observed at temperature 750 °C for 0 min, 15 min in 30 min. After these preset times the furnace was turned off. The cooling was continued down to the room temperature.

The samples were cut into two halves next to the iron wire (Figure 4). The samples were investigated using a scanning

Table 2. Chemical composition of investigated alloys in wt.%
Tabela 2. Kemijska sestava preiskovanih zlitin v mas.%

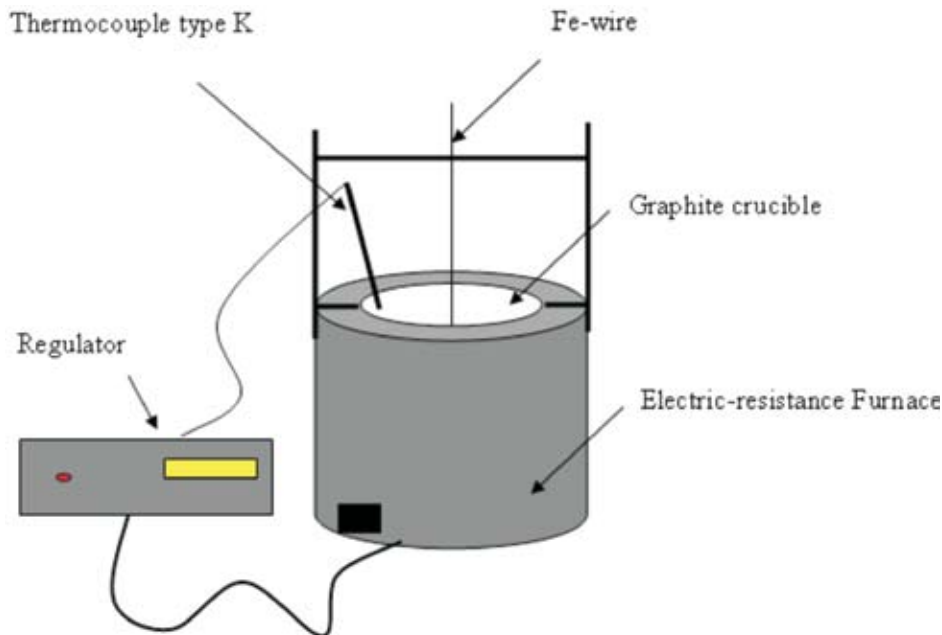|	SI	FE	CU	MN	MG	ZN	TI	AL
Electrolytic Al	0.041	0.1497	<0.0008	<0.0001	0.0011	0.0089	0.0001	rest
AlSi12Cu(Fe) alloy	11.5584	0.8292	0.7159	0.1915	0.0546	0.4673	0.0466	rest

Figure 3. Scheme of the experimental set-up
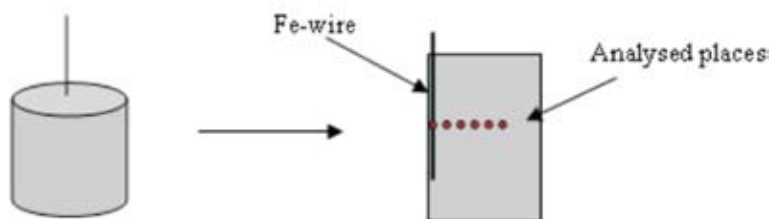**Slika 3.** Shema eksperimentalne naprave

Figure 4. Scheme of a cut sample and analysed places
Slika 4. Shema razreza vzorca s prikazanimi analiziranimi mesti

electron microscope (SEM) JEOL JSM-5610. They were prepared by the standard metallographic procedure. The samples were analysed at sites shown in Figure 4. On the basis of iron analysis in Al and AlSi12Cu(Fe) a diagram, iron concentration versus distance from the iron wire was constructed.

AlSi12Cu(Fe) samples were researched with simultaneous thermal analysis (STA) on the STA 449 NETZSCH apparatus. The specimens were heated to 720 °C with heating rate of 10 K/min in an argon protective atmosphere and cooled with the same rate down to the room temperature.

With computer simulation Thermo-Calc were defined existence of thermodynamic equilibrium phases in electrolytic aluminium and AlSi12Cu(Fe) alloy with 0.8 wt.% Fe. The aim was to determine which iron phases may form during solidification.

RESULTS AND DISCUSSION

Using computer simulation Thermo-Calc the existence of thermodynamic equilibrium phases in electrolytic aluminium and AlSi12Cu(Fe) alloy were calculated. Then the equilibrium isoplet phase diagram: vertical cross-section through Al-corner with variable contents of Al and Fe (a) and Si (b), and constant contents of all other element was constructed (Figure 5). Graphs show that during solidification in Al-Fe system $Al_{13}Fe$ phase precipitate and in Al-Si system β-AlFeSi phase precipitate.

Figure 6 a) presents a concentration of iron in dependence from the distance from the iron wire at temperature 750 °C. The dissolution time was 30 min. It also shows the microstructure of interface between iron wire and aluminium, and at the distances 3 mm and 9 mm from the iron wire. In Figure 6 b) the interface between iron wire and aluminium could be seen, and also the needles of iron phases. It is assumed that this is $Al_{13}Fe_4$ phase, formed during peritectic reaction between the electrolytic aluminium and the iron wire. Concentration of iron in aluminium decreased to 0.5 wt.% Fe at distance 3 mm from iron wire.

Figure 7 a) presents a concentration of iron in dependence from distance from iron wire at temperature 750 °C in electrolytic aluminium. The dissolution time was 15 min. Microstructures on distance b) 1 , c) 3 and d) 9 mm from the iron wire are shown on Figure 7. Needles of iron phases are barely visible, interface between iron wire
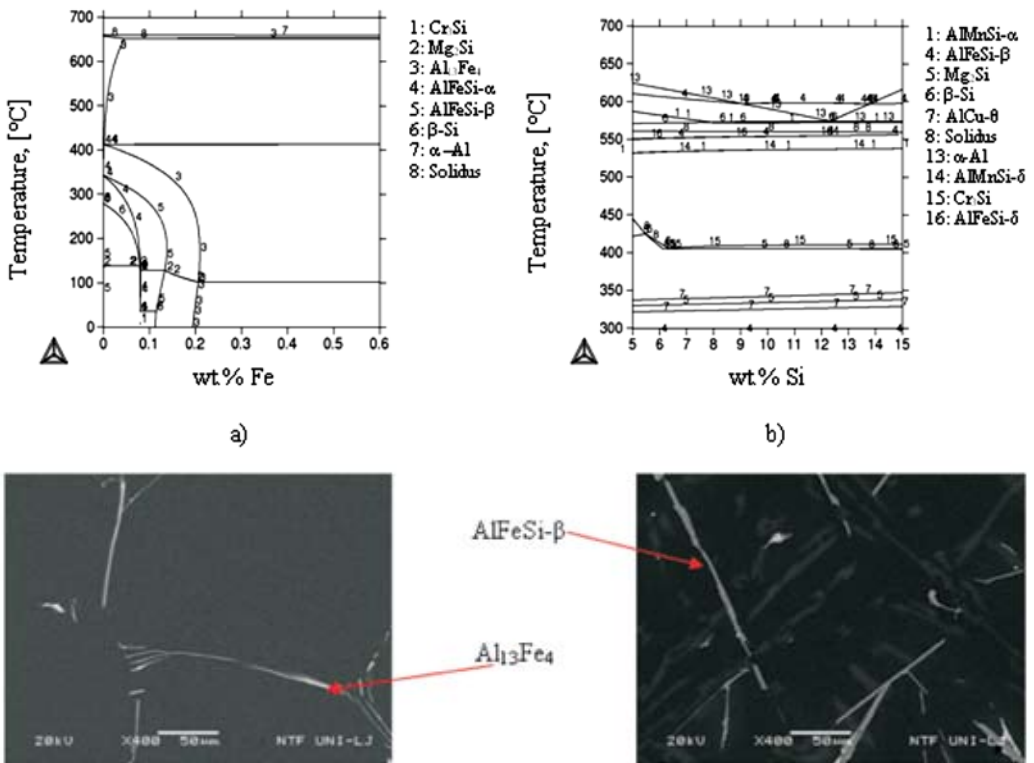
Figure 5. Equilibrium isoplet phase diagram of electrolytic aluminium with belonging microstructure of $Al_{13}Fe_4$ phase (a) and AlSi12Cu(Fe) alloy with belonging microstructure of AlFeSi-β phase (b)

Slika 5. Ravnotežni izopletni fazni diagram za elektrolizni aluminij s pripadajočimi mikrostrukturnimi fazami $Al_{13}Fe_4$ (a) in zlitino AlSi12Cu(Fe) s pripadajočimi mikrostrukturami faze AlFeSi-β (b)

and aluminium is not shown, concentration of iron in aluminium decreased to 0.8 wt.% at distance 1 mm.

Figure 8 a) presents a concentration of iron in dependence from distance from iron wire at temperature 750 °C in electrolytic aluminium. The dissolution time was 0 min. When the temperature of melt reached 750 °C, the iron wire was placed in the melt and the heating was turned off. On microstructure the interface between iron wire and aluminium is not present and

needles of iron phases are barely visible. Microstructure presents iron phases at the distance 1, 3 in 9 mm from iron wire.

Microstructures were made also on AlSi12Cu(Fe) alloy, which is shown by Figures 9-11. Figure 9 a) presents concentration of iron in dependence from distance from iron wire at temperature 750 °C and dissolution time of 30 min in AlSi12Cu(Fe) alloy. Shown are also microstructures of interface b) between iron wire and aluminium alloy, and on the

Figure 6. a) Concentration of iron in electrolytic aluminium at different distances from the iron wire (the results of EDS analyses). Scanning electron micrographs (BSE) at different distances from the iron wire after 30 min dissolution time at 750 °C: b) at the interface iron wire – electrolytic aluminium, c) 3 mm and d) 9 mm from the interface.

Slika 6. a) Koncentracija železa v elektroliznem aluminiju pri različnih razdaljah od železove žičke (rezultati EDS analize). Posnetki elektronskega mikroskopa (odbiti elektroni) pri različnih razdaljah od železove žičke po 30 min raztapljanja pri 750 °C: b) na prehodu železova žička – elektrolizni aluminij, c) 3 mm in d) 9 mm od prehoda.

Figure 7. a) Concentration of iron in electrolytic aluminium at different distance from iron wire (the results of EDS analyses). Scanning electron micrographs (BSE) at different distances from the iron wire after 15 min dissolution time at 750 °C: b) 1 mm, c) 3 mm and d) 9 mm from the iron wire.
Slika 7. a) Koncentracijski železa v elektroliznem aluminiju pri različnih razdaljah od železove žičke (rezultati EDS analize). Posnetki elektronskega mikroskopa (odbiti elektroni) pri različnih razdaljah od železove žičke po 15 min raztapljanja pri 750 °C: b) 1 mm, c) 3 mm in d) 9 mm od železove žičke.
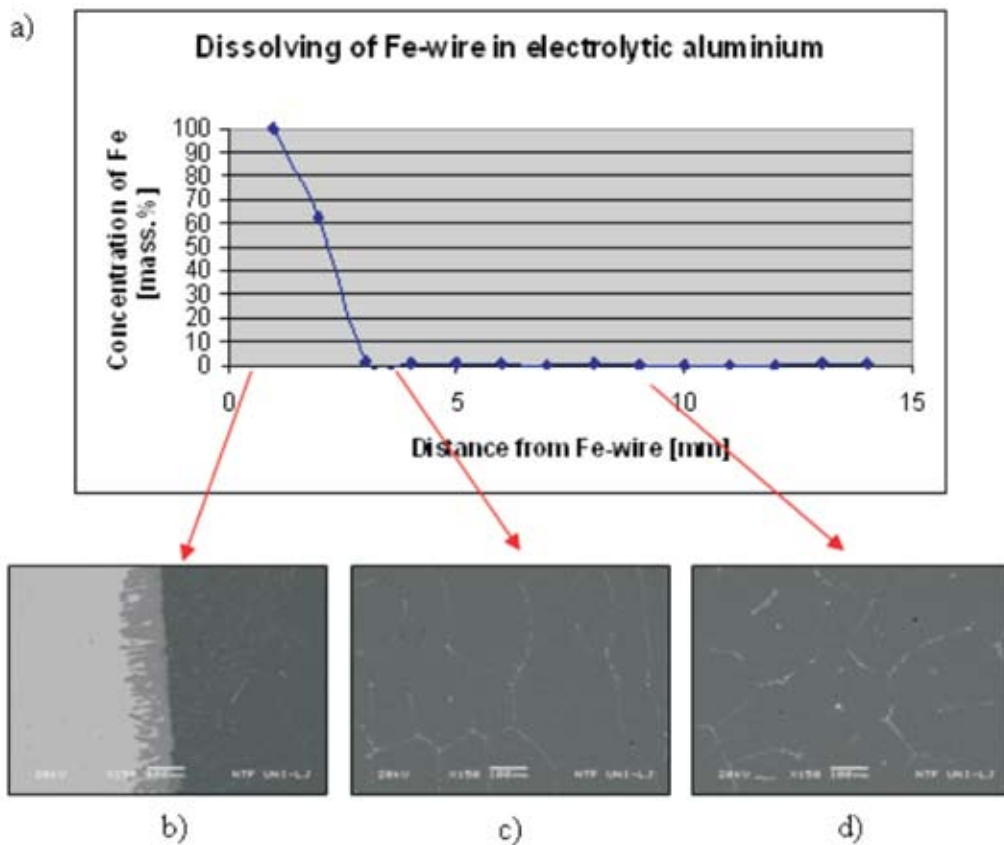
Figure 8. a) Concentration of iron in electrolytic aluminium at different distance from iron wire (the results of EDS analyses). Scanning electron micrographs (BSE) at different distances from the iron wire after 0 min dissolution time at 750 °C: b) 1mm, c) 3 mm and d) 9 mm from the iron wire.

Slika 8. a) Koncentracijski železa v elektroliznem aluminiju pri različnih razdaljah od železove žičke (rezultati EDS analize). Posnetki elektronskega mikroskopa (odbiti elektroni) pri različnih razdaljah od železove žičke po 0 min raztapljanja pri 750 °C: b) 1mm, c) 3mm in d) 9mm od železove žičke.

Figure 9. a) Concentration of iron in AlSi12Cu(Fe) alloy at different distances from the iron wire (the results of EDS analyses). Scanning electron micrographs (BSE) at different distances from the iron wire after 30 min dissolution time at 750 °C: b) at the interface iron wire – AlSi12Cu(Fe) alloy, c) 3 mm and d) 9mm from the interface.
Slika 9. a) Koncentracija železa v zlitini AlSi12Cu(Fe) pri različnih razdaljah od železove žičke (rezultati EDS analize). Posnetki elektronskega mikroskopa (odbiti elektroni) pri različnih razdaljah od železove žičke po 30 min raztapljanja pri 750 °C: b) na prehodu železova žička – zlitina AlSi12Cu(Fe), c) 3 mm in d) 9 mm od prehoda.
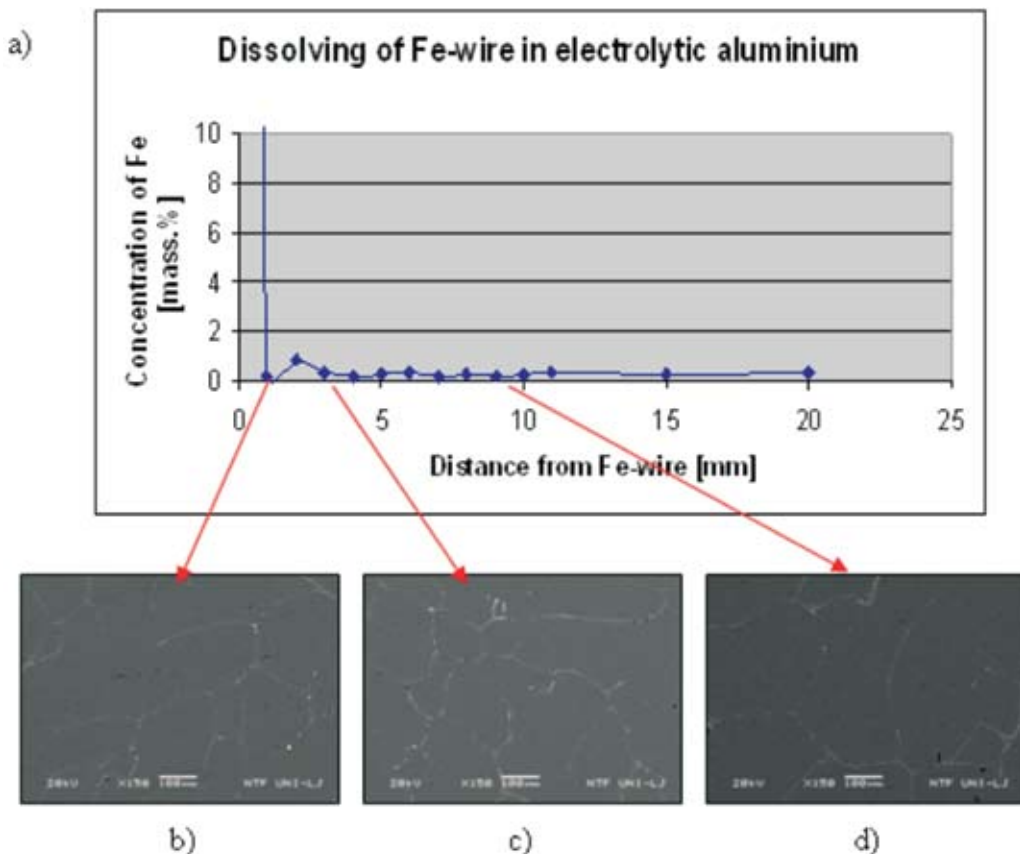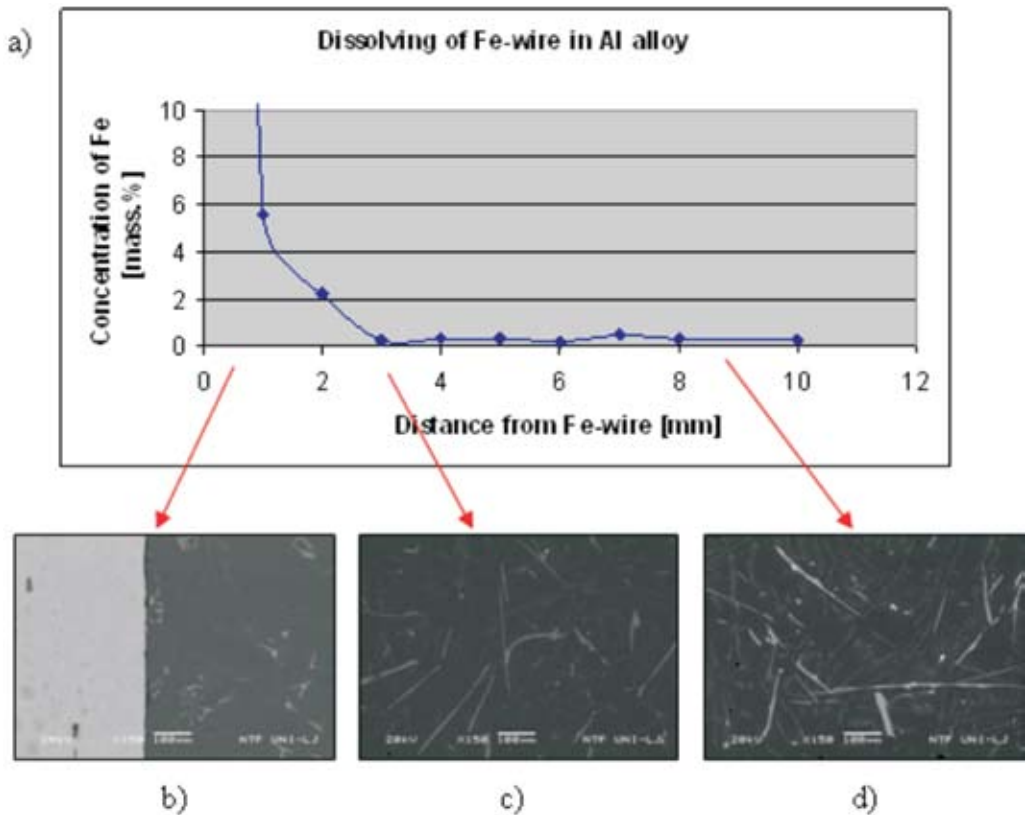
Figure 10. a) Concentration of iron in AlSi12Cu(Fe) alloy at different distances from the iron wire (the results of EDS analyses). Scanning electron micrographs (BSE) at different distances from the iron wire after 15 min dissolution time at 750 °C: b) at the interface iron wire – AlSi12Cu(Fe) alloy, c) 3 mm and d) 9 mm from the interface.

Slika 10. a) Koncentracija železa v zlitini AlSi12Cu(Fe) pri različnih razdaljah od železove žičke (rezultati EDS analize). Posnetki elektronskega mikroskopa (odbiti elektroni) pri različnih razdaljah od železove žičke po 15 min raztapljanja pri 750 °C: b) na prehodu železova žička – zlitina AlSi12Cu(Fe), c) 3 mm in d) 9 mm od prehoda.
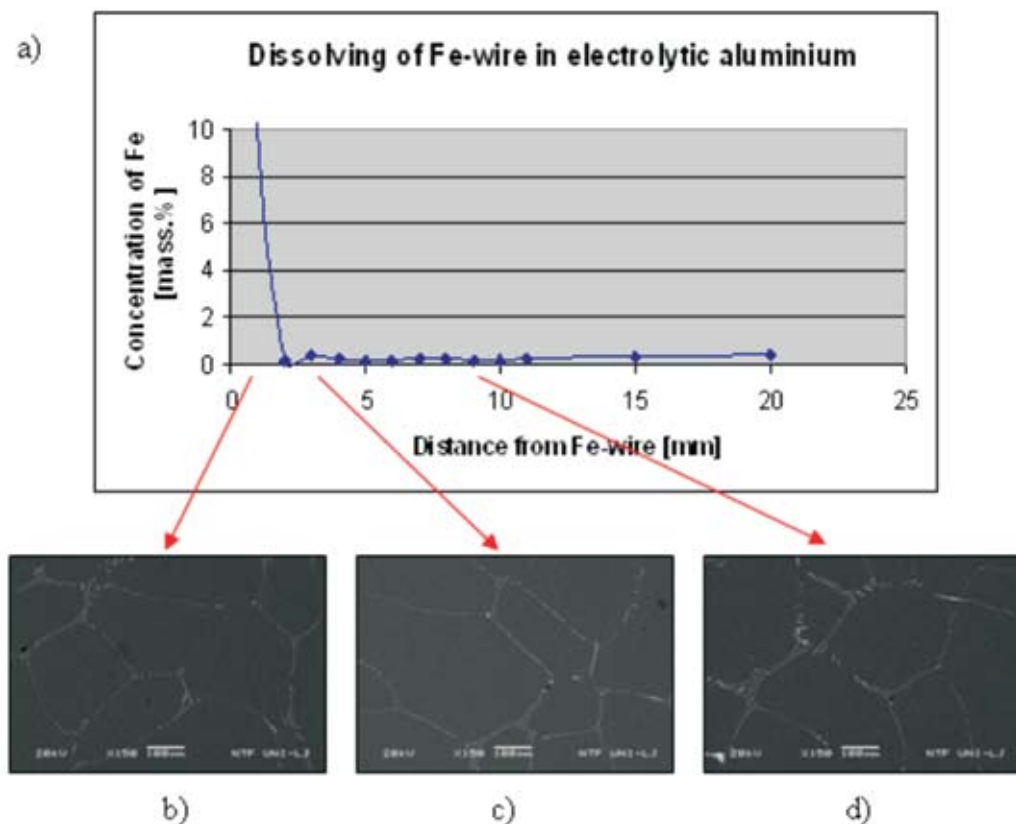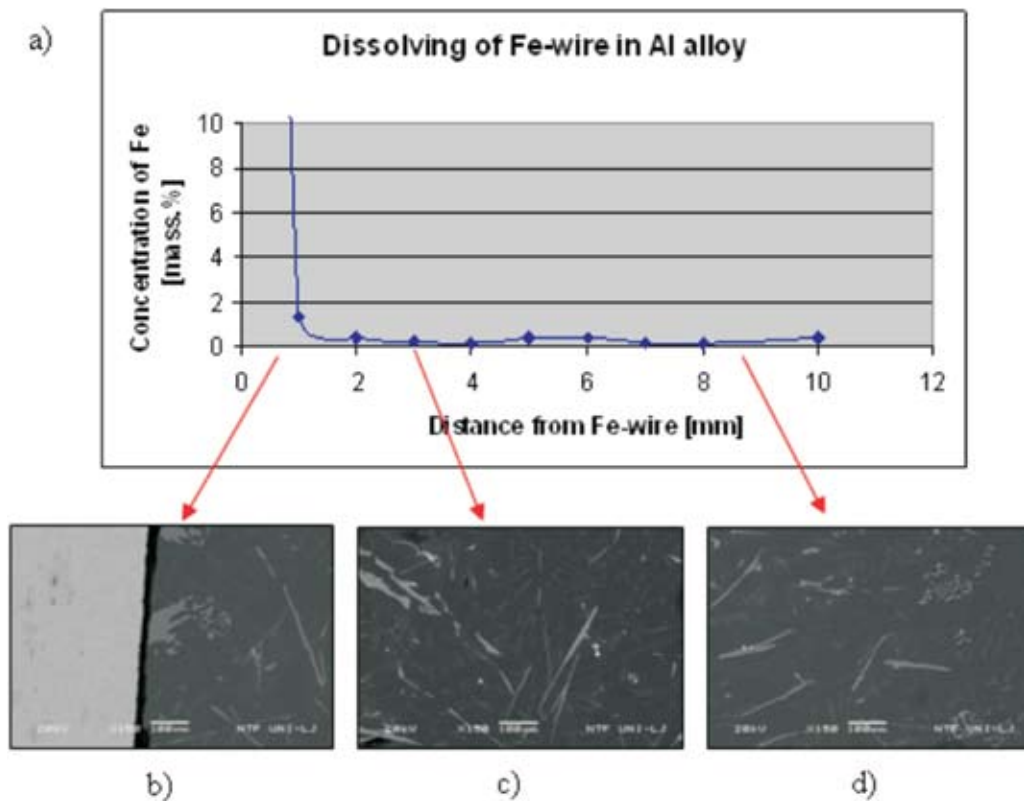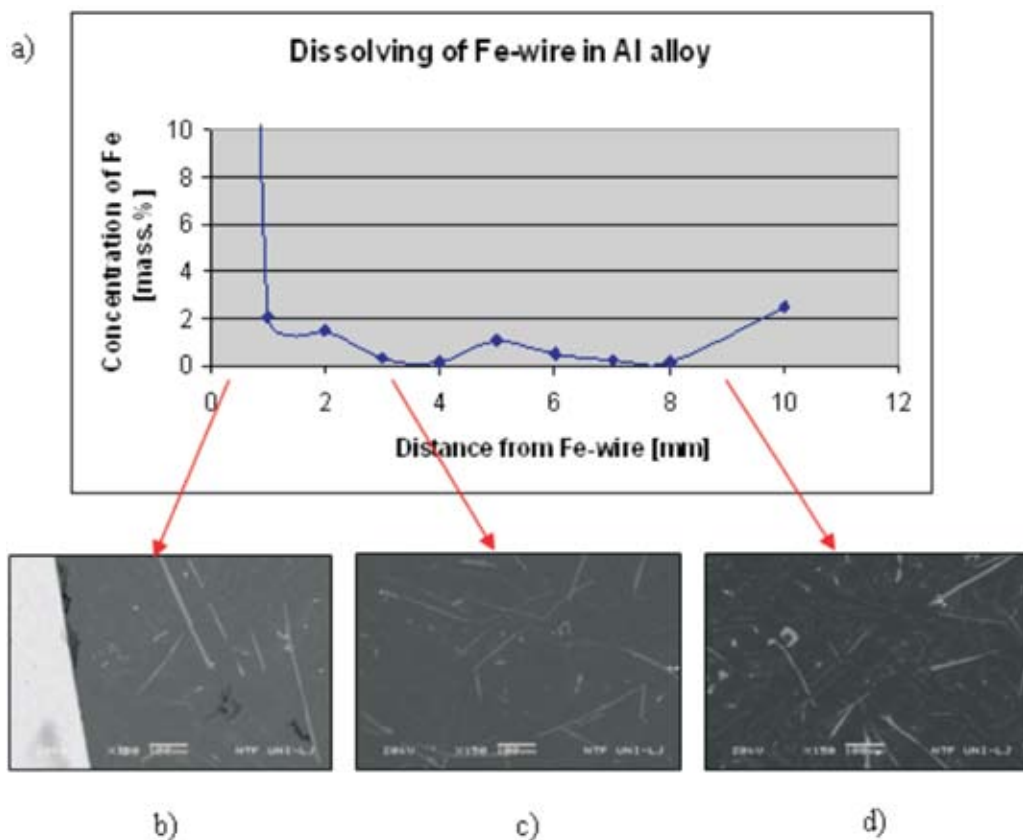
Figure 11. a) Concentration of iron in AlSi12Cu(Fe) alloy at different distances from the iron wire (the results of EDS analyses). Scanning electron micrographs (BSE) at different distances from the iron wire after 0 min dissolution time at 750 °C: b) at the interface iron wire – AlSi12Cu(Fe) alloy, c) 3 mm and d) 9 mm from the interface.

Slika 11. a) Koncentracija železa v zlitini AlSi12Cu(Fe) pri različnih razdaljah od železove žičke (rezultati EDS analize). Posnetki elektronskega mikroskopa (odbiti elektroni) pri različnih razdaljah od železove žičke po 0 min raztapljanja pri 750 °C: b) na prehodu železova žička – zlitina AlSi12Cu(Fe), c) 3 mm in d) 9 mm od prehoda.

distance 3mm c) and 9 mm d) from iron wire. Dissolving iron combines with Al and Si and forms β-AlFeSi phase. Interface between iron wire and aluminium alloys is not present as by electrolytic aluminium. Concentration of iron in aluminium alloy decreased to 0.3 wt.% at the distance 1 mm from iron wire.

Figure 10 presents concentration of iron in dependence from distance from iron wire at temperature 750 °C and dissolution time of 15 min in AlSi12Cu(Fe) alloy. Shown are also microstructures of interface between iron wire and aluminium alloy, and at the distance 3 mm and 9 mm from iron wire. Interface between iron wire and aluminium alloys, and needles from iron wire are not visible. Concentration of iron in aluminium alloy decreased to 0.2 wt.% at distance 3 mm from iron wire.

Figure 11 presents concentration of iron in dependence from distance from iron wire in AlSi12Cu(Fe) alloy and dissolution time of 0 min, which was heated up to 750 °C. Shown are also microstructures of interface between iron wire and aluminium alloy, and on the distance of 3 mm and 9 mm from iron wire. When the temperature of the melt reached 750 °C, the iron wire was placed into the melt and the heating was turned off. Interface between iron wire and aluminium alloy is seen on microstructures. The concentration of iron in alloy varies between 0.2 and 2 wt.% of iron.

For samples of AlSi12Cu(Fe) alloy with iron wires was made simultaneous thermal analysis. Figure 12 and 13 presents comparison between heating curves of investigated AlSi12Cu(Fe) alloy and heat of fusion. Notice that with increasing dissolution time of iron wire in melt at 750 °C, the liquidus temperature decreased and eutectic temperature increased. This can be a consequence of increasing iron concentration in the alloy. Comparison of solidus temperatures and their heats of fusion is presented in Table 3.

With the simultaneous thermal analysis were measured temperatures of precipitation and the heats of fusion. From diagram on Figures 6 is shown that at specified temperature AlCu-θ is precipitated. The curves in Figure 14 can show that increasing dissolution time of iron wire in the melt at 750 °C, the precipitation temperature and therefore heats of fusion decreased. Comparison of precipitation temperatures and heats of fusion are presented in Table 4.

Figure 15 compares cooling curves after different dissolution times of iron wire in AlSi12Cu(Fe) alloy. The curves show that the temperature of primary solidification and temperature of eutectic solidification are similar. The longer is the dissolution time of the iron wire in the melt at 750 °C, less heat is released during solidification. Table 5 shows temperatures of primary solidification, eutectic solidification and heats of fusion.
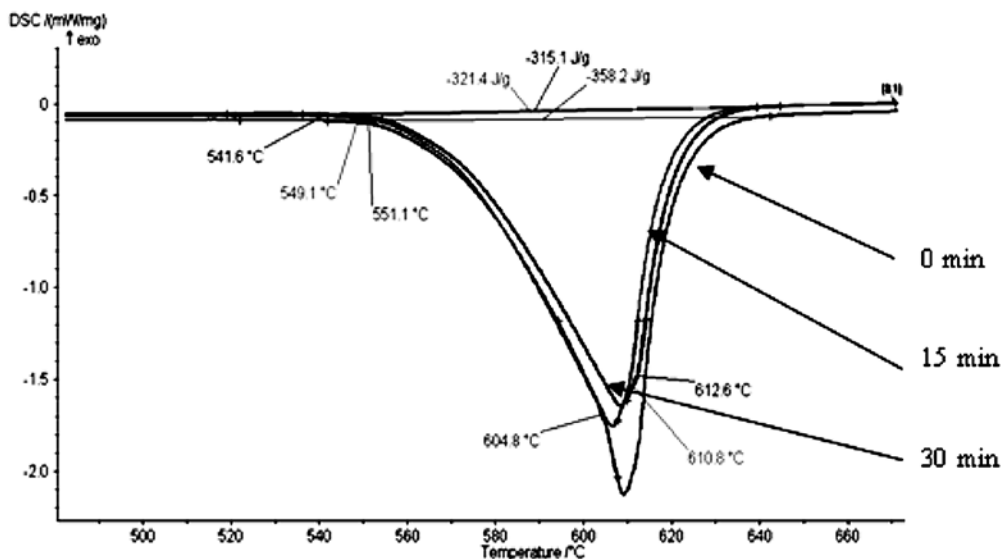
Figure 12. Comparison of heating curves of investigated samples in the AlSi12Cu(Fe) alloy
Slika 12. Primerjava segrevalnih krivulj preiskovanih vzorcev v zlitini AlSi12Cu(Fe)

Table 3. Comparison of melting temperatures and their heats of fusion
Tabela 3. Primerjava temperatur začetka taljenja in latentnih toplot, ki se porabijo pri taljenju

DISSOLUTION TIME	0 MIN	15 MIN	30 MIN
$T_{solidus}$	551.1 °C	549.1 °C	541.6 °C
$T_{eutectic}$	604.8 °C	610.8 °C	612.6 °C
Heat of fusion	358.2 J/g	321.4 J/g	315.1 J/g

Table 4. Segregation temperatures for AlCu-θ phase and their latent heats after different dissolution times of iron wire in AlSi12Cu(Fe) alloy
Tabela 4. Primerjava temperatur izločanja za fazo AlCu-θ in njihovih latentnih toplot po različnih časih raztapljanja železove žičke v zlitini AlSi12Cu(Fe)

DISSOLUTION TIME	0 MIN	15 MIN	30 MIN
$T_{segregation}$	261.4 °C	235.5 °C	237.5 °C
Precipitation heat	8.739 J/g	6.337 J/g	5.737 J/g
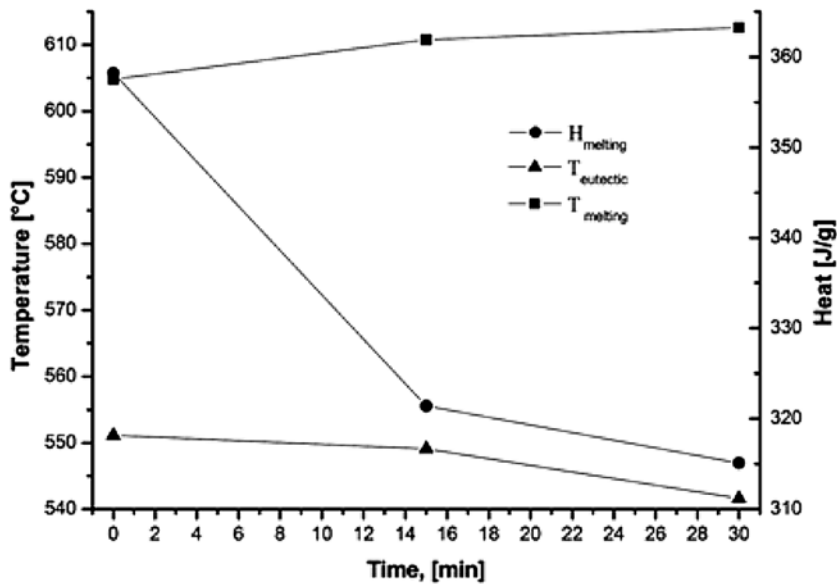
Figure 13. Melting temperatures and heats of fusion depending on dissolution time of iron wire in AlSi12Cu(Fe)
Slika 13. Temperature taljenja in porabljena latentna toplota v odvisnosti od časa raztapljanja Fe-žičke v zlitini AlSi12Cu(Fe)
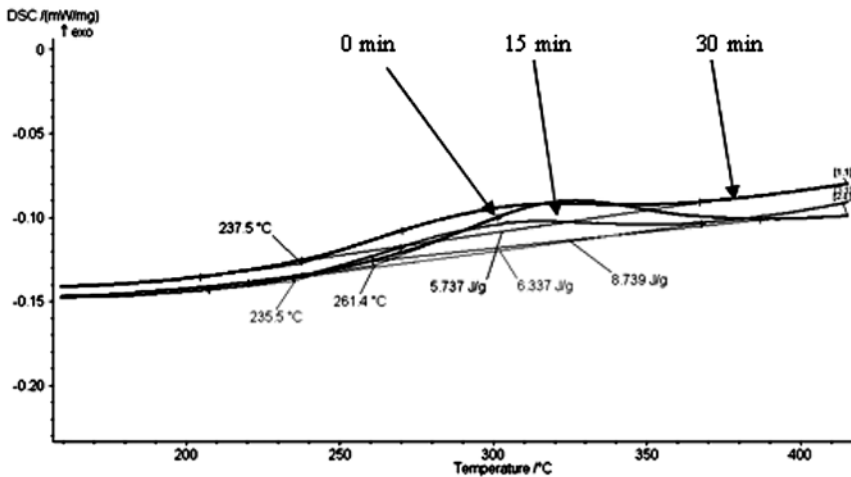
Figure 14. Comparison of cooling curves after different dissolution times of iron wire in AlSi12Cu(Fe) alloy in the temperature region, where precipitation of AlCu-θ phase is expected. The latent heats of precipitation are also given.
Slika 14. Primerjava ohlajevalnih krivulj po različnih časih raztapljanja železove žičke v zlitini AlSi12Cu(Fe) v temperaturnem območju, kjer se pričakuje izločanje faze AlCu-θ. Podane se tudi latentne toplote izločanja.
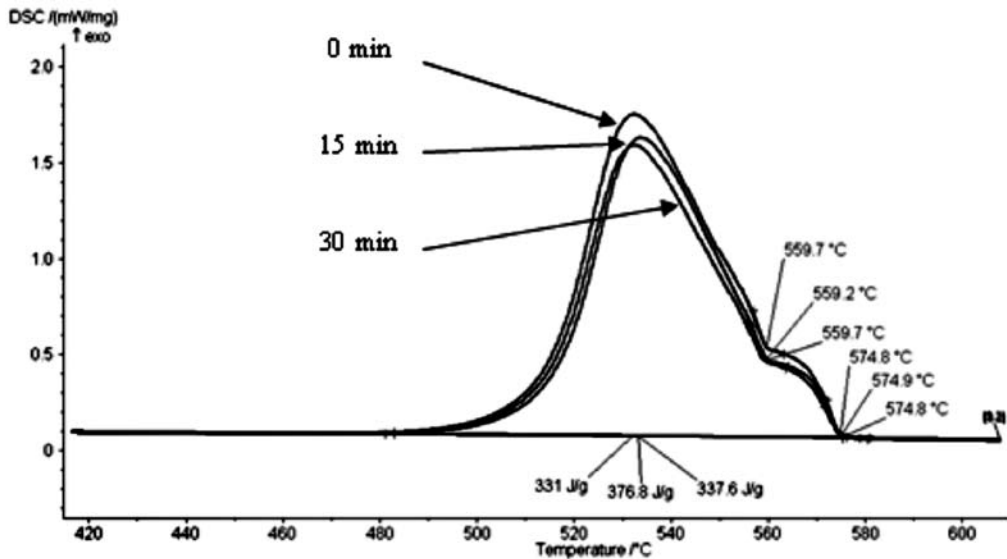
Figure 15. Cooling curves after different dissolution times of iron wire in AlSi12Cu(Fe) alloy and corresponding heats of fusion (solidification)
Slika 15. Ohlajevalne krivulje po različnih časih raztapljanja železove žičke v zlitini AlSi12Cu(Fe) ter pripadajoče latentne toplote

Table 5. Temperatures of primary solidification, eutectic solidification and heats of fusion (solidification) after different dissolution times of iron wire in AlSi12Cu(Fe) melt
Tabela 5. Temperature začetka strjevanja, strjevanja evtektika in latentnih toplot, po različnih časih raztapljanja železove žičke v talini zlitine AlSi12Cu(Fe)

DISSOLUTION TIME	0 MIN	15 MIN	30 MIN
$T_{liquidus}$	574.9 °C	574.8 °C	574.8 °C
$T_{eutectic}$	559.7 °C	559.7 °C	559.2 °C
Heat of fusion	376.8 J/g	337.6 J/g	331 J/g

CONCLUSIONS

The purpose of experiments was to determine of iron dissolution in electrolytic aluminium and in AlSi12Cu(Fe) alloy. According to the results the following conclusions can be drawn:

- In Al-Fe system most often iron phase $Al_{13}Fe_4$ is present. In AlSi12Cu(Fe) alloy β-AlFeSi phase crystallized as a primary phase, in which most of the iron from Fe-wire is present.
- The highest concentration of iron in electrolytic aluminium is obtained after dissolution iron wire for 30 min at 750 °C. Iron concentration diagram becomes apparently constant 4 mm from Fe- wire, when the content of Fe in aluminium decreased to 0.5 wt.% Fe.
- Concentration profile of dissolving iron in Al-Si alloy is different probably due to binding of iron from iron wire in the primary solidified β-AlFeSi phase. Concentration of Fe in AlSi12Cu(Fe) alloy drops to 0.3 wt.% Fe at distance 1 mm from iron wire after 30 min dissolution time at 750 °C.
- With the help of simultaneous thermal analysis we can claim that by increasing concentration of iron in alloy the solidus temperature decreased and eutectic temperature increased.
- By increasing the concentration of iron the latent heat for melting (heat of fusion) decreased. Iron phases released less heat during solidification, which was proven by simultaneous thermal analysis.

- By increasing concentration of iron in alloy the temperature for precipitation of AlCu-θ phase and amount of released latent heat were decreased.

POVZETEK

Raztapljanje železa v aluminijevih zlitinah

Železo predstavlja v aluminijevih zlitinah glavno nečistočo. Pri nekaterih aluminijevih zlitinah pa je glavni zlitinski element, ki izboljša trdoto zlitine, vendar s tem poveča krhkost. V tem delu smo preiskovali kako se železo raztaplja v elektroliznem aluminiju in zlitini AlSi12Cu(Fe). Raztapljanje železa smo preiskovali z vstavljanjem Fe-žičke v elektrolizni aluminij in zlitino AlSi12Cu(Fe), pri temperaturi 750 °C in različnih časih raztapljanja: 0, 15 in 30 minut. Ko je talina dosegla temperaturo 750 °C, smo vanj vstavili železovo žičko in jo pri tej temperaturi držali v talini različno dolgo. Nato smo vzorce razrezali tik ob žički in jih preiskali z vrstičnim elektronskim mikroskopom (SEM), kjer smo ugotavljali koncentracijo Fe v aluminiju in aluminijevi zlitini ter katere železove faze se izločajo. Z računalniško simulacijo Thermo-Calc smo ugotovili, da se v sistemu Al-Fe pri strjevanju elektroliznega aluminija izloča faza $Al_{13}Fe_4$ pri zlitini AlSi12Cu(Fe) pa faza AlFeSi-β. Z elektronskim mikroskopom smo analizirali železovo žičko, in vsak milimeter vstran od železove žičke ter naredili posnetek. Nato smo izdelali koncentracijski diagram koncentracije železa v odvisnosti od oddaljenosti žičke.

S simultano termično analizo (STA) smo določali karakteristične temperature in toplote taljenja, strjevanja in izločanja. Opazili smo, da dlje kot smo držali Fe-žičko pri 750 °C, nižje so likvidus temperature in višje so temperature taljenja evtektika, kar je posledica povečanja deleža železa v zlitini. Prav tako lahko rečemo, da dlje ko smo žičko držali pri temperaturi 750 °C, nižjo temperaturo izločanja faze AlCu-θ smo dobili in s tem tudi nižje toplote. Iz ohlajevalnih krivulj simultane termične analize pa je razvidno, da dlje kot smo Fe-žičko držali na temperaturi 750 °C v talini, manj toplote se sprosti pri strjevanju.

Najpogostejša faza, ki se pojavlja v sistemu aluminij-železo je faza $Al_{13}Fe_4$. V Al-Si zlitinah lahko srečamo številne železove intermetalne spojine, kar je odvisno od kemijske sestave in pogojev strjevanja. Najpogostejše primarno izločene faze so α-Al_8Fe_2Si, β-Al_5FeSi in δ-Al_9FeSi_2. V zlitini AlSi12Cu(Fe) je bila primarno izločena faza β-AlFeSi, na katero se je nalagalo tudi železo od raztapljanja Fe-žičke. Najvišjo koncentracijo železa aluminiju smo dobili z raztapljanjem žičke pri 750 °C in času 30 min. Krivulja koncentracijskega diagrama se izravna nekje na oddaljenosti 4 mm od žičke, vsebnost Fe v aluminiju pa pade na 0,5 mas.% Fe. Pri aluminijevi zlitini pa vsebnost železa v aluminijevi zlitini pade že na 1 mm od žičke na 0,3 mas. %, pri raztapljanju žičke na 750 °C 30 min. Z večanjem deleža železa v zlitini se znižuje temperatura tališča, temperatura tališča evtektika pa se zvišuje. Z večanjem deleža železa v zlitini se zniža tudi toplota, ki se porablja pri taljenju. Prav tako lahko rečemo, da železove faze oddajo manj toplote pri strjevanju, kar je razvidno tudi iz preiskav s simultano termično analizo.

REFERENCES

[1] BELOV, N.A., AKSENOV, A.A., ESKIN, D.G. (2002): *Iron in Aluminum Alloys: Impurity and Alloying Element*. London and New York, pp. 3-7.

[2] MARKOLI, B., SPAIČ, S., ZUPANIČ, F. (2004): The intermetallic phases containing transition elements in common Al-Si cast alloys. *Aluminium.*; Vol. 80, No. ½, pp. 84-88.

[3] MASSALSKI, T.B. (1990): *Binary Alloys Phase Diagrams*. 2nd ed., ASM, Metals Park, Ohio.

The kinetics of precipitation in Al-Mg and Al-Mg-Cu alloy

Kinetika izločanja v zlitinah Al-Mg in Al-Mg-Cu

Maja Vončina[1], Primož Mrvar[1], Franc Zupanič[2], Jožef Medved[1]

[1]University of Ljubljana, Faculty of Natural Sciences and Engineering, Department of materials and metallurgy, Aškerčeva cesta 12, SI-1000 Ljubljana, Slovenia;
E-mail: maja.voncina@ntf.uni-lj.si, primoz.mrvar@ntf.uni-lj.si, jozef.medved@ntf.uni-lj.si
[2] University of Maribor, Faculty for Mechanical Engineering, University Center for Electron Microscopy, Smetanova ulica 17, 2000 Maribor, Slovenia; E-mail: franc.zupanic@uni-mb.si

Abstract: Aluminium alloys usually contain many alloying elements which form many phases. However, most of the heat-treatable alloys contain combinations of magnesium with one or more of the elements such as copper, silicon and zinc. In this work a triple simple thermal analysis (TETA) was used in order to achieve three different cooling rates and consequently three different stages of supersaturated solid solution. In addition melt spinning was used to obtain highly supersaturated solid solution. The course of equilibrium solidification of the alloys was calculated using the computer simulation (Thermo-Calc). To pursue the sequence of precipitation of hardening precipitates the differential scanning calorimetry (DSC) was used enabling determination of precipitation energy and the temperature of precipitation of precipitates from supersaturated solid solution. Scanning electron microscopy (SEM) and energy dispersive spectroscopy (EDS) was used to determine the phases formed during solidification. Using the DSC method the kinetics of precipitation from supersaturated solid solution in our case in AlMg7.5 and AlMg3Cu can be followed very precisely. The precipitation kinetics is related to increasing tendency for energy relaxation on heating DSC curve, and is enhanced with strongly supersaturated solid solutions. If the portion of the precipitation energy is calculated, it can be evident that, in the AlMg7.5 alloy, it increases with the increasing supersaturation. In the AlMg3Cu alloy the precipitation energy also increases from 0.8 % in specimen that was cooled in MC1 to 1.6 % in specimen that was rapidly solidified.

Izvleček: Aluminijeve zlitine običajno vsebujejo veliko zlitinskih elementov, zato imajo v mikrostrukturi več faz. Večina toplotno utrjevalnih aluminijevih zlitin vsebuje kombinacijo magnezija z enim ali več elementi, kot so baker, silicij in cink. V tem delu je bila, za dosego različnih stanj prenasičene trdne raztopine, izvedena trojna enostavna termična analiza (TETA), pri čemer so bile dosežene tri različne ohlajevalne hitrosti ter posledično tri različne

---

Scientific paper

prenasičene trdne raztopine. Z napravo za hitro strjevanje (Melt Spinner) pa je bila dosežena najbolj prenasičena trdna raztopina. Potek ravnotežnega strjevanja je bil določen z računalniško simulacijo Thermo-Calc. Za zasledovanje zaporedja izločanja utrjevalnih izločkov je bila uporabljena simultana termična analiza (STA) in sicer diferenčna vrstična kalorimetrija (DSC), s katero so bile določene energije izločanja ter temperature izločanja izločkov iz različnih prenasičenih trdnih raztopin. S pomočjo elektronske mikroskopije (SEM) ter energijsko disperzijske spektroskopije (EDS) so bili določeni tipi nastalih izločkov. Ob uporabi DSC metode je omogočeno izredno natančno zasledovanje kinetike izločanja iz prenasičene trdne raztopine, v našem primeru v zlitini AlMg7,5 in AlMg3Cu. Kinetika izločanja je razvidna iz povečevanja sproščene energije izločanja, ki pa s se povečano prenasičenostjo samo še povečuje. Pri izračunu deleža sproščene energije je opaziti, da energija izločanja s prenasičenostjo v zlitini AlMg7,5 naraste. Pri zlitini AlMg3Cu energija izločanja prav tako naraste od 0,8 % v vzorcu predhodno ohlajanem v MC1 na 1,6 % v vzorcu predhodno ohlajenem na Melt Spinnerju.

Key words: Al-Mg alloy, Al-Mg-Cu alloy, thermal analysis, differential scanning calorimetry (DSC), precipitation kinetics

Ključne besede: zlitina Al-Mg, zlitina Al-Mg-Cu, termična analiza, diferenčna vrstična kalorimetrija (DSC), kinetika izločanja

Introduction

Al-Mg and Al-Mg-Cu alloys are usually strengthened by nanoparticles that precipitate from a supersaturated solid solution. Nevertheless, most of the heat-treatable alloys contain combinations of magnesium with one or more of the elements like copper, silicon and zinc. Characteristically, even a small amount of magnesium in concert with these elements accelerates and accentuates precipitation hardening. The structural changes, which are formed as a result of precipitation of atoms from solid solution, have extraordinary technological and industrial meaning.

The majority of heat-treatable aluminium alloy systems exhibit multistage precipitation and undergo accompanying strength changes. Multiple alloying additions of elements employed in commercial alloys are strictly functional and with different heat treatments serve to provide many different combinations of properties[1].

Heat treatment to increase strength of aluminium alloys is a three-step process:
1. Solution heat treatment: dissolution of soluble phases.
2. Quenching: development of supersaturated solid solution.
3. Age hardening: precipitation of solute atoms either at room temperature (natural aging) or elevated temperature (artificial aging)[1].

The classical Al-Mg alloy is typically used for car body construction, where certain problems can occur during the paint-bak-

ing treatment, due to the softening of Al-Mg parts. The undesirable softening can be overcome either by using precipitation hardening at paint-baking temperatures (160-180 °C) either with small additions of copper, which makes the alloys precipitation hardenable during paint-baking treatment[1].

During aging of Al-Mg-Cu alloy the precipitation takes place in following sequence:

SSS → GPB zone → S''/GPB2 → S' → S

SSS stands for supersaturated solid solution and GPB for Guinier-Preston-Bagaryatsky[1,2]. The transition phases (GPB zone, S'', S') are formed because they have a lower activation energy barrier for nucleation than the equilibrium phases. S-phase prefers to nucleate on defects, therefore dislocations and dislocation loops are the favoured nucleation sites[1].

In this work we investigated the precipitation kinetics from different supersaturated solid solutions in two alloys: binary AlMg7.5 and ternary AlMg3Cu. The latter alloy was chosen in order to determine the influence of copper on precipitation kinetics. The most important goals were to determine energies and temperatures of precipitation.

Experimental

The investigated AlMg7.5 and AlMg3Cu alloys were made out of pure electrolytic aluminium (99.98 %), pure magnesium and pure copper. Alloys were melted in graphite crucible and cast into three measuring cells (Table 1) of triple simple thermal analysis (TETA)[1] with a purpose to obtain three different supersaturated solid solutions.
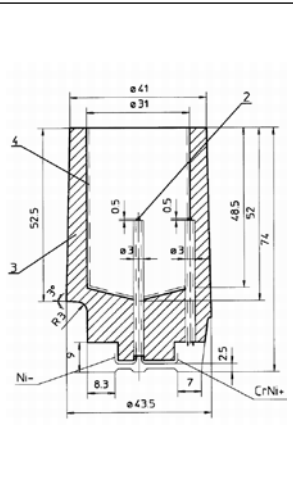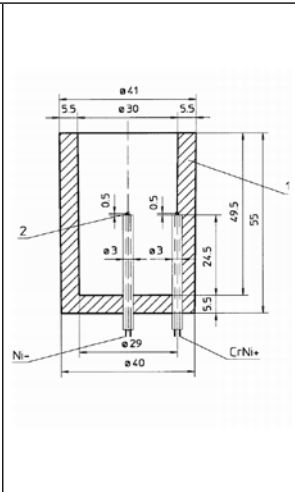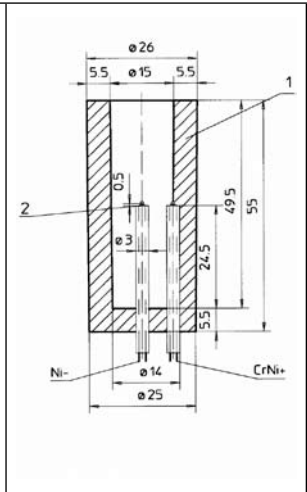
These alloys were also casted on the device for rapid solidification (Melt Spinner). The process is schematically presented in Figure 1. During melt spinning the liquid metal is cast upon a fast rotating copper wheel. A stable melt puddle appears when the wheel's velocity attains the critical point (up to 35 m/s). The thickness, width and length of ribbons depend on the wheel's velocity, substrate material, melt superheat, injection pressure, nozzle diameter and the distance between the nozzle and the wheel. Consequently, the ribbons with a thickness range of 10 μm to a few mm, and with width range of 1 to 12 mm at solidification rate from 10^2 to 10^6 K/s are produced[1].

After TETA the specimens were chemically analysed. In order to determine the intensity and the energy of precipitation from various supersaturated solutions the differential scanning calorimetry (DSC) of simultaneous thermal analysis (STA) Jupiter 449c of NETZSCH enterprise was used.

With a purpose to determine phase formed during solidification in investigated alloys the Scanning Electron Microscopy (SEM) with EDS analyser (Sirion 400 NC equipped with INCA 350) was used.

Table 1. Measuring cells of triple simple thermal analysis
Tabela 1. Merilne celice trojne enostavne termične analize

Figure			
Material	Cronning sand	Gray cast iron	Gray cast iron
Designation	MC1	MC2	MC3

Figure 1. Scheme of a free jet melt spinner[7]
Slika 1. Shematski prikaz naprave Melt Spinner[7]

Table 2. Chemical composition of the investigated alloys
Tabela 2. Kemijska sestava preiskovanih zlitin

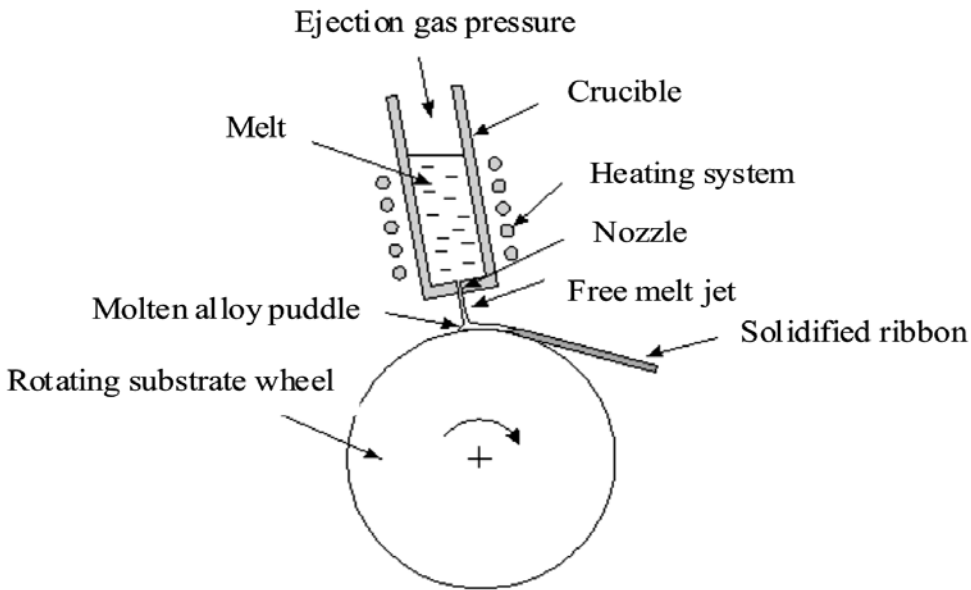| Alloy	Element/mass.%							
	Cu	Zn	Mg	Mn	Si	Ti	Fe	Al
AlMg7.5	0.00061	0.0114	7.572	0.0035	0.0534	0.00012	0.1417	rest
AlMg3Cu	0.8451	0.0107	3.253	0.0030	0.0547	0.00002	0.1932	rest

Table 3. The course of equilibrium solidification calculated using Thermo-Calc program
Tabela 3. Potek ravnotežnega strjevanja, izračunanega s programom Thermo-Calc

AlMg7.5		AlMg3Cu	
Temp. /°C	Reaction	Temp. /°C	Reaction
620	$L \rightarrow \alpha_{Al}$	640	$L \rightarrow \alpha_{Al}$
606	$L \rightarrow \alpha_{Al} + Al_{13}Fe_4$	622	$L \rightarrow \alpha_{Al} + Al_{13}Fe_4$
546	$L \rightarrow \alpha_{Al} + Mg_2Si$	550	$\alpha_{Al} \rightarrow Mg_2Si$
314	$\alpha_{Al} \rightarrow Al_3Mg$	396	$\alpha_{Al} \rightarrow Al_xMg_yCu_z$
230	$\alpha_{Al} \rightarrow Al_{15}Mg_{10}Cu$	293	$\alpha_{Al} \rightarrow Al_{15}Mg_{10}Cu$
156	$\alpha_{Al} \rightarrow Al_6Mn$	253	$\alpha_{Al} + Al_xMg_yCu_z \rightarrow Al_{15}Mg_{10}Cu$
50	$\alpha_{Al} \rightarrow Al_5Ti$	111	$\alpha_{Al} \rightarrow Al_6Mn$
		9	$\alpha_{Al} \rightarrow Al_5Ti$

RESULTS AND DISCUSSION

The chemical composition of the investigated alloys is presented in Table 2.

In Table 3 the course of equilibrium solidification of the alloys was calculated using the computer application Thermo-Calc. Equilibrium phase diagrams are shown in Figure 2. From Table 3 and Figure 2 the temperature of primary solidification, eutectic solidification and precipitation at equilibrium conditions can be determined. The sequence of solidification can be influenced by concentration of alloying elements (i. e. chemical composition).

From the cooling curves in Figure 3 the temperature of primary solidification, solidification of eutectic and the temperature of precipitation in the investigated alloys are evident. With the increasing cooling rate the peaks in differential cooling curve decreases. The alloy is now supersaturated with magnesium in case of AlMg7.5 alloy and magnesium and copper in case of AlMg3Cu alloy. The characteristic temperatures are also changing in dependence of the type and concentration of alloying elements.

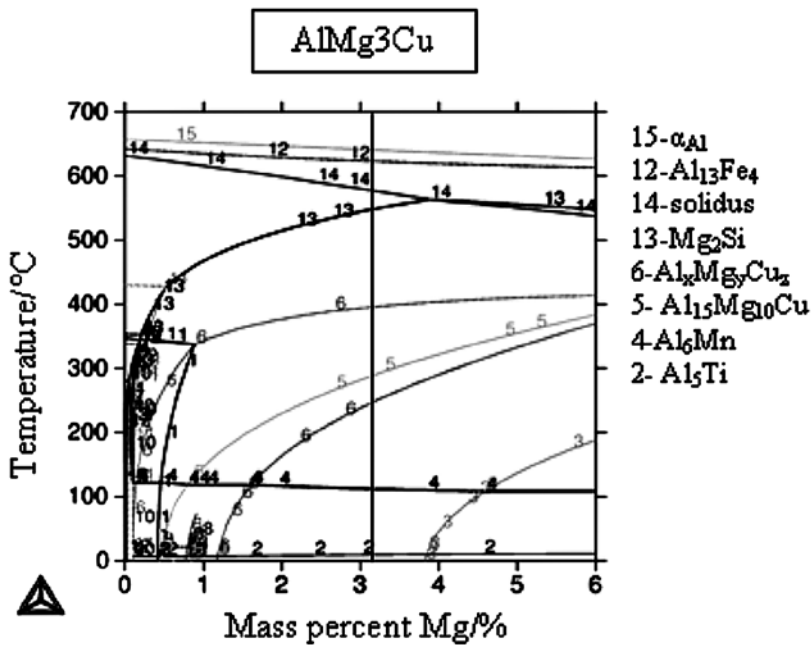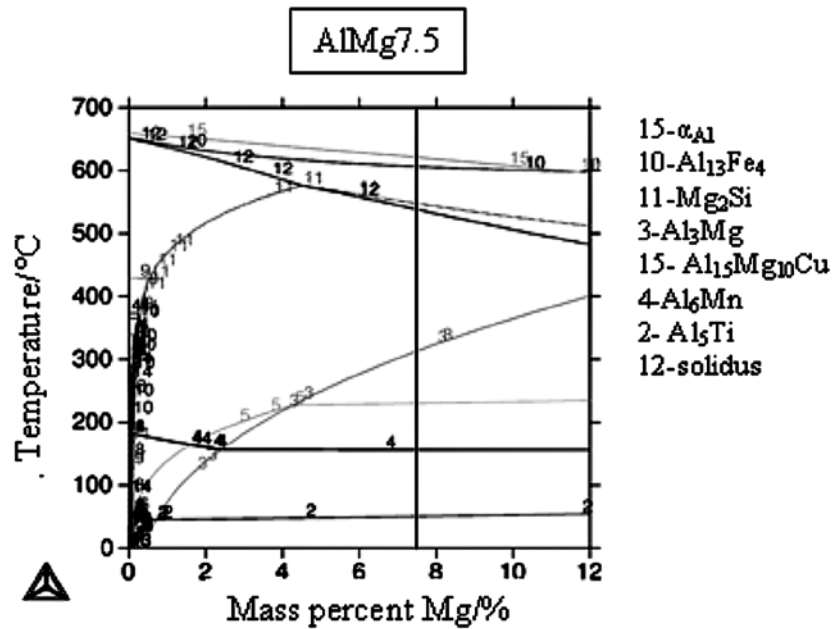The solidification of AlMg7.5 and AlMg3Cu alloys is presented in Figure

Figure 2. Isopleth equilibrium phase diagram of AlMg7.5 and AlMg3Cu alloy
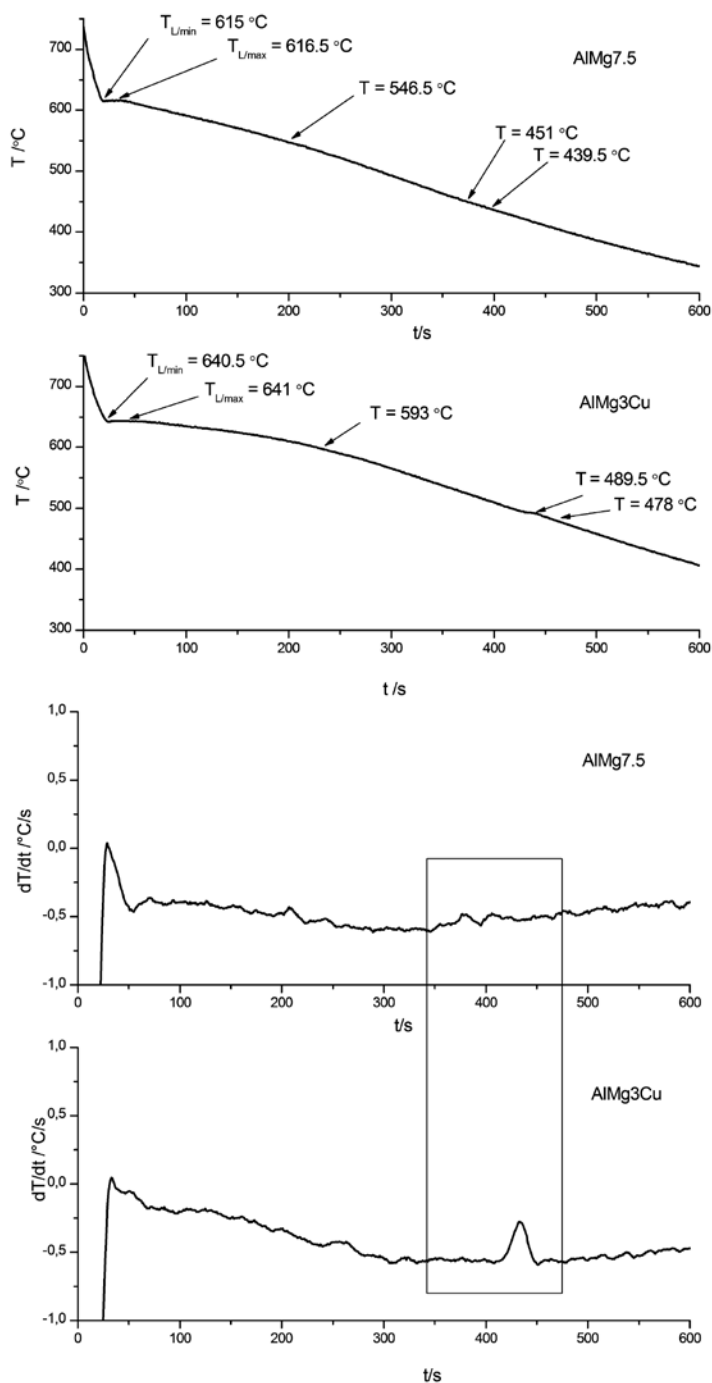**Slika 2.** Izopletni ravnotežni fazni diagrami zlitin AlMg7,5 ter AlMg3Cu

Figure 3. Cooling curves and differential cooling curves of investigated alloys
Slika 3. Ohlajevalne in diferencirane ohlajevalne krivulje preiskovanih zlitin

Table 4. The energy and temperature of solidification and melting of specific phases in investigated alloys

Tabela 4. Energije in temperature strjevanja in taljenja posameznih faz pri preiskovanih zlitinah

Temp. /°C	Reaction	Energy (x0.9513 J/g)	Temp. /°C	Reaction	Energy (x0.9513 J/g)
	AlMg7.5 – MC1				
	DSC - heating			DSC - cooling	
576.1	$L \to \alpha_{Al}$		609.4	$L \to \alpha_{Al}$	
529.7	$L \to \alpha_{Al} + Al_{13}Fe_4$	-135.47	550.5	$L \to \alpha_{Al} + Al_{13}Fe_4$	161.15
447.1	$L \to \alpha_{Al} + Mg_2Si$	-1.27	521.5	$L \to \alpha_{Al} + Mg_2Si$	
308.6	$\alpha_{Al} \to AlMg$	0.07			
	AlMg7.5 – MC2				
606.5	$L \to \alpha_{Al}$		612.4	$L \to \alpha_{Al}$	
532.2	$L \to \alpha_{Al} + Al_{13}Fe_4$	-262.56	566.7	$L \to \alpha_{Al} + Al_{13}Fe_4$	275.40
447.2	$L \to \alpha_{Al} + Mg_2Si$	-0.23	551.1	$L \to \alpha_{Al} + Mg_2Si$	
279.5	$\alpha_{Al} \to AlMg$	0.47			
	AlMg7.5 – MC3				
574.0	$L \to \alpha_{Al}$		609	$L \to \alpha_{Al}$	
532.7	$L \to \alpha_{Al} + Al_{13}Fe_4$	-287.96	545	$L \to \alpha_{Al} + Al_{13}Fe_4$	280.44
336.1	$\alpha_{Al} \to AlMg$	-6.63	520	$L \to \alpha_{Al} + Mg_2Si$	
	AlMg7.5 – rapid solidification				
556.1	$L \to \alpha_{Al}$		618.7	$L \to \alpha_{Al}$	
536.1	$L \to \alpha_{Al} + Al_{13}Fe_4$	-221.94	565.4	$L \to \alpha_{Al} + Al_{13}Fe_4$	220.04
310.0	$\alpha_{Al} \to AlMg$	-0.89	540.3	$L \to \alpha_{Al} + Mg_2Si$	
	AlMg3Cu – MC1				
	DSC - heating			DSC - cooling	
575.5	$L \to \alpha_{Al}$	-205.10	633.7	$L \to \alpha_{Al}$	
508.2	$L \to \alpha_{Al} + Mg_2Si$	-3.521	580.3	$L \to \alpha_{Al} + Al_{13}Fe_4$	211.66
293.4	$\alpha_{Al} \to Al_xMg_yCu_z$	1.708	489.8	$L \to \alpha_{Al} + Mg_2Si$	1.59
	AlMg3Cu – MC2				
577.5	$L \to \alpha_{Al}$	-207.38	633.0	$L \to \alpha_{Al}$	
511.3	$L \to \alpha_{Al} + Mg_2Si$	-2.04	576.7	$L \to \alpha_{Al} + Al_{13}Fe_4$	211.09
254.5	$\alpha_{Al} \to Al_xMg_yCu_z$	2.19	477.7	$L \to \alpha_{Al} + Mg_2Si$	2.71
	AlMg3Cu – MC3				
576.3	$L \to \alpha_{Al}$	-303.75	636.0	$L \to \alpha_{Al}$	
510.0	$L \to \alpha_{Al} + Mg_2Si$	-1.88	583.0	$L \to \alpha_{Al} + Al_{13}Fe_4$	303.56
251.4	$\alpha_{Al} \to Al_xMg_yCu_z$	1.38	484.0	$L \to \alpha_{Al} + Mg_2Si$	2.34
	AlMg3Cu – rapid solidification				
574.4	$L \to \alpha_{Al}$	-260.09	635.9	$L \to \alpha_{Al}$	
246.5	$\alpha_{Al} \to Al_xMg_yCu_z$	4.28	592.6	$L \to \alpha_{Al} + Al_{13}Fe_4$	256.37
			476.6	$L \to \alpha_{Al} + Mg_2Si$	0.44

* 0.9513 is a correction factor of STA machine for aluminium alloys at current conditions.

3. The primary solidification at the alloy AlMg7.5 occurred at 615 °C or 616.5 °C. The undercooling was 5 °C and the recalescence 1.5 °C. The eutectic (α_{Al} + $Al_{13}Fe_4$) solidified at 546.5 °C, eutectic (α_{Al} + Mg_2Si) solidified at 451 °C. These characteristic temperatures are somewhat lower than theoretical ones, because of the unequilibrium solidification of the alloy.

AlMg3Cu alloy started to solidify at 640.5 °C or 641 °C (Figure 3). The solidification of eutectic (α_{Al} + $Al_{13}Fe_4$) started at temperature 593 °C. Eutectic (α_{Al} + Mg_2Si) solidified at 489.5 °C. As mentioned above, these temperatures result differ from the theoretical ones because of the unequilibrium solidification.

At higher cooling rates the characteristic temperatures of primary and eutectic solidification move to lower temperatures.

From DSC curves on Figure 4 and 5 and from Table 4 the energy of formation and melting of specific phases are determined. The temperature where the solidification of specific phase starts (in cooling DSC curve) and temperature where the solidification of specific phase ends (in heating DSC curve) are also determined. Only heating DSC curves of investigated alloys are presented.

In AlMg7.5 alloy some changes between the heating DSC curves can be seen. These are the consequences of different cooling rates (Figure 4). It is obvious that the precipitation in specimens is intensified with higher supersaturation of Mg in solid solution; i.e. in specimens cooled with higher cooling rates. During reheating magnesium is precipitated from α_{Al} in a form of Al_xMg_y precipitates. In Figure 5 the precipitation kinetics can be even clearly seen. Namely, there is a stronger tendency for energy relaxation on heating DSC curves in samples previously cooled with higher rates and a fact that the solid solution in Al-Mg-Cu alloy is more supersaturated solid solutions. At higher magnification it can be clearly seen, that the precipitation temperature decreases with the increasing supersaturation. The energy of precipitation also increases with the increasing supersaturation of the alloy. Here the precipitation of $Al_xMg_yCu_z$ precipitates took place within the primary crystals of α_{Al}. In addition, if the portion of the energy for the precipitation is calculated it can be evident, that the fraction of the precipitation energy is increasing with the increasing supersaturation, so the portion of the precipitates in the microstructure increases. The portion of precipitation energy in AlMg7.5 alloy increases from 0.05 % in specimen that was cooled in MC1 to 0.18 % in specimen that was cooled in MC2 and to 0.3 % at specimen that was rapidly solidified. In the AlMg3Cu alloy the precipitation energy increases from 0.8 % in specimen that was cooled in MC1 to 1.0 % in specimen that was cooled in MC2 and to 1.6 % in specimen that was rapidly solidified. As already mentioned the copper in the alloy accelerates and accentuates precipitation hardening. That is evident from the fraction of precipitation energy in heating DSC curves of AlMg7.5 and AlMg3Cu alloys. The portion of precipitation is higher in AlMg3Cu alloy at each level of the supersaturation. The portion of precipitation energy was calculated as a portion from the total solidification energy (precipitation energy divided with the total

Figure 4. Heating DSC curves of specimens made of AlMg7.5 alloy: previously cooled in MC1, previously cooled in MC2 and previously cooled with Melt Spinner

Slika 4. Segrevalne DSC krivulje vzorca iz zlitine AlMg7,5: predhodno ohlajene v MC1, predhodno ohlajene v MC2 in predhodno ohlajene na napravi Melt Spinner

solidification energy). Furthermore, when the specimen was cooled very quickly the melting of eutectics (α_{Al} + $Al_{13}Fe_4$) and (α_{Al} + Mg_2Si), and primary phase takes place in one step. On the other hand, when the cooling of the specimen was slow, the melting of eutectics (α_{Al} + $Al_{13}Fe_4$) and (α_{Al} + Mg_2Si), and primary phase takes place in two steps.

Using the scanning electron microscope and energy dispersive spectroscopy the microstructure constituents in all investigated alloys were analysed. In Figure 6 the microstructure of AlMg7.5 alloy with the EDS analysis are presented. In the microstructure primary crystals of α_{Al} and the eutectic (α_{Al} + $Al_{13}Fe_4$) are visible. When the specimen was ached in a diluted solution of HF acid for approximately 10 minutes also Al_3Mg_2 precipitates become visible.

In the specimen AlMg3Cu in Figure 7 the primary crystals of α_{Al} and the eutectic (α_{Al} + $Al_{13}Fe_4$) were determined. In the structure the phase on the basis of aluminium with some magnesium and copper were also determined, which did not correspond to stoichiometry that was described in literature[5].
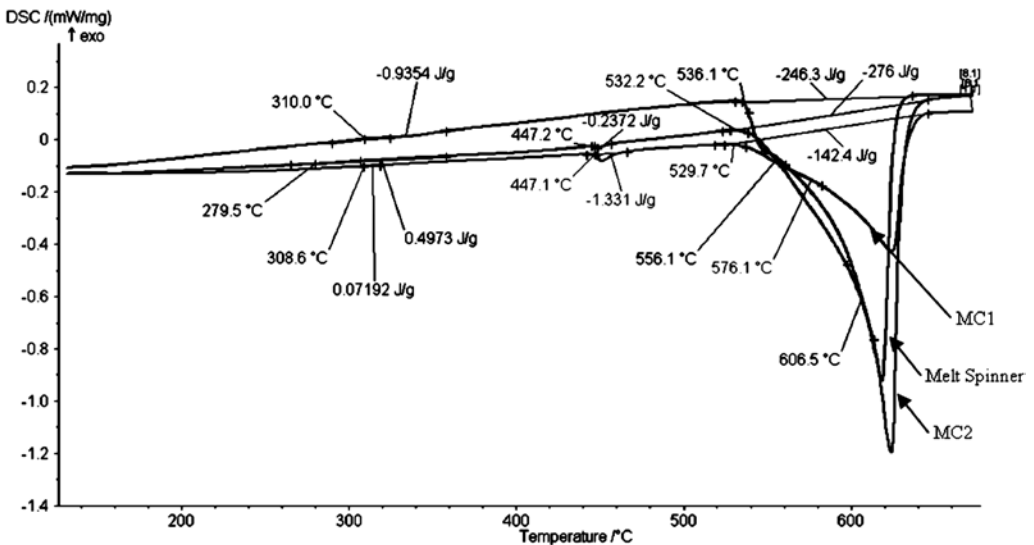
a)
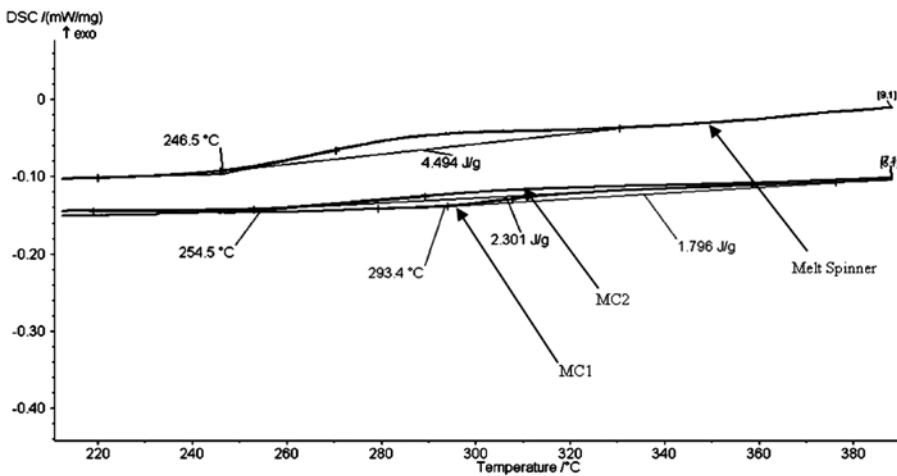
b)

Figure 5. Heating DSC curves of specimens made of AlMg3Cu alloy: previously cooled in MC1, previously cooled in MC2 and previously cooled with Melt Spinner: whole heating curve (a) and heating curve at the precipitation (b)
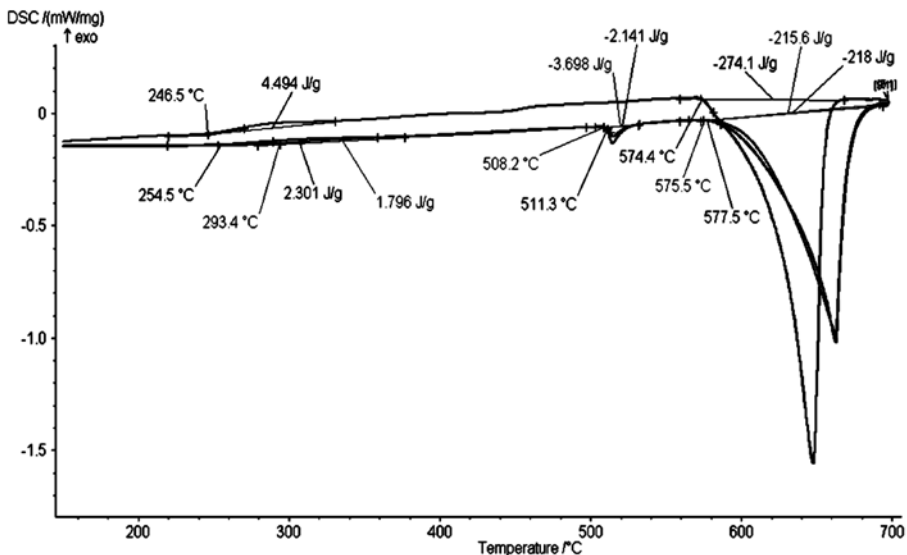**Slika 5.** Segrevalne DSC krivulje vzorca iz zlitine AlMg3Cu: predhodno ohlajene v MC1, predhodno ohlajene v MC2 in predhodno ohlajene na napravi Melt Spinner: celotna segrevalna krivulja (a) ter segrevalna krivulja pri izločanju (b)
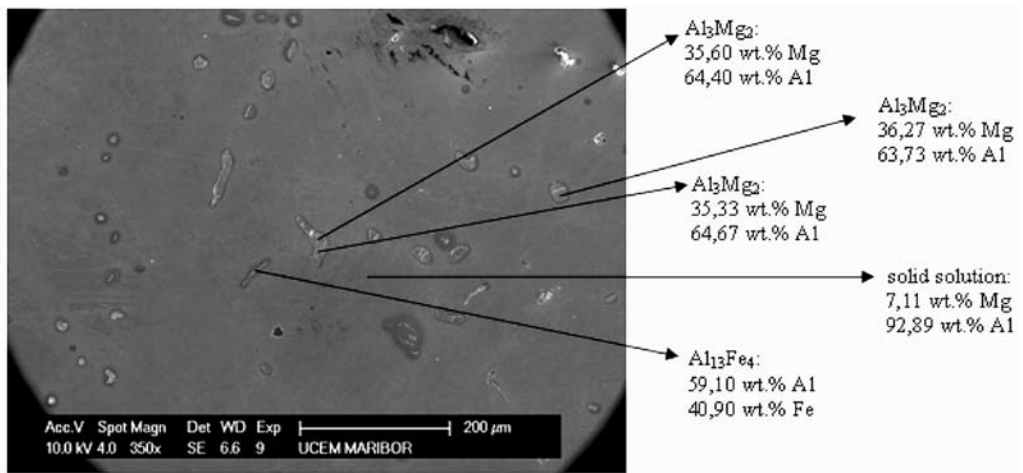
Figure 6. Secondary elektron image of AlMg7.5 alloy (SEM)
Slika 6. SEM mikroposnetek zlitine AlMg7,5 (SEM)
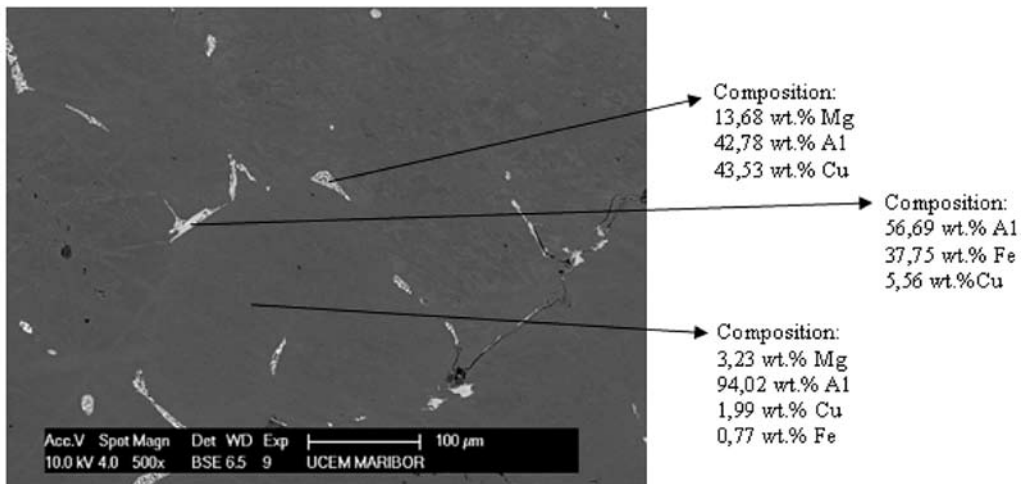
Figure 7. Secondary elektron image of AlMg3Cu alloy (SEM)
Slika 7. SEM mikroposnetek zlitine AlMg3Cu (SEM)

CONCLUSIONS

From the above presented results a few conclusions can be made:

- Using the DSC method the kinetics of precipitation from supersaturated solid solution in our case in AlMg7.5 and AlMg3Cu can be followed very precisely.
- The precipitation kinetics is related to increasing tendency for energy relaxation on heating DSC curve, and is enhanced with strongly supersaturated solid solutions.
- The temperature of precipitation decreases with the increasing supersaturation. The energy of precipitation also increases with the increasing supersaturation of solid solution. If the portion of the precipitation energy is calculated, it can be evident that, in the AlMg7.5 alloy, it increases with the increasing supersaturation from 0.05 % in specimen that was cooled in MC1 to 0.18 % in specimen that was cooled in MC2 and to 0.3 % at specimen that was rapidly solidified. In the AlMg3Cu alloy the precipitation energy increases from 0.8 % in specimen that was cooled in MC1 to 1.0 % in specimen that was cooled in MC2 and to 1.6 % in specimen that was rapidly solidified.
- When comparing the behaviour of both alloys, it becomes evident that copper in the alloy enhances the precipitation. The portion of precipitation was higher in AlMg3Cu alloy in each level of supersaturation. Consequently, more precipitates in the microstructure of the AlMg3Cu alloy can be expected.
- Microstructure constituents have been analysed. In specimens, primary crystals of α_{Al} and eutectic (α_{Al} +$Al_{13}Fe_4$) have been observed. In case of AlMg7.5 alloy the Al_3Mg_2 precipitates were found. In case of AlMg3Cu alloy the precipitates on base of aluminium with some magnesium and copper were determined, which stoichiometry did not correspond to that described in literature[5].

POVZETEK

Kinetika izločanja v zlitinah Al-Mg in Al-Mg-Cu

Aluminijeve zlitine običajno vsebujejo veliko zlitinskih elementov, zato imajo v mikrostrukturi več faz. Večina toplotno utrjevalnih aluminijevih zlitin vsebujejo kombinacijo magnezija z enim ali več elementi, kot so baker, silicij in cink. Že majhna koncentracija magnezija v povezavi s temi elementi pospeši in poudari izločevalno utrjevanje. Strukturne spremembe, ki so posledica izločanja atomov iz trdne raztopine, so izrednega tehnološkega in industrijskega pomena.

Večino aluminijevih zlitin utrjujemo večstopenjsko. Dodajanje večjega števila zlitinskih elementov je nujno samo za funkcijske namene ter za določene toplotne obdelave ter tako omogočajo različne kombinacije lastnosti: fizikalne, mehanske, elektromehanske, ki so potrebne za različne aplikacije[1].

Zlitine Al-Mg ter Al-Mg-Cu se utrjujejo z izločanjem nanodelcev iz prenasičene trdne raztopine. V tem delu smo za doseganje različnih stopenj prenasičenja trdne raztopine izvedli trojno enostavno termič-

no analizo (TETA), pri čemer so bile dose-
žene tri različne ohlajevalne hitrosti. S hi-
trim strjevanjem (Melt Spinner) pa je bila
dosežena najbolj prenasičena trdna razto-
pina. Za zasledovanje zaporedja izločanja
utrjevalnih izločkov je bila uporabljena
simultana termična analiza (STA) in sicer
diferenčna vrstična kalorimetrija (DSC), s
katero so bile določene energije izločanja
ter temperature izločanja izločkov iz raz-
ličnih prenasičenih trdnih raztopin. S po-
močjo elektronske mikroskopije (SEM) so
bili določeni tipi nastalih izločkov.

Na osnovi rezultatov preiskav smo prišli
do naslednjih zaključkov. S pomočjo DSC
metode lahko dokaj podrobno zasleduje-
mo kinetiko izločanja iz prenasičene trdne
raztopine, v našem primeru pri zlitinah
AlMg7,5 ter AlMg3Cu. Kinetika izločanja
je razvidna iz tendence večanja količine
sproščene energije na segrevalnih DSC kri-
vuljah pri povečevanju ohlajevalne hitrosti
zlitin in vse bolj prenasičeni trdni raztopi-
ni. Poleg tega temperatura pričetka izloča-
nja izločkov pada ob povečanju prenasiče-
nja trdne raztopine. Če izračunamo delež
izločevalne energije opazimo, da se ta pri
obeh preiskovanih zlitinah povečuje s pre-
nasičenjem trdne raztopine. Pri primerjavi
obeh zlitin med seboj lahko zaključimo, da
baker v zlitini izločanje izrazito poveča.
Z elektronsko mikroskopijo smo v zlitini
AlMg7,5 našli izločke Al_3Mg_2, v zlitini Al-
Mg3Cu pa izločke na osnovi aluminija z
nekaj magnezija in bakra, katerih stehio-
metrija pa ni ustrezala stehiometriji podani
v literaturi[5].

References

[1] ASM handbook (1991): *Volume 4, Heat Treating*. ASM International, The Materials Information Company.

[2] Romhanji, E., Popovic, M., Glisic, D., Dodok, R., Jovanovic, D. (2006): Effect of annealing temperature on the formability of Al-Mg4.5-Cu0.5 alloy sheets. *Journal of Materials Processing Technology*.; Vol. 177, pp. 386-389.

[3] Wang, S.C., Starink, M.J. (2007): Two types of S phases precipitates in Al-Cu-Mg alloys. *Acta Materialia*.; Vol. 55, pp. 933-941.

[4] Wang, M.J., Starink, N., Gao, N. (2006): Precipitation hardening in Al-Cu-Mg alloys revisited. *Scripta Materialia*.; Vol. 54, pp. 287-291.

[5] Kovarik, L., Miller, M.K., Court, S.A., Mills, M.J. (2006): Origin of the modified orientation relationship for S(S'')-phase in Al-Mg-Cu alloys. *Acta Materialia*.; Vol. 54, pp. 1731-1740.

[6] Medved, J., Mrvar, P. (2006): Thermal Analysis of Mg-Al Alloy. *Materials Science Forum*.; Vol. 508, pp. 603-608.

[7] Lojen, G., Anžel, I., Kneissl, A., Križman, A., Unterweger, E., Kosec, B., Bizjak, M. (2005): Microstructure of rapidly solidified Cu-Al-Ni shape memory alloy ribbons. *Journal of Materials Processing Technology*.; Vol. 162-163, pp. 220-229.

Review of materials in medical applications

Pregled materialov v medicinskih aplikacijah

David Bombač[1], Miha Brojan[2], Peter Fajfar[1], Franc Kosel[2], Rado Turk[1]

[1]University of Ljubljana, Faculty of Natural Sciences and Engineering, Aškerčeva cesta 12, SI-1000 Ljubljana, Slovenia; E-mail: david.bombac@ntf.uni-lj.si, peter.fajfar@ntf.uni-lj.si, rado.turk@ntf.uni-lj.si
[2]University of Ljubljana, Faculty of Mechanical Engineering, Aškerčeva cesta 6, SI-1000 Ljubljana, Slovenia; E-mail: miha.brojan@fs.uni-lj.si, franc.kosel@fs.uni-lj.si

Abstract: Medical implants are products that have to satisfy functionality demands defined by the human body as working environment. Ideally, they should have biomechanical properties comparable to those of autogenous tissues without any adverse effects and are regulated in order to ensure safety and effectiveness. The choice of material used for designing a medical implant is governed by biocompatibility, bioadhesion, biofunctionality, corrosion resistance, etc. In these review metallic biomaterials are divided into four subgroups: stainless steels, the cobalt alloys, titanium alloys, and other metals. Some attention is also given to shape memory, polymeric, and ceramic biomaterials for their innovative use in practical medical applications.

Izvleček: Medicinski vsadki so izdelki, ki morajo zadovoljiti stroge funkcijske zahteve, ki jih narekuje človeško telo kot delovno okolje. V idealnem primeru naj bi imeli biomehanske lastnosti primerljive avtogenim tkivom brez škodljivih efektov in so evidentirani, da zagotavljajo varnost in uspešnost. Izbira materiala pri načrtovanju medicinskih vsadkov je pogojena z biokompatibilnostjo, bioadhezijo, biofunkcionalnostjo, korozijsko odpornostjo, itd. V tem pregledu so kovinski biomateriali razdeljeni v štiri podskupine: nerjavna jekla, kobaltove zlitine, titanove zlitine in druge kovine. Nekaj pozornosti je posvečene tudi zlitinam s spominom, polimernim in keramičnim biomaterialom zaradi njihove inovativne uporabe v praktičnih medicinskih aplikacijah.

Key words: medical implants, biomaterials, AISI 316L, titanium alloys, shape memory alloys, polymeric biomaterials, ceramic biomaterials
Ključne besede: medicinski vsadki, biomateriali, AISI 316L, titanove litine, materiali z oblikovnim spominom, polimerni biomateriali, keramični biomateriali

---

Review paper

INTRODUCTION

The development of medical implants utilizing new materials continues to attract considerable academic and commercial interest. The development of new biomaterials involves a complicated mix of materials science and cell biology. Collaboration of various experienced specialists such as material scientists, metallurgists, traumatologists, orthopedists, chemists, mechanical engineers, pharmacists and others in order to achieve better results in research, development and implementation of the extracted knowledge into the practice is of essential importance.

Biomaterials are nonviable materials used in a medical devices intended to interact with biological systems[1] and cover several classes of materials, such as metallic, ceramic, and polymeric materials. Medical implants are products that have to satisfy functionality demands defined by the human body as working environment. Ideally, they should have biomechanical properties comparable to those of autogenous tissues without any adverse effects and are regulated in order to ensure safety and effectiveness. The choice of material used for designing a medical implant is governed by biocompatibility, bioadhesion, biofunc-

tionality, corrosion resistance, etc. To better understand implant material-biological organism interaction most of the studies are directed into the releases of particles from the material and offer screens for genotoxicity, carcinogenicity, cytotoxicity, irritation, sensitivity and sterilization agent residues[2]. Focus of this contribution is on metallic, shape memory, polymeric and ceramic biomaterials used in modern medical applications.

METALLIC BIOMATERIALS

Metallic biomaterials are often used to support and/or replace components of the skeleton. They are used e.g. as artificial joints, bone plates, screws, intramedullary nails, spinal fixations, spinal spacers, external fixators, pace maker cases, artificial heart valves, wires, stents, and dental implants. They possess greater tensile strength, fatigue strength, and fracture toughness when compared to polymeric and ceramic materials. Most widely used metallic biomaterials for implants devices are 316L stainless steels, cobalt alloys, commercially pure titanium, and Ti-6Al-4V alloys[3-6]. Originally, these materials were developed for industrial purposes. Their excellent mechanical properties and relatively high

Table 1. Mechanical characteristics of metal alloys used in medicine*
Tabela 1. Mehanske lastnosti kovinskih zlitin uporabljenih v medicini*

Characteristics	Stainless steel	Cobalt alloys	Titanium alloys
Stiffness	High	Medium	Low
Strength	Medium	Medium	High
Corrosion Resistance	Low	Medium	High
Biocompatibility	Low	Medium	High

* the scale is relative

corrosion resistance, which results in very small release of harmful toxins when exposed to bodily fluids, are the main reasons for these materials can be left inside the body for a longer period of time and are therefore appropriate for medical uses. In Table 1 some mechanical and biological characteristics of stainless steel, cobalt and titanium alloys are presented.

As additional information let us mention that production of metallic-based medical devices in general involves cutting operations (turning, milling, drilling, etc.); forming operations (pressing, hydroforming, forging, etc.) and other alternative machining operations (laser and waterjet cutting, different layer-by-layer sintering techniques such as direct metal laser sintering, selective laser melting, selective laser sintering, electron beam melting, and laser engineered net shaping).

In these review metallic biomaterials will be divided into four subgroups: stainless steels, the cobalt alloys, titanium alloys, and other metals.

Stainless steels

Stainless steel used for medical implants is mainly austenitic type 316L due to its resistance to corrosion, together with a wide range of other physical and mechanical properties coupled with inert, easily-to-clean surfaces. The chemical composition of type 316L stainless steel was developed to obtain stable austenitic structure which has numerous advantages, namely:

- Austenitic stainless steel has a face-centered cubic structure and is characterized by very low yield strength-to-tensile strength ratio and high form-

ability.
- To increase strength, cold working and successive strain aging treatment can be applied.
- Austenitic stainless steel is superior to ferritic stainless steel in corrosion resistance because the crystallographic atomic density of the former is higher than that of the latter.
- Austenitic stainless steel is essentially nonmagnetic.

The disadvantages of austenitic stainless steels generally are higher sensitivity toward pitting corrosion and stress corrosion cracking[3]. Pitting corrosion causes deep pits on the metal surface. It is initiated when an oxidant such as dissolved oxygen reacts with chloride ions. Pitting is further accelerated by the existence of an oxygen concentration cell at the early growth stage. The chemical composition of type 316L (ASTM F138, F139) austenitic stainless steel where "L" denotes low carbon content is as follows: ≤ 0.030 % C, ≤ 1.0 % Si, ≤ 2.0 % Mn, ≤ 0.045 % P, ≤ 0.030 % S, 12.0-15.0 % Ni, 16.0-18.0 % Cr, and 2.0-3.0 % Mn [1]. Its corrosion resistance is improved by adding molybdenum, increasing nickel and reducing carbon to less than 0.030 %. This steel has less than 0.03 wt.% carbon in order to reduce the possibility of in vivo corrosion. If the carbon content of the steel significantly exceeds 0.03 %, there is increased danger of formation of carbides such as $Cr_{23}C_6$. These tend to precipitate at grain boundaries when the carbon concentration and thermal history have been favorable to the kinetics of carbide growth. In turn, this carbide precipitation depletes the adjacent grain boundary regions of chromium, which has the effect of dimin-

ishing formation of the protective chromium-based oxide Cr_2O_3[7]. The presence of molybdenum as an alloying element in stainless steel reduces both the number and the size of nucleations and metastable pits. This is because bonds in the oxide film are strengthened and active sites caused by the formation of molybdates or of molybdenum oxyhyroxides are eliminated[8].

Due to high content of chromium, 316L stainless steel forms a protective, adherent and coherent oxide film that envelops the entire outer surface. This oxide film, often called passive layer, is intentionally formed when device is manufactured as chromium in the surface layer reacts with oxygen creating Cr_2O_3. The passive film serve as a barrier to corrosion processes in alloy systems that would otherwise experience very high corrosion rates[9] and has ability of self-healing, when damaged, as chromium in the steel reacts with oxygen and moisture in the environment to reform the protective oxide layer[10].

Cobalt alloys

Cobalt alloys may be generally described as nonmagnetic, corrosion and heat resistant where exhibit high strength even at elevated temperature and are also resistant to wear[11]. Many of its properties originate from the crystallographic nature of cobalt, and formation of extremely hard carbides and the corrosion resistance imparted by chromium. Cobalt alloys are difficult to fabricate which is why their use has been limited, but continuous work led to the development of specialized casting methods[12] and recently to selective laser sintering. Due to cobalt alloy excellent resistance to degradation in the oral environment, the first medical use was in the cast of dental implants. Various in-vitro and in-vivo tests have shown that the alloys are biocompatible and suitable for use as surgical implants. Today the use of Co alloys for surgical applications is mainly related to orthopaedic prostheses for the knee, shoulder and hip as well as to fracture fixation devices. Joint endoprostheses are typical long-term implants, and the applied implant material must therefore meet extremely high requirements with regard to biocompatibility with the surrounding body tissue material and corrosion resistance to bodily fluids[13].

Nowdays the CoCrMo cast and wrought versions of alloy are highly biocompatible materials[14,15] and are widely used as orthopedic implant materials in clinical practice such as hip joint and knee replacement. The biocompatibility of CoCrMo alloy is closely related to its excellent corrosion resistance due to the presence of an extremely thin passive oxide film that spontaneously forms on the alloy surface. Similar to AISI 316L stainless steel predominant oxide film is Cr_2O_3 with some minor contribution from Co and Mo oxides[16,17].

In spite of the alloys excellent corrosion resistance, there is still some concern about metal ion release from orthopedic implants into the human body environment. Implant components fabricated from Co-Cr based alloys have been reported to produce elevated Co, Cr and Ni concentrations in the surrounding tissue[18,19].

Other Co alloys used in medicine are MP35N or CoNiCrMo (ASTM F 562) with a nickel content of 35 % used for car-

diovascular pacing leads, stylets, catheters and orthopaedic cables. Increased content of nickel exhibits an improved resistance to stress-corrosion cracking in aqueous solution, but also increase the possibility of nickel allergy reactions. Therefore these alloys are not ideal for orthopaedic applications. The biocompatibility of the wear particles produced can be troublesome because of the increased surface area of these small particles which are in direct contact with the surrounding medium or tissue material. In work-hardened or work-hardened and aged conditions, this alloy has very high tensile properties which are among the strongest available for implant applications. Other Co-based alloy is L-605 cobalt alloy or CoCrWNi (ASTM F 90) which is used for heart valves and in an annealed condition (ASTM F 1091) for surgical fixation wires. Its mechanical properties are approximately the same as those of CoCrMo alloys, but after the material is cold worked the mechanical properties more than double.

Titanium and its alloys

Titanium and its alloy grades started gaining widespread usage as implant materials in the early 1970s. Material specifications and forms of them are detailed in a number of specifications, including ASTM and BS7252/ISO 5832 standards. The majority of Ti-based implants are made of commercially pure titanium (CP-Ti), mainly in Europe, and titanium alloy grade 5 Ti-6Al-4V (ASTM F 1472), mainly in North America. Although CP-Ti offer better corrosion resistance and tissue tolerance than stainless steel, its comparatively lower strength and unfavorable wear properties restricted its usage to certain applications such as pace-

maker cases, heart valve cages and reconstruction devices. Selection of titanium alloys for implementation is determined by a level and combination of the most desirable characteristics including immunity to corrosion, biocompatibility, shear strength, density and capability of ossteointegration[20]. The cold worked CP-Ti has been used for dental implant and maxillofacial applications. Interest in the Ti-6A1-4V alloy for total joint prostheses grew significantly in the United States toward the late 1970s because of its high strength, low elastic modulus, excellent corrosion resistance, and good tissue tolerance. Currently, its applications include hip and knee prostheses, trauma fixation devices (nails, plates, screws, and wires), instruments, and dental implants. Due to its relatively poor wear resistance, it was soon realized that the Ti-6A1-4V alloy was not suitable for bearing surface applications as are hip heads and femoral knees, without a coating or surface treatment[21]. Application from titanium alloys for bone trauma fixation applications as spinal fusion devices, pins, bone-plates, screws and intramedullary nails are shown in Figure 1.

Number of medical devices being made from titanium alloys which are generally preferred comparing to stainless steel and Co-alloys and is increasing, because of their lower modulus of elasticity (it is closer to that of bone), superior biocompatibility and corrosion resistance[22,23]. Recently, new titanium alloy compositions, specifically tailored for biomedical applications, have been developed. These first generation of orthopaedic alloys included Ti-6Al-7Nb[24] and Ti-5Al-2.5Fe [25,26], two alloys with properties similar to Ti-6Al-4V that were developed in response to concerns

Figure 1. Examples of implants made of metallic biomaterials
Slika 1. Primeri implantatov narejenih iz kovinskih biomaterialov

relating V to potential cytotoxicity[27,28] and adverse reaction with body tissues[29]. Further, biocompatibility enhancement and lower modulus has been achieved through the introduction of second generation titanium orthopaedic alloys including Ti-12-Mo-6Zr-2Fe [30,31], Ti-15Mo-5Zr-3Al [32], Ti-15Zr-4Nb-2Ta-0.2Pd and Ti-15Sn-4Nb-2Ta-0.2Pd alloys[33] as well as the almost completely biocompatible Ti-13Nb-13Zr alloy[34,35]. Titanium and its alloys have the inherent property to osseointegrate, enabling use in implants that can remain in place for longer period of time. Since titanium is non-magnetic, patients with titanium implants can be safely examined with magnetic resonance imaging which is convenient for long-term implants. Preparing titanium for implantation in the body involves subjecting it to a high-temperature plasma arc which removes the surface atoms, exposing fresh titanium that is instantly oxidized, whereas may be anodized to produce various colors[36]. Titanium is also used for the surgical instruments used in image-guided surgery.

To stimulate ossteointegration, limit resorption and thus increase the implant lifetime, some designs (cementless prostheses) use roughened bioactive coated surfaces. Hydroxyapatite (HA) coatings are used as bioactive surface of titanium implants, of which many surface treatment techniques have been developed[37]. Those techniques are plasma spraying, electrophoretic deposition of HA and micro-arc oxidation. Another form of implant coating is diamond-like carbon (DLC) coatings. DLC coatings can address the main biomechanical problems with the implants currently used, e.g. friction, corrosion and biocompatibility[38]. Metallic surfaces in contact with bodily fluids corrode as their surface dissolves and the dissolved metals enter the blood stream. The frequency of skin sensitivity to metals in patients with artificial joints is substantially higher than that in the general population[39]. At present, the risk to patients to develop such skin reaction after implantation of artificial joints may be considered minimal, cf. Table 2.

Table 2. Sensitivity to metal
Tabela 2. Občutljivost na kovine

	Percent Metal Sensitive
General population	10 %
Patients with stable total joints	25 %
Patients with loose total joints	60 %

Other metals

Conventional metal materials with use of numerous surface coatings and porous designs have been developed to enhance biological fixation of medical implants to bone for use in orthopedic procedures[40]. Other metals used for medical purposes include tantalum, gold, dental amalgams and other special metals. Although excellent clinical results of classical metal materials have been shown, they have several inherent limitations i.e. low volumetric porosity, relatively high modulus of elasticity and low frictional characteristics. To address the limitations of these solid metals, a new porous tantalum biomaterial has been developed. Porous tantalum is an open-cell tantalum structure of repeating dodecahedrons with an appearance similar to cancellous bone comercially known as trabecular metal. Tantalum is a transition metal that remains relatively inert in in-vivo. In the past multiple medical devices have been fabricated that utilize this material, including: pacemaker electrodes, foil and mesh for nerve repair, radiopaque markers, and cranioplasty plates[41,42]. Tantalum-based implants have displayed an exceptional biocompatibility and safety record in orthopedic, cranio-facial, and dentistry literature[43]. The basic structure of this po-rous tantalum metal yields a high volumetric porosity, a low modulus of elasticity, and relatively high frictional characteristics. Porous tantalum implants are fabricated from the pyrolysis of a thermosetting polymer foam which in turn creates a low-density vitreous carbon skeleton with 98 % porosity and a repeating dodecahedron array of regular pores. Commercially pure tantalum is then deposited onto this interconnected vitreous carbon scaffold using chemical vapor deposition [40,44,45].
Figure 2 [46], demonstrates the distinct microtexture and overall geometry of this nanostructured porous metal construct and some examples of medical implants.

Oxidized zirconium is a metal with a ceramic surface that was introduced commercially for knee arthroplasty components[47,48]. Commercial medical alloy under trade name Oxinium consists of a zirconium and niobium alloy (Zr-2.5Nb) that has been oxidized to transform the surface into zirconia ceramic. The ceramic is not a coating but a transition of metal to ceramic approximately 4-5 μm thick that is produced by reaction to oxygen during a thermal treatment. The ceramic surface is a monoclinic zirconia ceramic[49,50].

Because the bulk of the material is metal, it does not have the same risk of fracture as a monolithic ceramic head. Thus, the oxidized zirconium implant offers the potential to decrease wear and thereby increase the life span of implants. First oxidized zirconium implants were introduced in 1996 as simple implants. For total knee replacements it has not been used until 2001, and was later used also for hip replacements since 2003.

Figure 2. Microstructure of the porous nanostuctured tantalum material and examples of medical devices
Slika 2. Mikrostuktura nanostrukturiranega poroznega tantala in primeri medicinskih izdelkov

In Figure 3 [51], knee and hip replacemt component from oxidized zirconium are shown.

Shape memory materials

Shape memory alloys (SMA) have been given a lot of attention mainly for their innovative use in practical applications using shape memory effect (SME). The SME is unique property that some alloys possess according to which, after being deformed at one temperature, they re- cover their original shape by increasing to the alloys second temperature. This effect arises from reversible and usually rate-independent martensitic transformation and resulting changes of crystal structure of the solid phases of the material. The low temperature phase is called martensite phase and the high temperature austenite phase. Large residual strains of even more than 10 % can be recovered in this way and the process is often referred to as free recovery. The return to the original shape starts at a temperature called austenite start transformation temperature A_s, and com-

pletes at the austenite finish transformation temperature A_F. Pseudoelasticity or superelastic effect and shape memory effect are two separate mechanical effects which characterize the response of SMA. At constant high temperature, above temperature A_F, a mechanical loading-unloading cycle induces highly-nonlinear large deformations. At the end of the loading-unloading cycle no permanent deformations are present. The cycle usually presents a hysteresis loop, Figure 4a.

In the early 1960s, researchers at the U.S. Naval Ordnance Laboratory discovered the shape memory effect in an equiatomic alloy of nickel and titanium. Discovered alloy was patented and named Nitinol (Nickel-Titanium Naval Ordnance Laboratory). This discovery is considered a breaktrought in the field of shape memory materials and since that time, intensive investigations have been made to elucidate the mechanics of its basic behavior. The use of NiTi as a biomaterial is fascinating because of its superelasticity and shape

memory effect, which are completely new properties compared to the conventional metal alloys. Composition and metallurgical treatments have dramatic impacts on the described transition temperatures. From the applications point of view, NiTi can have three different forms: martensite, stress induced martensite (superelastic), and austenite. In martensite form alloy is soft and ductile and can be easily deformed. Superelastic NiTi is highly elastic, whereas austenitic NiTi is quite strong and hard. The NiTi alloy can exhibit all these properties depending on the temperature in which it is used.

In vast majority of medical applications is utilized superelastic effect. Result of slightly nickel richer alloys is superelasticity which could be exhibited in a narrow temperature range of the human body. The Simon Inferior Vena Cava filter was the first SMA cardiovascular device. It is used for blood vessel interruption for preventing pulmonary embolism[52]. The Simon filter is filtering clots that travel inside blood-
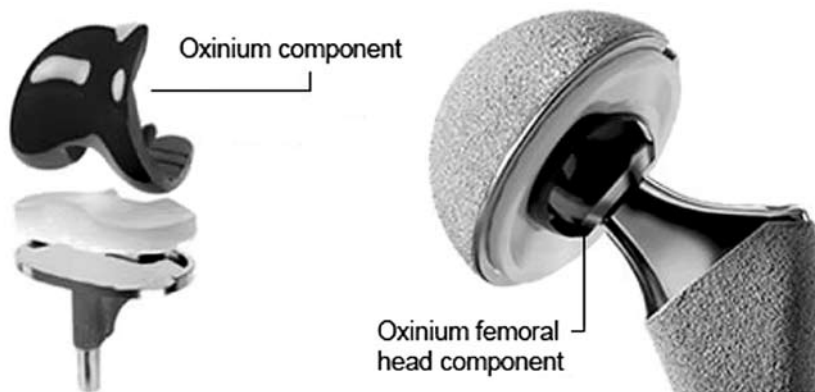

Figure 3. Microstructure of the porous nanostuctured tantalum material and examples of medical devices
Slika 3. Mikrostuktura nanostrukturiranega poroznega tantala in primeri medicinskih izdelkov

Figure 4. The stress-strain diagram, SE stents, Nitinol clamps, orthodontic wire
Slika 4. Diagram napetost-raztezek, SE stent, Nitinol spona, ortodontska žica

stream. The device is made of SMA wire curved similary to an umbrella which traps the clots which are better dissolved in time by the bloodstream. For insertion, the device is exploiting the shape memory effect, i.e. the original form in martensitic state is deformed and mounted into a catheter. When the device is released, body heat causes the filter to return to its original shape.

Stents are most rapidly growing cardiovascular products which are used to maintain the inner diameter of a blood vessel. The product has been developed in response to limitations of balloon angioplasty, which resulted in repeated blockages of the vessel in the same area. NiTi alloys have become the material of choice for superelastic self-expanding (SE) stents[53], Figure 4b.

The self-expanding nitinol stents are produced in open state and later compressed and inserted into the catheter. The basic open form is obtained mainly by SMA tubing, the final shape is then obtained by alternative machining operations such as laser cutting. Stents can also be produced from wire and laser welded or coiled

striped etched sheet. During the operation procedure, when the catheter is in correct position in the vessel, the self-expanding stent is pushed out and then it expands against the vessel wall due to a rise in temperature.

Superelastic SMA wires have found wide use as orthodontic wires as well, Figure 4c. Nitinol wires have large elastic deformation combined with a low plateau stress. This results a smaller number of visits to the orthodontist due to the larger elastic stroke and more comfort due to lower stress levels. In dental medicine, special plates for fixing a loose tooth have become available, Figure 4c. They are produced with laser cutting from sheet metal.

Orthopedic implants far exceed any other by weight or volume. They are used as fracture fixation devices, which may or may not be removed and as joint replacement devices. As shown in Figure 4a, bone and nitinol have similar stress-strain characteristics, which make nitinol a perfect material for production of bone fixation plates, nails and other trauma implants[54]. In the past, acceptability of nitinol as material for

permanent bone implants was conditioned by releasing Ni3^{+} ions from NiTi and integrity of contact between the bone and the implant. To solve these two vital problems, coating the bioactive layer on the device surface has been introduced[55].

Medical equipment is also a branch where nitinol has found its place. Because modern surgery is aiming less invasive operations, smaller diameters of tubing are very important. Reducing the diameters of medical devices was possible compared to polymer materials due to superelasticity when tubing of NiTi alloys became available.

Polymeric biomaterials

Polymeric biomaterials are used as a substitute for metal alloys in trauma and orthopedic implant devices or as an aid at surgical procedures. First polymeric material, used in medicine since the 1960s, was ultra-high molecular weight polyethylene (UHMWPE). It is a thermoplastic with extremely long chains and molecular weight numbering between 2 and 6 million. The longer chain serves to transfer load more effectively to the polymer backbone by strengthening intermolecular interactions. Results of this are a very tough material, with the highest impact strength of any thermoplastic presently made. UHMWPE is highly resistant to corrosive chemicals, with exception of oxidizing acids and has extremely low moisture absorption, very low coefficient of friction, characteristic of self lubrication and high resistance to abrasion. The mechanical and tribological properties of UHMWPE favor its use as a bearing material in many joint replacement devices. UHMWPE is used in buttons to resurface the patella in total knee arthroplasty, in sleeves to permit semi-constrained rotation in elbow and wrist arthroplasty designs, and in counterfaces inserted into the glenoid in shoulder arthroplasty. However, for the purposes of this review we will focus on the most common uses of UHMWPE in medical devices, those of tibial bearings in knee arthroplasties and of acetabular bearings in hip arthroplasties[56]. UHMWPE was first used clinically in 1962 and emerged as the dominant bearing material for total hip and knee replacements in the 1970s. Since the 1980s UHMWPE is successfully used for spine implants[57]. Thus, even though UHMWPE components are typically in no imminent danger of wearing through during a patient's lifetime, the generation of particulate debris from the articulating surface has been associated with osteolysis and loosening of implants[58-61]. To address these problems a highly crosslinked UHMWPE materials were clinically introduced in 1998 and has rapidly become the standard of care for total hip replacements[62-68]. Another important medical advancement for UHMWPE in the past decade has been the increase in use of fibers for sutures, where maximum strength and minimum weight are required. It is ideal for orthopedic implants, for example, as it allows smaller implants to be used, and is flexible and resistant to abrasion. Similarly, its strength can be used for surgical instruments for minimally invasive procedures[69].

Polymethyl methacrylate (PMMA) is the synthetic polymer of methyl methacrylate and is in field of medical technologies and implants used because of its good de-

gree of compatibility with human tissue. In orthopaedics, PMMA bone cement is used to affix implants and to remodel lost bone. It is supplied as a powder with liquid methyl methacrylate (MMA). When mixed these yield dough like cement that gradually hardens. Surgeons can judge the curing of the PMMA bone cement by pressing their thumb on it. Although PMMA is biologically compatible, MMA is considered to be an irritant and a possible carcinogen and therefore PMMA has also been linked to cardiopulmonary events in the operating room due to hypotension[70-75]. Bone cement acts like a grout and not so much like a glue in arthroplasty. Although sticky, it does not bond to either the bone or the implant, it primarily fills the spaces between the prosthesis and the bone preventing motion. A big disadvantage to this bone cement is that it heats to quite a high temperature while setting and because of this it kills the bone in the surrounding area. It has a Young modulus between the one of cancellous bone and the one of cortical bone, thus it is a load sharing entity in the body not causing bone resorption[76]. Dentures are often made of PMMA, and can be color matched to the patient's teeth and gum tissue. In cosmetic surgery, tiny PMMA microspheres suspended in some biological fluid are injected under the skin to reduce wrinkles or scars permanently. PMMA also is used for replacement intraocular lenses in the eye when the original lens is removed in the treatment of cataracts. Hard contact lenses are frequently made of this material. Soft contact lenses are often made of a related polymer, where acrylate monomers containing one or more hydroxyl groups make them hydrophilic[77-80].

Another polymeric material used as biomaterials for trauma, orthopedic, and spinal implants is polyetheretherketones (PEEK). It is thermoplastic polymer obtained from aromatic dihalides and bisphenolate salts by nucleophilic substitution. The bisphenolate salt is formed in situ from bisphenol and either added sodium or added alkali metal carbonate or hydroxide and have extraordinary mechanical properties. PEEK is partially crystalline and has unusual property in exhibiting two glass transition temperatures, at approximately 140 °C and 275 °C, depending on cure cycle and precise formulation. It is also highly resistant to thermal degradation[81]. By the late 1990s, PEEK had emerged as the leading high-performance thermoplastic candidate for replacing metal implant components, especially in orthopedics[82,83] and trauma[84,85]. Numerous studies documenting the successful clinical performance of PEEK polymers in orthopedic and spine patients continue to emerge in the literature[86-91]. Recent research has also investigated the biotribology of PEEK composites as bearing materials and flexible implants used for joint arthroplasty[92-95]. Due to interest in further improving implant fixation, PEEK biomaterials research has also focused on compatibility of the polymer with bioactive materials, including hydroxyapatite (HA), either as a composite filler, or as a surface coating[96-100]. As a result of ongoing biomaterials research, PEEK and related composites can be engineered today with a wide range of physical, mechanical, and surface properties, depending upon their implant application. Mechanical properties of PEEK implants can be tailored by preparing carbon-fiber-reinforced (CFR)

Table 3. Typical average physical properties of UHMWPE, PMMA and PEEK
Tabela 3. Značilne povprečne mehanske lastnosti UHMWPE, PMMA in PEEK

	UHMWPE	PMMA	PEEK	CRF-PEEK
Polymer type	Semi-crystalline	Amorphous	Semi-crystalline	Semi-crystalline
Degree of crystallinity [%]	39 – 75	Noncrystalline	30 – 35	30 – 35
Molecular weight [10^6 g/mol]	2 – 6	0.1 -0.8	0.08 – 0.12	0.08 – 0.12
Poisson ratio	0.46	0.35	0.36	0.38 – 0.40
Specific gravity	0.932 – 0.945	1.180 – 1.246	1.3	1.4 – 1.6
Flexural modulus [GPa]	0.8 – 1.6	1.5 – 4.1	4	20 – 135
Tensile strength [MPa]	39 – 48	24 – 49	93	170 – >2000
Tensile elongation [%]	350 – 525	1 – 2	30 – 40	1 – 2

composites with varying fiber length and orientation. Comparison of physical properties of UHMWPE, PMMA, PEEK and CFR-PEEK is presented in Table 3 [81].

Property of polymeric materials reviewed earlier (UHMWPE, PMMA and PEEK) is that they are not biadsorbable and biodegradable. Due to high cost of secondary operations, where implants are extracted scientists started research and development of medical devices which are made form bioabsorbable and biodegradable materials. These types of materials have ability to gradually decline in the strength of implant during the healing process where the area of fracture is filled with bone and connective tissue. The rate of dissolving can be engineered in order to be consistent with the rate of new bone growth and under ideal conditions, a bioabsorbable polymer could encourage bone healing while the body slowly metabolizes it[101]. The main advantage of biodegradable implants is elimination of need for a second surgery whereas the main disadvantage is a tendency to release harmful acids and other toxins during the dissolving process. The physical properties required for reliable bioabsorbable and biodegradable implants such as appropriate initial strength, initial modulus of elasticity, controlled strength, etc. could be engineered carefully[102]. In general bioabsorbable polymers used in medicine are thermoplastics, linear-chain, partially crystalline or totally amorfous with a definitive melting temperature and/or a glass transition region. The most used medical polymers are polyglycolide acid (PGA), polylactide acid (PLA) and poly(ε-caprolactone) (PCL). Polymers prepared from glycolic acid and lactic acid have found a multitude of uses in the medical industry, beginning with biodegradable sutures first approved in the 1960s [103]. Since that time other medical devices, based on lactic and glycolic acid, as well as other materials, including poly(dioxanone), poly(trimethylene carbonate) copolymers, and poly(ε-caprolactone) homopolymers and copolymers, have been accepted for use as medical devices[104].

In addition to these approved devices, a great deal of research continues on polyanhydrides[105] polyorthoesters[106] and other materials[107,108].

Fibers from PGA exhibit high strength and modulus and are too stiff to be used as sutures except as braided material. Sutures of PGA lose about 50 % of their strength after two weeks and 100 % at four weeks and are completely absorbed in 4-6 months[101]. PGA is immunological inert, but it leads to slight non-specific lymphocyte activation, as it induces inflammatory mononuclear cell migration[109].

Lactide is the cyclic dimer of lactic acid, which exists as two optical isomers, D and L. L-lactide, is the naturally occurring isomer, and DL-lactide is the synthetic blend of D-lactide and L-lactide. The homopolymer of -lactide (LPLA) is a semicrystalline polymer. PGA and LPLA exhibit high tensile strength and low elongation and consequently have a high modulus that makes them more applicable than the amorphous polymers for load-bearing applications such as in orthopedic fixation and sutures. Poly(DL-lactide) (DL-PLA) is an amorphous polymer having lower tensile strength and higher elongation and much more rapid degradation time making it more attractive as a drug delivery system. The degradation time of LPLA is much slower than that of DL-PLA requiring greater than 2 years to be completely absorbed[110]. Copolymers of ε-caprolactone with DL-lactide have been synthesized to yield materials with more rapid degradation rates[111]. A copolymer of ε-caprolactone with glycolide that has reduced stiffness compared to pure PGA is being sold as a monofilament suture.

Non-specific inflammatory reactions in living tissue associated with the degradation of the implant sometimes lead to a clinical complication, either to small fluid accumulation under the skin needing no treatment, or to painful fluid accumulation under the skin treated by aspiration with a needle[112]. Polymeric bio-implants are made by traditional melt-molding techniques such as blow molding and injection molding, extrusion, vacuum forming, fiber spinning and sintering technique. They could be produced in the final or semifinal form. The main requirements for polymer bioimplants are sterile production and sterile techniques. To gain better mechanical

Figure 5. Bone-fracture fixation polymer screws, rods and plates
Slika 5. Polimerni vijaki, žeblji in plošče za fiksacijo fraktur kosti

properties the self-reinforcing technique has been introduced[101]. Examples of polymeric material medical devices are sutures, small staple devices, drug delivery devices, small pins, bone-plates and screws, depicted in Figure 5.

Ceramic biomaterials

In order to avoid the problems associated with random dissolution which include uncontrolled physical degradation, particulate release and long-term durability, the materials need to remain essentially insoluble only to be removed by specific cell activity. Ceramic biomaterials have been developed that not only act as suitable substrates for bone mineralization by osteoblasts but are essentially insoluble in biological media and are resorbed when acted upon by osteoclasts[113]. Zirconium dioxide or zirconia ceramics (ZrO_2) is a bioinert non-resorbable metal oxide which has a good chemical and dimensional stability, and a high strength and toughness[114]. Currently, zirconia ceramic is being recognized for its high strength and surface finish, making this material potentially suitable for the highly loaded environments found in joint replacement. Biomedical grade zirconia was introduced approximately 20 years ago to solve the problem of alumina brittleness and the consequent potential failure of implants[115]. Zirconia ceramic has been used to manufacture femoral heads for total hip replacements since the late 1980s [115]. Its color and excellent biocompatibility and mechanical properties have made it attractive for dental applications[116-120]. A prerequisite for successful bone implant integration is direct bone apposition which

was observed at bone-zircona interfaces in histological[121-123] and ultrastructural[124] studies suggesting that ZrO_2 may also be a suitable implant material. On the one hand, biomedical grade zirconia exhibits the best mechanical properties of oxide ceramics: this is the consequence of phase transformation toughening, which increases its crack propagation resistance. The stress-induced phase transformation involves the transformation of metastable tetragonal grains to the monoclinic phase at the crack tip, which, accompanied by volume expansion, induces compressive stresses[125]. On the other hand, due to this meta-stability, zirconia is prone to ageing in the presence of water[126]. Up to date clinical reports appear to be again somewhat opposite where some results show excellent behavior of some femoral heads after several years in vivo[127] while others show poor follow up results[128] with severe wear and osteolysis around the implant. Few case studies report surface degradation of zirconia implants, which could be related to ageing[129,130].

Alumina ceramics (Al_2O_3) have been used for implants and prostheses for several decades now[131]. The material is characterised by its excellent biocompatibility[132] and high strength, hardness and fracture resistance[133,134]. The resultant high wear resistance is of particular interest for implant components with articulating surfaces like artifical joints. The outstanding wear resistance is the major reason for the predominant use of this material for the femoral joint head [135]. A common material pairing used for hip arthroplasty is a femoral joint head made of alumina and an acetabular liner made of UHMWPE. Inauspiciously alumina is not suitable for

implant components with bone contact, because the material is bioinert and thereby no bony ongrowth, and subsequently loosening of the implant occurs[136].

No difference between the biocompatibility of zirconia and that of alumina ceramics has been found in the biological reaction in vivo. Furthermore, the wear factor of UH-MWPE against zirconia ceramic is 40-60 % less than that against alumina ceramic counterfaces and 10-20 % less than that against SUS 316L metal counterfaces[137]. Hydroxyapatite ceramic (HAC) granules are used successfully world-wide as a bone substitute material because of their high biocompatibility. In an orthotopic site, such as a bony defect, bone formation occurs on ceramic surfaces. This newly formed bone bonds tightly to the ceramic surface without any mechanical interlock[138]. Bioactive glasses have been used in many medical applications. However, due to their poor mechanical properties, these glasses cannot be used in load-bearing applications, whereas metallic alloys are still the materials of choice. It was recognized early on that one of the main applications of bioactive glasses could be coatings for prosthetic metallic implants. These coatings serve two purposes: improving the osseointegration of the implants, and protecting the metal against corrosion from the body fluids and the tissue from the corrosion products of the alloys. Unfortunately, most of the attempts to coat metallic implants with bioactive glasses have had limited success due to poor adhesion of the coating and/or degradation of the glass properties during the coating procedure, typically enameling, or flame or plasma spray coating[139].

In recent years, transition metal nitrides like TiN, ZrN, TiAlN, NbN, TaN and VN were successfully used as protective coatings against wear and corrosion in order to increase the life expectancy of surgical implants and prosthesis[140-142].

CONCLUSIONS

As presented in the article, a variety of different materials and processing technologies are available for medical applications. Which material should be used depends on the type of injury. Medical implants used for temporary healing should be made of conventional metallic biomaterials. The question of the long-term effects of bio-metal, on patients is very important. Further studies relating to long-term effects of materials on biological tissues are necessary, and are likely to lead to an increased understanding of the biocompatibility of materials in the future. Medical implants used for permanent healing are made of titanium alloy due to its inertness and good material characteristics, or polymeric degradable materials due to their properties and possibility of using them together with medicaments and bone healing stimulants. SMA medical devices and implants have been successful because they offered a possibility of performing less invasive surgeries. Nitinol wires in medical instruments are more kink resistant and have smaller diameter compared to 316L or polymer devices. Research to develop a porous SMA which enables the transport of body fluids from outside to inside the bone is currently underway. It was also an intention to provide an overview of uses of polymers in medicine, the field, where is expected an increased number of

applications. To addresses the limitations of current surgical techniques a diverse and large number of roles exist for bone biomaterials that are capable of incorporation into the natural process of healing. We expect that in the future, surgeons will have available even more products that will accelerate patient recovery and eliminate secondary surgeries.

In the future research and developement of a new perspective that conflates in solid-state physics, biological science as well as materials engineering. The perspective is one that recognizes that future new advances in all these areas will be based on a fundamental understanding of the atomic and molecular infrastructure of materials that has resulted from te past achievemts of physics and chemistry. Major advances will be achieved when the novel behavior, in particular the quantum mechanical behavior, that nanoscale structures possess, can be controlled and harnessed. The next decade should see the emergence of new technologies based on nano-systems with not only improved but hopefully also fundamentally new physico-chemical properties produced at reasonable costs. Experimental and theoretical research should lead to industrial applications yielding important breakthroughs.

Povzetek

Pregled materialov v medicinskih aplikacijah

Medicinski vsadki so izdelki, ki morajo zadovoljiti stroge funkcijske zahteve, ki jih narekuje človeško telo kot delovno okolje.

V idealnem primeru naj bi imeli biomehanske lastnosti primerljive z avtogenim tkivom brez škodljivih efektov in so evidentirani tako, da zagotavljajo varnost in uspešnost. Izbira materiala pri načrtovanju medicinskih vsadkov je pogojena z biokompatibilnostjo, bioadhezijo, biofunkcionalnostjo, korozijsko odpornostjo, itd. V tem pregledu so kovinski biomateriali razdeljeni v štiri podskupine: nerjavna jekla, kobaltove zlitine, titanove zlitine in druge kovine. Nekaj pozornosti je posvečene tudi zlitinam s spominom, polimernim in keramičnim biomaterialom zaradi njihove inovativne uporabe v praktičnih medicinskih aplikacijah.

V delu so predstavljeni različni materiali in procesne tehnike, ki so mogoče za medicinske aplikacije. Izbira materiala je pogojena s tipom poškodbe. Medicinski vsadki, ki so začasno v telesu naj bi bili narejeni iz klasičnih kovinskih biomaterialov. Vprašanje kako na pacienta vpliva dolgoročni efekt stika tkivo-kovina je izjemnega pomena. Potrebne so nadaljne študije v zvezi z dolgoročnim vplivom materialov na biološka tkiva, ki bodo po vsej verjetnosti vodile povečanemu razumevanju biokompatibilnosti materialov v prihodnosti. Medicinski vsadki, namenjeni permanentni uporabi so običajno narejeni iz titanovih zlitin, zaradi njihove inertnosti in dobrih lastnosti, ali iz razgradljivih polimernih materialov zaradi posebnih lastnosti in možnosti hkratne uporabe z zdravili ali stimulanti rasti kosti. Medicinski pripomočki in vsadki narejeni iz materialov s spominom (SMA) so razširjeni in uspešni, ker ponujajo možnost izvršiti manj invazivnih kirurških posegov. Žice in medicinski instrumenti iz nitinola so bolj odporne proti vozljem in omogo-

čajo manjše premere v primerjavi z nerjavečim jeklom AISI 316L ali polimernimi pripomočki. Veliko raziskav in razvoja je narejenega tudi na poroznem SMA, ki omogoča prenos telesnih sokov proti kostem. Namen študije je bil tudi zagotovitev pregleda uporabe polimerov v medicini, ki je področje kjer pričakujemo povešanje števila aplikacij.

Za odpravo omejitev kururških tehnik obstaja veliko število različnih vlog biomaterialov, ki so se sposobni vključiti v naravni proces zdravljnja. V prihodnosi pričakujemo, da bodo imeli kirurgi še precej več produktov, ki bodo pospešili pacientovo okrevanje in izključili potrebe po sekundarnih operacijah.

References

[1] Ratner, B.D., Schoen, F., Hoffman, A., Lemons, J. (2004): *Biomaterials Science: An Introduction to Materials in Medicine*. Elsevier Science & Technology Books, ISBN: 978-0-125-82463-7.

[2] Balazic, M., Brojan, M., Bombac, D., Caram, R. Jr., Kosel, F., Kopac, J. (2007): Titanium and titanium alloy applications in medicine. *Surface Engineered Surgical Tools and Medical Devices*. Editors: Jackson, J. , Ahmed, W., Springer, ISBN: 978-0-387-27026-5.

[3] Sumita, M., Hanawab, T., Teoh, S.H. (2004): Development of nitrogen-containing nickel-free austenitic stainless steels for metallic biomaterials - review. *Materials Science and Engineering: C*.; Vol. 24, No. 6-8, pp. 753-760.

[4] *Annual Book of ASTM Standards*. Section 13 - Medical Devices and Services: Medical Devices, 1999.

[5] Williams, D.F. (1993): Volume 14: Medical and Dental Materials. *Materials Science and Technology: A Comprehensive Treatment*. Editors: Cahn, R.W., Haasen, P., Kramer, E.J., Wiley-VCH, ISBN: 978-3-527-26825-2.

[6] Breme, J., Biehl, V. (1998): Metallic biomaterials. *Handbook of Biomaterials Properties*. Editors: Black, J., Hastings, G., Springer, ISBN: 978-0-412-60330-3.

[7] Bombac, D., Brojan, M., Krkovic, M., Turk, R., Zalar, A. (2007): Characterization of titanium and stainless steel medical implants

surfaces. *RMZ - Materials and geoenvironment*.; Vol. 54, No. 2, pp. 151-164.

[8] ILEVBARE, G.O., BURSTEIN, G.T. (2001): The role of alloyed molybdenum in the inhibition of pitting corrosion in stainless steels. *Corrosion Science*.; Vol. 43, No. 3, pp. 485-513.

[9] LIU, C., BI, Q., MATTHEWS, A. (2003): Tribological and electrochemical performance of PVD TiN coatings on the femoral head of Ti-6Al-4V artificial hip joints. *Surface and Coatings Technology*.; Vol. 163-164, pp. 597-604.

[10] NEWSON, T. (2002): Stainless Steel – A Family of Medical Device Materials. *Business briefing: medical device manufacturing & technology*.

[11] DAVIDS, J.R. (1998): *Metals Handbook*. ASM International.

[12] SHETTY, R.H., OTTERSBERG, WI-I. (1995): Metals in Orthopedic Surgery. *Encyclopedic Handbook of Biomaterials and Bioengineering*. Editors: Wise, D., Trantolo, J.D., Altobelli, E.D., Yaszemski, J.M., Gresser, J.D., Schwartz, E.R., Marcel Dekker, ISBN: 978-0-824-79649-5.

[13] SURY, P., SEMLITSCH, M. (1978): Corrosion behavior of cast and forged cobalt-based alloys for double-alloy joint endoprostheses. *Journal of Biomedical Materials Research*.; Vol. 12, No. 5, pp. 723-741.

[14] KATTI, K.S. (2004): Biomaterials in total joint replacement. *Colloids and Surfaces B: Biointerfaces*.; Vol. 39, No. 3, pp. 132-142.

[15] LONG, M., RACK, H.J. (1998): Titanium alloys in total joint replacement - a materials science perspective. *Biomaterials*.; Vol. 19, No. 18, pp. 1621-1639.

[16] MILOSEV, I., STREHBLOW, H.-H. (2003): The composition of the surface passive film formed on CoCrMo alloy in simulated physiological solution. *Electrochimica Acta*.; Vol. 48, No. 19, pp. 2767-2774.

[17] KOCIJAN, A., MILOSEV, I., PIHLAR, B. (2004): Cobalt-based alloys for orthopaedic applications studied by electrochemical and XPS analysis. *Journal of Material Science: Materials in Medicine*.; Vol. 15, pp. 643-650.

[18] OKAZAKI, Y., GOTOH, E. (2005): Comparison of metal release from various metallic biomaterials in vitro. *Biomaterials*.; Vol. 26, No. 1, pp. 11-21.

[19] JACOBS, J.J., SKIPOR, A.K., PATTERSON, L.M., HALLAB, N.J., PAPROSKY, W.G., BLACK, J., GALANTE, J.O. (1998): A prospective, controlled, longitudinal study of metal release in patients undergoing primary total hip arthroplasty. *Journal of Bone and Joint Surgery*.; Vol. 80 A, No. 10, pp. 1444-1458.

[20] RACK, H.J., QAZI, J.I. (2006): Titanium alloys for biomedical applications. *Materials Science and Engineering: C*.; Vol. 26, No. 8, pp. 1269-1277.

[21] WANG, K. (1996): The use of titanium for medical applications in the USA. *Materials Science and Engineering: A*.; Vol. 213, No. 1-2, pp. 134-137.

[22] DOWSON, D. (1992): Friction and wear of medical implants and prosthetic devices. *ASM Handbook*.; Vol. 18, ASM International, Gereland, Materials Park, OH, pp. 656-664.

[23] PARK, J.B., LAKES, R.S. (1992): *Biomaterials - An introduction*. 2nd ed, Springer, ISBN: 978-0-306-43992-6.

[24] SEMLITSCH, M.F., WEBER, H., STREICHER, R.M., SCHOÖN, R. (1992): Joint replacement components made of hot-forged and surface-treated Ti-6Al-7Nb alloy. *Biomaterials*.; Vol. 13, No. 11, pp. 781-788.

[25] BOROWY, K-H., KRAMER, K-H. (1985): On the properties of a new titanium alloy (TiAl5Fe2.5) as implant material. *Titanium '84 Science and Technology*.; Vol. 2, Munich, Deutsche Gesellschaft Für Metallkunde EV, pp. 1381-1386.

[26] ZWICKER, R., BÜHLER, K., MÜLLER, R., BECK, H., SCHMID, H-J., FERSTL, J. (1980): *Titanium '80 Science and Technology*. Warrendale, PA, TMS-AIME, pp. 505-514.

[27] STEINEMANN, S.G. (1980): Corrosion of surgical implants-in vivo and in vitro tests. *Evaluation of Biomaterials*. Editors: Winter, G.D., Leray, J.L., de Groot, K., John Wiley, ISBN 978-0-471-27658-6.

[28] STEINEMANN, S.G. (1985): Corrosion of titanium and titanium alloys for surgical implants. *Titanium '84 Science and Technology*.; Vol. 2, Munich, Deutsche Gesellschaft Für Metallkunde EV, 1373-1379.

[29] LAING, P.G., FERGOSUN, A.B. JR., HODGE, E.S. (1967): Tissue reaction in rabbit muscle exposed to metallic implants. *Journal of Biomedical Materials Research*.; Vol. 1, No. 1, pp. 135-149.

[30] WANG, K., GUSTAVSON, L., DUMBLETON, J. (1993): The characterization of Ti-12Mo-6Zr-2Fe. A new biocompatible titanium alloy developed for surgical implants. *Beta Titanium in the 1990's*. The Minerals, Metals&Materials Society, pp. 49-60.

[31] WANG, K., GUSTAVSON, L., DUMBLETON, J. (1993): Low modulus, high strength, biocompatible titanium alloy for medical implants. *Titanium '92 Science and Technology*. The Minerals, Metals & Materials Society, 2697-2704.

[32] STEINEMANN, SG., MAÜSLI, P-A., SZMUKLER-MONCLER, S., SEMLITSCH, M., POHLER, O., HINTERMANN, H-E., PERREN, SM. (1993): Beta-titanium alloy for surgical implants. *Titanium '92 Science and Technology*. The Minerals, Metals & Materials Society, pp. 2689-2696.

[33] OKAZAKI, Y., ITO, Y., ITO, A., TATEISHI, T. (1993): Effect of alloying elements on mechanical properties of titanium alloys for medical implants. *Materials Transactions JIM*.; Vol. 34, No. 12, pp. 1217-1222.

[34] KOVACS, P., DAVIDSON, JA. (1993): The electrochemical behavior of a new titanium alloy with superior biocompatibility. *Titanium '92 Science and Technology*. The Minerals, Metals& Materials Society, pp. 2705-2712.

[35] MISHRA, A.K., DAVIDSON, J.A., KOVACS, P., POGGIE, R.A. (1993): Ti-

13Nb-13Zr: a new low modulus, high strength, corrosion resistant near-beta alloy for orthopaedic implants. *Beta Titanium in the 1990's*. The Minerals, Metals & Materials Society, pp. 61-72.

[36] EDWARDS, J. (1997): *Coating and Surface Treatment Systems for Metals*. Finishing Publications and ASM International, pp. 39-40, ISBN 0-904477-16-9.

[37] CHEN, J.Z., SHI, Y.L., WANG, L., YAN, F.Y., ZHANG, F.Q. (2006): Preparation and properties of hydroxyapatite-containing titania coating by micro-arc oxidation. *Materials Letters*.; Vol. 60, No. 20, pp. 2538-2543.

[38] DEARNALEY, G., ARPS, J. (2005): Biomedical applications of diamond-like carbon (DLC) coatings: a review. *Surface and Coatings Technology*.; pp. 2518-2524.

[39] HALLAB, N., MERRITT, K., JACOBS, J.J. (2001): Metal sensitivity in patients with orthopaedic implants. *Journal of Bone and Joint Surgery*.; Vol. 83 A, No. 3, pp. 428-433.

[40] BOBYN, J.D., STACKPOOL, G.J., HACKING, S.A., TANZER, M., KRYGIER, J.J. (1999): Characteristics of bone ingrowth and interface mechanics of a new porous tantalum biomaterial. *Journal of Bone and Joint Surgery*.; Vol. 81 B, No. 5, pp. 907-914.

[41] BLACK, J. (1994): Biological performance of tantalum. *Clinical Materials*.; Vol. 16, No. 3, pp. 167-173.

[42] LEVINE, B.R., SPORER, S., POGGIE, R.A., DELLA VALLE, C.J., JACOBS, J.J. (2006): Experimental and clinical performance of porous tantalum in orthopedic surgery. *Biomaterials*.; Vol. 27, No. 27, pp. 4671-4681.

[43] KATO, H., NAKAMURA, T., NISHIGUCHI, S., MATSUSUE, Y., KOBAYASHI, M., MIYAZAKI, T., KIM, H.-M., KOKUBO, T. (2000): Bonding of alkali- and heat-treated tantalum implants to bone. *Journal of Biomedical Materials Research*.; Vol. 53, No. 1, pp. 28-35.

[44] ZARDIACKAS, L.D., PARSELL, D.E., DILLON, L.D., MITCHELL, D.W., NUNNERY, L.A., POGGIE, R.A. (2001): Structure, metallurgy, and mechanical properties of a porous tantalum foam. *Journal of Biomedical Materials Research*.; Vol. 58, No. 2, pp. 180-187.

[45] HACKING, S.A., BOBYN, J.D., TOH, K., TANZER, M. and KRYGIER, J.J. (2000): Fibrous tissue ingrowth and attachment to porous tantalum. *Journal of Biomedical Materials Research*.; Vol. 52, No. 4, pp. 631-638.

[46] http://www.zimmer.com/z/ctl/op/global/action/1/id/33/template/MP/navid/312.

[47] RIES, M., SALEHI, A., WIDDING, K., HUNTER, G. (2002): Polyethylene wear performance of oxidized zirconium and cobalt-chromium knee components under abrasive conditions. *Journal of Bone and Joint Surgery*.; Vol. 84 A, No. 2, pp. 129-135.

[48] HUNTER, G., LONG, M. (2000): Abrasive wear of oxidized Zr-2.5Nb, CoCrMo, and Ti-6Al-4V against bone cement. *6th World Biomate-*

rials Congress Transactions. Society For Biomaterials, Minneapolis.

[49] Bᴇɴᴇᴢʀᴀ, V., Mᴀɴɢɪɴ, S., Tʀᴇꜱᴋᴀ, M., Sᴘᴇᴄᴛᴏʀ, M., Hᴜɴᴛᴇʀ, G., Hᴏʙʙꜱ, L.W. (1999): Microstructural investigation of the oxide scale on Zr-2.5Nb and its interface with the alloy substrate. *Biomedical Materials: Drug Delivery, Implants and Tissue Engineering*. Editors: Neenan, T., Marcolongo, M., Valentini, R.F., Materials Research Society Symposium Proceedings, Vol. 550, Materials Research Society, pp. 337-342, ISBN: 978-1-558-99456-0.

[50] Hᴜɴᴛᴇʀ, G. (2001): Adhesion testing of oxidized zirconium. *Transactions of the Society for Biomaterials*.; Vol. 24, pp. 540.

[51] http://www.oxinium.co.uk/patients/material.php

[52] Yᴀɴʟɪ, C., Cʜᴜɴʏᴏɴɢ, L., Sʜᴇɴɢʟɪ, Z., Zʜᴇɴᴅᴜᴏ, C., Xɪᴀɴᴊɪɴ, Y. (2006): Formation of bonelike apatite - collagen composite coating on the surface of NiTi shape memory alloy. *Scripta Materialia*.; Vol. 54, No. 1, pp. 89-92.

[53] Dᴜᴇʀɪɢ, T.W., Tᴏʟᴏᴍᴇᴏ, D.E., Wʜᴏʟᴇʏ, M. (2000): An overview of superelastic stent design. *Minimally Invasive Therapy & Allied Technologies*.; Vol. 9, No. 3-4, pp. 235-246.

[54] Mᴏʀɢᴀɴ, N.B. (2004): Medical shape memory alloy applications the market and its products. *Materials Science and Engineering A*.; Vol. 378, No. 1-2, pp. 16-23.

[55] Dᴜᴇʀɪɢ, T.W., Pᴇʟᴛᴏɴ, A., Sᴛᴏᴇᴄᴋᴇʟ, D. (1999): An overview of nitinol medical applications. *Materials Science and Engineering A*.; Vol. 273-275, pp. 149-160.

[56] Kᴜʀᴛᴢ, S.M., Mᴜʀᴀᴛᴏɢʟᴜ, O. K., Eᴠᴀɴꜱ, M., Eᴅɪᴅɪɴ, A. A. (1999): Advances in the processing, sterilization, and crosslinking of ultra-high molecular weight polyethylene for total joint arthroplasty. *Biomaterials*.; Vol. 20, No. 18, pp. 1659-1688.

[57] Kᴜʀᴛᴢ, S.M. (2004): *The UHMWPE Handbook: Ultra-High Molecular Weight Polyethylene in Total Joint Replacement*. Academic Press, New York, ISBN: 978-0-124-29851-4.

[58] Lᴇᴡɪꜱ, G. (1997): Polyethylene wear in total hip and knee arthroplasties. *Journal of Biomedical Materials Research*., Vol. 38, No. 1, pp. 55-75.

[59] Sᴄʜᴍᴀʟᴢʀɪᴇᴅ, T.P., Kᴡᴏɴɢ, L.M., Jᴀꜱᴛʏ, M., Sᴇᴅʟᴀᴄᴇᴋ, R.C., Hᴀɪʀᴇ, T.C., O'Cᴏɴɴᴏʀ, D.O., Bʀᴀɢᴅᴏɴ, C.R., Kᴀʙᴏ, J.M., Mᴀʟᴄᴏʟᴍ, A.J., Hᴀʀʀɪꜱ, W.H. (1992): The mechanism of loosening of cemented acetabular components in total hip arthroplasty. Analysis of specimens retrieved at autopsy. *Clinical Orthopaedics and related research*.; Issue 274, pp. 60-78.

[60] Xᴇɴᴏꜱ, J.S., Hᴏᴘᴋɪɴꜱᴏɴ, W.J., Cᴀʟʟᴀɢʜᴀɴ, J.J., Hᴇᴇᴋɪɴ, R.D., Sᴀᴠᴏʀʏ, C.G. (1995): Osteolysis around an uncemented cobalt chrome total hip arthroplasty: Polyethylene wear. *Clinical Orthopaedics and related research*.; Issue 317, pp. 29-36.

[61] LIVINGSTON, B.J., CHMELL, M.J., SPECTOR, M., POSS, R. (1997): Complications of total hip arthroplasty associated with the use of an acetabular component with a Hylamer liner. *Journal of Bone and Joint Surgery*.; Vol. 79 A, Issue 10, pp. 1529-1538.

[62] LI, S., BURSTEIN, A.H. (1994): Ultrahigh molecular weight polyethylene. The material and its use in total joint implants. *Journal of Bone and Joint Surgery*.; Vol. 76 A, No. 7, pp. 1080-1090.

[63] PREMNATH, V., HARRIS, W.H., JASTY, M., MERRILL, E.W. (1996): Gamma sterilization of UHMWPE articular implants: an analysis of the oxidation problem. *Biomaterials*.; Vol. 17, No. 18, pp. 1741-1753.

[64] SAUER, W.L., ANTHONY, M.E. (1998): Predicting the clinical wear performance of orthopaedic bearing surfaces. *Alternative bearing surfaces in total joint replacement*. Editors: Jacobs, J.J., Craig, T.L., American Society for Testing and Materials, West Conshohoken, ISBN: 978-0-803-12490-5.

[65] MCKELLOP, H.A. (1998): Wear assessment. *The adult hip*. Editors: Callaghan, J.J., Rosenberg, A.G., Rubash, H.E., Lippincott-Raven Publishers, Philadelphia, ISBN: 978-0-397-51704-6.

[66] EYERER, P., ELLWANGER, R., FEDEROLF, H.-A., KURTH, M., MADLER, H. (1990): Polyethylene. *Concise encyclopaedia of medical and dental materials*. Editors: Williams, D., Cahn, R., Pergamon, Oxford, ISBN: 978-0-080-36194-9.

[67] FISHER, J., DOWSON, D. (1991): Tribology of total artificial joints. *Proceedings of the Institution of Mechanical Engineers*, *Part H*.; Vol. 205, No. 2, pp. 73-79.

[68] KLEIN, P.G., GONZALEZ-OROZCO, J.A., WARD, I.M. (1991): Structure and morphology of highly oriented radiation crosslinked polyethylene fibres. *Polymer*.; Vol. 32, No. 10, pp. 1732-1736.

[69] http://www.dsm.com/en_US/html/ hpf/dyneema_purity.htm.

[70] ELLIS, R.H., MULLVEIN, J. (1974): The cardiovascular effects of methylmethacrylate. *Journal of Bone and Joint Surgery*.; Vol. 56 B, No. 1, pp. 59-61.

[71] GRESHAM, G.A., KUCZYŃSKI, A., ROSBOROUGH, D. (1971): Fatal fat embolism following replacement arthroplasty for transcervical fractures of femur. *British Medical Journal*.; Vol. 2 (5762), pp. 617-619.

[72] HOMSY, C.A., TULLOS, H.S., ANDERSON, M.S., DIFERRANTE, N.M., KING, J.W. (1972): Some physiological aspects of prosthesis stabilization with acrylic polymer. *Clinical Orthopaedics and related research*.; Issue 83, pp. 317-328.

[73] PHILLIPS, H., COLE, P.V., LETTIN, A.W.F. (1971): Cardiovascular effects of implanted acrylic bone cement. *British Medical Journal*.; Vol. 3(5772), pp. 460-461.

[74] ORSINI, E.C., BYRICK, R.J., MULLEN, J.B.M., KAY, J.C., WADDELL, J.P. (1987): Cardiopulmonary function and pulmonary microemboli during arthroplasty using cemented or

non-cemented components. *Journal of Bone and Joint Surgery*.; Vol. 69, No. 6, pp. 822-832.

[75] KAUFMANN, T.J., JENSEN, M.E., FORD, G., GILL, L.L., MARX, W.F., KALLMES, D.F. (2002): Cardiovascular Effects of Polymethylmethacrylate Use in Percutaneous Vertebroplasty. *American Journal of Neuroradiology*.; Vol. 23, No. 4, pp. 601-604.

[76] MILLER, M.D. 82004): *Review of Orthopaedics 4th Edition*. W.B. Saunders Company, ISBN: 978-0-721-60364-3, 129.

[77] OLSON, R.J., CRANDALL, A.S. (1998): Silicone vs polymethylmethacrylate intraocular lenses with regard to capsular opacification. *Ophthalmic Surgery and Lasers*.; Vol. 29, No. 1, pp. 55-58.

[78] OSHIKA, T., NAGAHARA, K., YAGUCHI, S. (1998): Three-year prospective, randomized evaluation of intraocular lens implantation through 3.2 mm and 5.5 mm incisions. *Journal of Cataract & Refractive Surgery*.; Vol. 24, No. 4, pp. 509-514.

[79] KRUGER, A.J., SCHAUERSBERGER, J., ABELA, C., SCHILD, G., AMON, M. (2000): Two-year results: sharp vs rounded optic edges on silicone lenses. *Journal of Cataract & Refractive Surgery*.; Vol. 26, No. 4, pp. 566-570.

[80] FINDL, O., BUEHL, W., MENAPACE, R., SACU, S., GEORGOPOULOS, M.,RAINER, G. (2005): Long-term Effect of Sharp Optic Edges of a Polymethyl Methacrylate Intraocular Lens on Posterior Capsule Opacification: A Randomized Trial. *Ophthalmology*.; Vol. 112, No. 11, pp. 2004-2008.

[81] KURTZ, S.M., DEVINE, J. N. (2007): PEEK biomaterials in trauma, orthopedic, and spinal implants. *Biomaterials*.; Vol. 28, No. 32, pp. 4845-4869.

[82] LIAO, K. (1994): Performance characterization and modeling of a composite hip prosthesis. *Experimental Techniques*.; Vol. 18, No. 5, pp. 33-38.

[83] MAHARAJ, G.R., JAMISON, R.D. (1993): Intraoperative impact: characterization and laboratory simulation on composite hip prostheses. *Composite Materials for Implant Applications in the Human Body: Characterization and Testing*. Editors: Jamison, R.D., Gilbertson, L.N., ASTM, Philadelphia, ISBN: 978-0-803-11852-2, 98-108.

[84] KELSEY, D.J., SPRINGER, G.S., GOODMAN, S.B. (1997): Composite implant for bone replacement. *Journal of Composite Materials*.; Vol. 31, No. 16, pp. 1593-1632.

[85] CORVELLI, A.A., BIERMANN, P.J., ROBERTS, J.C. (1997): Design, analysis, and fabrication of a composite segmental bone replacement implant. *Journal of Advanced Materials*.; Vol. 2, No. 1, pp. 2-8.

[86] TOTH, J.M., WANG, M., ESTES, B.T., SCIFERT, J.L., SEIM, III H.B., TURNER, A.S. (2006): Polyetheretherketone as a biomaterial for spinal applications. *Biomaterials*.; Vol. 27, No. 3, pp. 324-334.

[87] BRANTIGAN, J.W., NEIDRE, A., TOOHEY, J.S. (2004): The Lumbar I/F Cage for posterior lumbar interbody fu-

sion with the variable screw placement system: 10-year results of a Food and Drug Administration clinical trial. *The Spine Journal*.; Vol. 4, No. 6, pp. 681-688.

[88] BRANTIGAN, J.W., STEFFEE, A.D., LEWIS, M.L., QUINN, L.M., PERSENAIRE, J.M. (2000): Lumbar interbody fusion using the Brantigan I/F cage for posterior lumbar interbody fusion and the variable pedicle screw placement system: two-year results from a Food and Drug Administration investigational device exemption clinical trial. *Spine*.; Vol. 25, No. 11, pp. 1437-1446.

[89] AKHAVAN, S., MATTHIESEN, M.M., SCHULTE, L., PENOYAR, T., KRAAY, M.J., RIMNAC, C.M., GOLDBERG, V.M. (2006): Clinical and histologic results related to a low-modulus composite total hip replacement stem. *Journal of Bone and Joint Surgery*.; Vol. 88 A, No. 6, pp. 1308-1314.

[90] GLASSMAN, A.H., CROWNINSHIELD, R.D., SCHENCK, R., HERBERTS, P. (2001): *A low stiffness composite biologically fixed prosthesis*. Clin Orthop Relat Res (393), pp. 128-136.

[91] KÄRRHOLM, J., ANDERBERG, C., SNORRASON, F., THANNER, J., LANGELAND, N., MALCHAU, H., HERBERTS, P. (2002): Evaluation of a femoral stem with reduced stiffness. A randomized study with use of radiostereometry and bone densitometry. *Journal of Bone and Joint Surgery*.; Vol. 84 A, No. 9, pp. 1651-1658.

[92] WANG, A., LIN, R., STARK, C., DUMBLETON, J.H. (1999): Suitability and limitations of carbon fiber reinforced PEEK composites as bearing surfaces for total joint replacements. *Wear*.; Vol. 225-229, Part 2, pp. 724-727.

[93] JONES, E., WANG, A., STREICHER, R. (2001): Validating the limits for a PEEK composite as an acetabular wear surface. *27th Annual Meeting of the Society for Biomaterials in conjunction with the 33rd International Biomaterials Symposium*.

[94] JOYCE, T.J., RIEKER, C., UNSWORTH, A. (2006): Comparative in vitro wear testing of PEEK and UHMWPE capped metacarpophalangeal prostheses. *Bio-Medical Materials and Engineering*.; Vol. 16, No. 1, pp. 1-10.

[95] MANLEY, M., ONG, K., KURTZ, S.M., RUSHTON, N., FIELD, R.E. (2007): Biomechanics of a PEEK horseshoe-shaped cup: comparisons with a predicate deformable cup. *Transactions of the 53rd Orthopedic Research Society*.; Vol. 32, 1717.

[96] YU, S., HARIRAM, K.P., KUMAR, R., CHEANG, P., AIK, K.K. (2005): In vitro apatite formation and its growth kinetics on hydroxyapatite/polyetheretherketone biocomposites. *Biomaterials*.; Vol. 26, No. 15, pp. 2343-2352.

[97] FAN, J.P., TSUI, C.P., TANG, C.Y., CHOW, C.L. (2004): Influence of interphase layer on the overall elasto-plastic behaviors of HA/PEEK biocomposite. *Biomaterials*.; Vol. 25, No. 23, pp. 5363-5373.

[98] TAN, K.H., CHUA, C.K., LEONG, K.F., CHEAH, C.M., CHEANG, P., ABU

Bakar, M.S., Cha, S.W. (2003): Scaffold development using selective laser sintering of polyetheretherketone - hydroxyapatite biocomposite blends. *Biomaterials.*; Vol. 24, No. 18, pp. 3115-3123.

[99] Abu Bakar, M.S., Cheng, M.H.W., Tang, S.M., Yu, S.C., Liao, K., Tan, C.T., Khor, K.A., Cheang, P. (2003): Tensile properties, tension - tension fatigue and biological response of polyetheretherketone - hydroxyapatite composites for load-bearing orthopedic implants. *Biomaterials.*; Vol. 24, No. 13, pp. 2245-2250.

[100] Ha, S.W., Kirch, M., Birchler, F., Eckert, K.-L., Mayer, J., Wintermantel, E., Sittig, C., Pfund-Klingenfuss, I., Textor, M., Spencer, N.D., Guecheva, M., Vonmont, H. (1997): Surface activation of polyetheretherketone (PEEK) and formation of calcium phosphate coatings by precipitation. *Journal of Materials Science: Materials in Medicine.*; Vol. 8, No. 11, pp. 683-690.

[101] Middleton, J.C., Tipton, A.J. (2000): Synthetic biodegradable polymers as orthopaedic devices. *Biomaterials.*; Vol. 21, No. 23, pp. 2335-2346.

[102] Törmälä, P., Pohjonen, T., Rokkanen, P. (1998): Bioabsorbable polymers: materials technology and surgical applications. *Journal of Engineering in Medicine.*; Vol. 212, No. 2, pp. 101-111.

[103] Gilding, D.K., Reed, A.M. (1979): Biodegradable polymers for use in surgery - polyglycolic/poly(lactic acid) homo-and copolymers: 1. *Polymer.*; Vol. 20, No. 12, pp. 1459-1464.

[104] Barrows, T.H. (1986): Degradable Implant Materials: A Review of Synthetic Absorbable Polymers and Their Applications. *Clinical Materials.*; Vol. 1, pp. 233-257.

[105] Domb, A.J., Amselem, S., Langer, R., Maniar, M. (1994): Polyanhydrides as carriers of drugs. *Biomedical Polymers: Designed-To-Degrade Systems.* Editor: Shalaby, S.W., Hanser Gardner Pubns, pp. 69-96, ISBN: 978-1-569-90159-5.

[106] Heller, J., Daniels, A.U. (1994): Poly(orthoesters). *Polymers: Designed-To-Degrade Systems.* Editor: Shalaby, S.W., Hanser Gardner Pubns, pp. 35-68, ISBN: 978-1-569-90159-5.

[107] Kohn, J., Abramson, S., Langer, R. (2004): Bioresorbable and Bioerodible Materials. *Biomaterials science.* Editors: Ratner, B.D., Hoffman, A.S., Schoen, F.J., Lemons, J.E., Academic Press, pp. 115-126, ISBN: 978-0-125-82463-7.

[108] Shalaby, S.W., Johnson, R.A. (1994): Synthetic absorbable polyesters. *Biomedical Polymers: Designed-To-Degrade Systems.* Editor: Shalaby, S.W., Hanser Gardner Pubns, pp. 1-34, ISBN: 978-1-569-90159-5.

[109] Santavirta, S., Konttinen, Y.T., Saito, T., Gronblad, M., Partio, E., Kemppinen, P., Rokkanen, P. (1990): Immune response to poly-

glycolic acid implants. *Journal of Bone and Joint Surgery*.; Vol. 72, No. 4, pp. 597-600.

[110] BERGSMA, J.E., DE BRUIJN, W.C., ROZEMA, F.R., BOS, R.R.M., BOERING, G. (1995): Late degradation tissue response to poly(L-lactide) bone plates and screws. *Biomaterials*.; Vol. 16, No.1, pp. 25-31.

[111] SCHINDLER, A., JEFFCOAT, R., KIMMEL, G.L., PITT, C.G., WALL, M.E., ZWIEDINGER, R. (1977): Biodegradable polymers for sustained drug delivery. *Contemporary Topics in Polymer Science*.; Vol. 2, pp. 251-289.

[112] BOSTMAN, O., HIRVENSALO, E., MAKINEN, J., ROKKANEN, P. (1990): Foreign-body reactions to fracture fixation implants of biodegradable synthetic polymers. *Journal of Bone and Joint Surgery*.; Vol. 72, No. 4, pp. 592-596.

[113] LANGSTAFF, S., SAYER, M., SMITH, T.J.N., PUGH, S.M. (2001): Resorbable bioceramics based on stabilized calcium phosphates. Part II: evaluation of biological response. *Biomaterials*.; Vol. 22, No. 2, pp. 135-150.

[114] PICONI, C., MACCAURO, G. (1999): Zirconia as a ceramic biomaterial. *Biomaterials*.; Vol. 20, No. 1, pp. 1-25.

[115] CHRISTEL, P., MEUNIER, A., DORLOT, J.M., CROLET, J.M., WITVOET, J., SEDEL, L., BOUTIN, P. (1988): Biomechanical compatibility and design of ceramic implants for orthopedic surgery, Bioceramics: material caracteristics versus in vivo behaviour. *Annals of the New York Academy of Sciences*.; Vol. 523, pp. 234-256.

[116] AHMAD, I. (1998): Yttrium-partially stabilized zirconium dioxide posts: an approach to restoring coronally compromised nonvital teeth. *International Journal of Periodontics & Restorative Dentistry*.; Vol. 18, No. 5, pp. 454-465.

[117] MEYENBERG, K.H., LUTHY, H., SCHÄRER, P., (1995): Zirconia Posts: New All-Ceramic Concept for Nonvital Abutment Teeth. *Journal of Esthetic Dentistry*.; Vol. 7, No. 2, pp. 73-80.

[118] FRITZSCHE, J. (2003): Zirconium oxide restorations with the DCS precident system. *International Journal of Computerized Dentistry*.; Vol. 6, No. 2, pp. 193-201.

[119] TINSCHERT, J., NATT, G., MAUTSCH, W., SPIEKERMANN, H., ANUSAVICE, K.J. (2001): Marginal fit of alumina- and zirconia-based fixed partial dentures produced by a CAD/CAM system. *Operative Dentistry*.; Vol. 26, No. 4, pp. 367-374.

[120] GLAUSER, R., SAILER, I., WOHLWEND, A., STUDER, S., SCHIBLI, M., SCHÄRER, P. (2004): Experimental zirconia abutments for implant-supported single-tooth restorations in esthetically demanding regions: 4-year results of a prospective clinical study. *The International Journal of Prosthodontics*.; Vol. 17, No. 3, pp. 285-290.

[121] AKAGAWA, Y., HOSOKAWA, R., SATO, Y., KAMAYAMA, K. (1998): Comparison between freestanding and

tooth-connected partially stabilized zirconia implants after two years' function in monkeys: a clinical and histologic study. *Journal of Prosthetic Dentistry*.; Vol. 80, No. 5, pp. 551-558.

[122] Akagawa, Y., Ichikawa, Y., Nikai, H., Tsuru, H. (1993): Interface histology of unloaded and early loaded partially stabilized zirconia endosseous implant in initial bone healing. *Journal of Prosthetic Dentistry*.; Vol. 69, No. 6, pp. 599-604.

[123] Scarano, A., Di Carlo, F., Quaranta, M., Piattelli, A. (2003): Bone response to zirconia ceramic implants: an experimental study in rabbits. *Journal of Oral Implantology*.; Vol. 29, No. 1, pp. 8-12.

[124] Albrektsson, T., Hansson, H.A., Ivarsson, B. (1985): Interface analysis of titanium and zirconium bone implants. *Biomaterials*.; Vol. 6, No. 2, pp. 97-101.

[125] Garvie, R.C., Hannink, R.H.J., Pascoe, R.T. (1975): Ceramic Steel?. *Nature*.; Vol. 258, pp. 703-704.

[126] Lawson, S. (1995): Environmental degradation of zirconia ceramics. *Journal of the European Ceramic Society*.; Vol. 15, No. 6, pp. 485-502.

[127] Caton, J., Bouraly, J.P., Reynaud, P., Merabet, Z. (2004): Phase Transformation in Zirconia Heads after THA Myth or Reality. *Proceedings of the Ninth BIOLOX Symposium*.; Vol. 26-27, pp. 73-74.

[128] Allain, J., Le Mouel, S., Goutallier, D., Voisin, M.C. (1999): Poor eighth year survival of cemented zirconia-polyethylene total hip replacements. *Journal of Bone and Joint Surgery*.; Vol. 81 B, No. 5, pp. 835-842.

[129] Haraguchi, K., Sugano, N., Nishii, T., Sakai, T., Yoshikawa, H, Ohzono, K. (2001): Phase transformation of a zirconia cermaic head after total hip arthroplasty. *Journal of Bone and Joint Surgery*.; Vol. 83 B, No. 7, pp. 996-1000.

[130] Catledge, S.A., Cook, M., Vohra, Y., Santos, E.M., McClenny, M.D., Moore, K.D. (2003): Surface crystalline phases and nanoindentation hardness of explanted zirconia femoral heads. *Journal of Materials Science: Materials in Medicine*.; Vol. 14, No. 10, pp. 863-867.

[131] Hulbert, S.F., Young, F.A., Mathews, R.S., Klawitter, J.J., Talbert, C.D., Stelling, F.H. (1970): Potential of ceramic materials as permanently implantable skeletal prostheses. *Journal of Biomedical Materials Research*.; Vol. 4, No. 3, pp. 433-456.

[132] Griss, P., Werner, E. (1980): Alumina ceramic, bioglass and silicon nitride. A comparative biocompatibility study. *Mechanical Properties of Biomaterials*. Editors: Hastings, G.W., Williams, D.F., John Wiley, pp. 217-225, ISBN: 978-0-471-27761-3.

[133] Green, D.J. (1998): *An Introduction to the Mechanical Properties of Ceramics*. Cambridge University Press, ISBN: 978-0-521-59913-9.

[134] Munz, D., Fett, T. (1999): *Ceramics: Mechanical Properties, Failure Behaviour, Materials Selection 1st*

Ed., Springer Verlag, ISBN: 978-3-540-65376-9.

[135] WILLMANN, G. (1998): Überlebensrate und Sicherheit von keramischen Kugelköpfen für Hüftendoprothesen (Survival rate and reliability of ceramic femoral heads for total hip arthroplasty). *Materialwissenschaft und Werkstofftechnik.*; Vol. 29, No. 10, pp. 595-604.

[136] FISCHER, H., NIEDHART, C., KALTENBORN, N., PRANGE, A., MARX, R., NIETHARD, F.U., TELLE, R. (2005): Bioactivation of inert alumina ceramics by hydroxylation. *Biomaterials.*; Vol. 26, No. 31, pp. 6151-6157.

[137] YEN, S.K., GUO, M.J., ZAN, H.Z. (2001): Characterization of electrolytic ZrO_2 coating on Co-Cr-Mo implant alloys of hip prosthesis. *Biomaterials.*; Vol. 22, No. 2, pp. 125-133.

[138] HOLTGRAVE, E.A., DONATH, H. (1995): Response of odontoblast-like cells to hydroxyapatite ceramic granules. *Biomaterials.*; Vol. 16, No. 2, pp. 155-159.

[139] LOPEZ-ESTEBAN, S., SAIZ, E., FUJINO, S., OKU, T., SUGANUMA, K., TOMSIA, A. P. (2003): Bioactive glass coatings for orthopedic metallic implants. *Journal of the European Ceramic Society.*; Vol. 23, No. 15, pp. 2921-2930.

[140] BRAIC, M., BALACEANU, M., BRAIC, V., VLADESCU, A., PAVELESCU, G., ALBULESCU, M. (2005): Synthesis and characterization of TiN, TiAlN and TiN/TiAlN biocompatible coatings. *Surface and Coatings Technology.*; Vol. 200, No. 1-4, pp. 1014-1017.

[141] LENG, Y.X., SUN, H., YANG, P., CHEN, J.Y., WANG, J., WAN, G.J., HUANG, N., TIAN, X.B., WANG, L.P., CHU, P.K. (2001): Biomedical properties of tantalum nitride films synthesized by reactive magnetron sputtering. *Thin Solid Films.*; Vol. 398-399, pp. 471-475.

[142] HÜBLER, R., COZZA, A., MARCONDES, T.L., SOUZA, R.B., FIORI, F.F. (2001): Wear and corrosion protection of 316-L femoral implants by deposition of thin films. *Surface and Coatings Technology.*; Vol. 142-144, pp. 1078-1083.

Regional sediment yield pattern for the west flowing rivers of Kerala state, India

Chandramohan T.[1], Balchand A.N.[2]

[1]National Institute of Hydrology, Belgaum-590001, Karnataka, India;
E-mail: cmohant@yahoo.com
[2]Cochin University of Science and Technology, Department of Physical Oceanography,
Kochi-16, Kerala, India; E-mail: balchand@rediffmail.com

Abstract: This study aims to understand the spatial and seasonal distribution of suspended sediment load carried by major west flowing rivers of Kerala State, India, which lies in the humid climatic zone. While comparing sediment yield pattern among individual rivers with the aid of daily discharge and sediment load data, it was noticed that the State could be broadly delineated into four distinct sediment yielding zones. This aspect was dealt in detail and the influencing factors were analyzed. The sediment yield characteristics for each of these zones were explained mainly with respect to the two major rainfall seasons of the State, namely Southwest (SW) monsoon and Northeast (NE) monsoon and their spatial and temporal coverage over the state.

Key words: suspended sediment, yield, erosion, discharge, monsoon, Kerala

Introduction

In recent times, due to various developmental activities within the river basins, the rate of soil erosion, its transport, and deposition downstream have considerably altered. Such changes in sediment movement will have its impact on the river system, reservoirs, estuaries and coastal regions.

While studying the environmental problems of a region, land, water, and biomass have to be considered together. An integrated approach has to be followed while suggesting solutions to such problems.

Kerala, which is the southernmost state of India, faces numerous environmental issues (Basak, 1998) such as uncontrolled developmental activities on the upstream reaches, land use changes, flash floods, droughts, sedimentation, excessive sand mining, deterioration of water quality, etc. Hence it is important to study the water and sediment yields together and its relation to the drainage basin environment.

The Kerala State, situated in the humid tropics lies between 8° 18' and 12° 48' N and 74° 52' and 77° 22' E. Based on the topography, the state can be divided into three well-defined natural landforms: the

Scientific paper

lowlands with altitude less than 7.5 m; midlands with altitude between 7.5 and 75 m; and the highlands with altitudes greater than 75 m. The state is a narrow strip of land with width varying from 30 km in the north and south to about 130 km in the central region. The Western Ghat forms a continuous mountain wall on the eastern border of the state while Arabian Sea is the margin to west.

Geologically the major formations of the state are, crystalline rocks of Archaen age; sedimentary rocks of Tertiary age; laterites capping the crystalline and sedimentary rocks; and recent to sub-recent sediments forming the low-lying areas and river valleys. Lateritic and coastal loams cover the major soil types of the State. There are mainly five broad categories of land use distributed unevenly, arable land, forestland, plantation, grassland and wasteland (Nair, 1987).

The average annual rainfall for the State is about 3000 mm. It ranges in the lowland, from 900 mm in the south to 3500 mm in the north; in the midland, from 1400 mm to 4000mm; and in the highland, from 2500 mm to 6000 mm (CWRDM, 1995). About 65 % of this rainfall is received during the southwest (SW) monsoon and 25 % during northeast (NE) monsoon. However, for the southern parts, NE monsoon is active compared to the northern Kerala.

Forty-four (44) rivers, with lengths more than 15 km, originate from the Western Ghat, out of which 41 flows towards west and the other three rivers towards east. Periyar, Bharathapuzha, Pamba, and Chal-iyar are the major rivers of the state. The net annual discharge from all these rivers is estimated to be 77,900 MCM (CWRDM, 1995). The drainage basin area and the discharge carried by these rivers are small compared to other major rivers in India.

Materials and methods

Numerous studies were undertaken in the past to analyze the sediment yield from large and medium rivers of the world (Holeman, 1968; Wilson, 1972; Griffiths, 1982; Keown et al., 1986; Lajczak and Jansson, 1993; Yang et al., 2002). In India also, such studies were carried out for most of the major rivers (Abbas and Subramanian, 1984; Goswami, 1985; Biksham and Subramanian, 1988; Ramesh & Subramanian, 1988; Vaithyanathan et al., 1992; Chakrapani and Subramanian, 1993; Rao et al., 1997). These studies have contributed much to the understanding of the sediment yield processes and the regional factors influencing these processes.

In the present study, an attempt was made to understand the spatial and temporal variation of sediment transport characteristics of the rivers of Kerala and the factors affecting this variability. The Central Water Commission (CWC), Govt. of India, is maintaining 16 sediment gauges in Kerala for daily river gauge measurements and sediment sampling. In order to utilize this long-term data, these 16 river basins were selected for the present study.

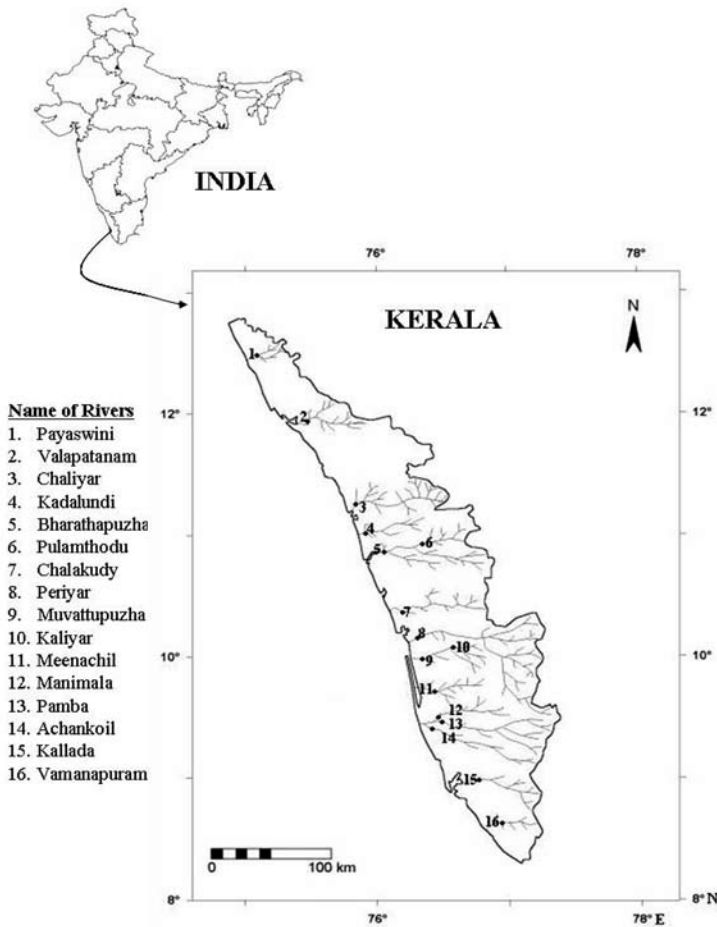Location of these rivers with the sediment gauge sites is shown in Figure 1. The daily

Figure 1. Location of rivers and the sediment gauge sites

suspended sediment concentration (mg/l) and corresponding discharge (cumec) data were collected for fifteen years, from 1986-87 to 2000-01. Average monthly rainfall (mm) for each river basin was calculated from the daily data of rain gauge stations located within these basins. Length of the main streams, average slope and drainage area were extracted from Survey of India toposheets. General and hydrological characteristic of the river basins are given in Table 1.

The daily data on suspended sediment concentration [C in mg/l] were converted into sediment load [S in ton]. Daily discharge values were added to get the monthly and yearly discharge in cumec-days. The monthly discharge and sediment load values were used to estimate the percentage monthly and seasonal contributions. While analyzing the sediment and discharge data for the rivers of Kerala, it is noticed that there is a marked change in the pattern (seasonal as well as annual) of carrying capacities of

these rivers from north to south. Hence this aspect was studied in detail. Such studies to delineate quantitatively, broad regions with similar erosional patterns were carried out earlier by GRIFFITHS (1982) for North Island basins, New Zealand and LAJCZAK and JANSSON (1993) for Baltic Drainage basins.

The analysis of seasonal and annual contribution of discharge and suspended sediment load will not yield much inference on the comparative characteristics of individual rivers originating and flowing through different topographical conditions. Sediment load from a river basin depends mainly on the size of the catchment and on the discharge, which carries the sediment. Hence, the erosion rate or sediment yield, which is the ratio of sediment load to catchment area [S/A]; and the ratio of sediment load to discharge [S/Q], which is a measure of average sediment concentration, were considered for analyzing the spatial yield characteristics of the rivers.

RESULTS AND DISCUSSION

Seasonal discharge and sediment contribution for individual rivers is given in Table 2. It can be seen that most of the rivers drain 95-98 % of its sediment load during the monsoon season. However, its distribution during the southwest (SW) and northeast (NE) monsoons gives an entirely different pattern for the rivers flowing through the northern and southern regions of the State. This aspect was analyzed in detail using different criterion.

Table 1. Characteristics of the river basins studied

Name of the River	Annual rainfall (mm)	River Basin area [A] (km²)	Length (km)	Slope (m/m)	Annual discharge (MCM)	Average annual sediment load (ton)	Max. observed sediment conc. (mg/l)
Payaswini	4000	957	105	0.012	2384	239934	1090
Valapatanam	3600	1070	101	0.013	3543	252144	613
Chaliyar	3800	1876	169	0.012	4175	401614	1024
Kadalundi	3400	750	86	0.013	1303	85171	345
Bharathpuzha	2300	5755	209	0.009	4326	369186	1163
Pulanthode	2600	940	78	0.013	1756	101771	791
Chalakudy	3600	1342	120	0.010	1798	50234	167
Periyar	3200	4234	244	0.007	6895	320029	739
Muvattupuzha	3100	1208	92	0.011	5068	157001	595
Kaliyar	3000	405	71	0.014	1194	44667	557
Meenachil	3000	615	61	0.017	1756	36566	1091
Manimala	3300	731	90	0.012	1795	70486	559
Pamba	3600	1654	176	0.009	4016	156851	896
Achankovil	2600	810	138	0.005	1247	77130	904
Kallada	2800	1210	92	0.016	1636	104447	802
Vamanapuram	2200	540	88	0.020	701	68619	2944

Table 2. Seasonal variation of % Q and % S for the rivers

Name of the River	% Discharge [Q]				% Sediment Load [S]			
	Monsoon			Non-monsoon	Monsoon			Non-monsoon
	SW	NE	Total		SW	NE	Total	
Payaswini	83.5	13.5	97.0	3.0	90.0	9.5	99.5	0.5
Valapatanam	86.2	11.3	97.5	2.5	94.0	5.3	99.3	0.7
Chaliyar	79.6	15.8	95.4	4.6	87.0	11.9	98.9	1.1
Kadalundi	77.3	20.0	97.3	2.7	79.0	19.6	98.6	1.4
Bharthapuza	74.5	19.7	94.2	5.8	79.9	18.1	98.0	2.0
Pulamthode	72.6	21.8	94.4	5.6	73.8	24.3	98.1	1.9
Chalakudy	75.7	16.8	92.5	7.5	84.2	14.1	98.3	1.7
Periyar	67.9	18.2	86.1	13.9	89.8	8.3	98.1	1.9
Muvattupuzha	56.9	19.2	76.1	23.9	65.9	25.4	91.3	8.7
Kaliyar	77.1	18.9	96.0	4.0	75.7	22.6	98.3	1.7
Meenachil	69.7	22.8	92.5	7.5	71.8	23.7	95.5	4.5
Manimala	69.4	23.6	93.0	7.0	68.1	27.4	95.5	4.5
Pamba	65.5	23.3	88.8	11.2	54.9	40.3	95.2	4.8
Achankovil	62.3	29.7	92.0	8.0	53.9	41.7	95.6	4.4
Kallada	50.7	32.4	83.1	16.9	39.8	53.8	93.6	6.4
Vamnapuram	50.3	35.2	85.5	14.5	41.4	51.4	92.8	7.2

* Seasons as per the Indian Meteorological Department (IMD) norms

M - Monsoon (June to Nov.)   NE - Northeast Monsoon (Oct. and Nov.)
NM - Non-Monsoon (Dec. to May)   W - Winter (Dec. to Feb.)
SW - Southwest Monsoon (June to Sept.)   S - Summer (March to May)

Seasonal and spatial variation of sediment load and discharge

Based on the 15 years of data, River Periyar carries maximum yearly discharge (9968 MCM) while Vamanapuram yields the minimum discharge of 288 MCM. Chaliyar supplies the maximum sediment load (0.8 x 10^6 ton) and Meenachil supplies the minimum (0.02 x 10^6 ton).

The seasonal variation of discharge and sediment load can be represented graphically (Figure 2). A definite grouping of data into four zones: north zone (NZ), north-central zone (NCZ), south-central zone (SCZ) and south zone (SZ), can be observed from the graph for SW and NE monsoon seasons. The rivers from the 4 zones are also shown in separate groups in Table 2.

Southwest (SW) monsoon is the major source of discharge for northern rivers. The percentage discharge during SW monsoon decreases steadily from north to south as shown in Table 2, about 84 % in the north to 50 % in the south. On the other hand, the northeast (NE) monsoon yields about 14 % discharge for the rivers from NZ, whereas the percentage increases to 32 % for the SZ rivers. The Muvattupuzha river shows 23 % yield during non-monsoon season, since it includes the diverted water from the tail-race of Idukki hydroelectric project in River Periyar.

Major amount of the annual sediment load is transported during monsoon season. SW monsoon sediment load ranges from 74-94 % for northern rivers (NZ + NCZ) whereas
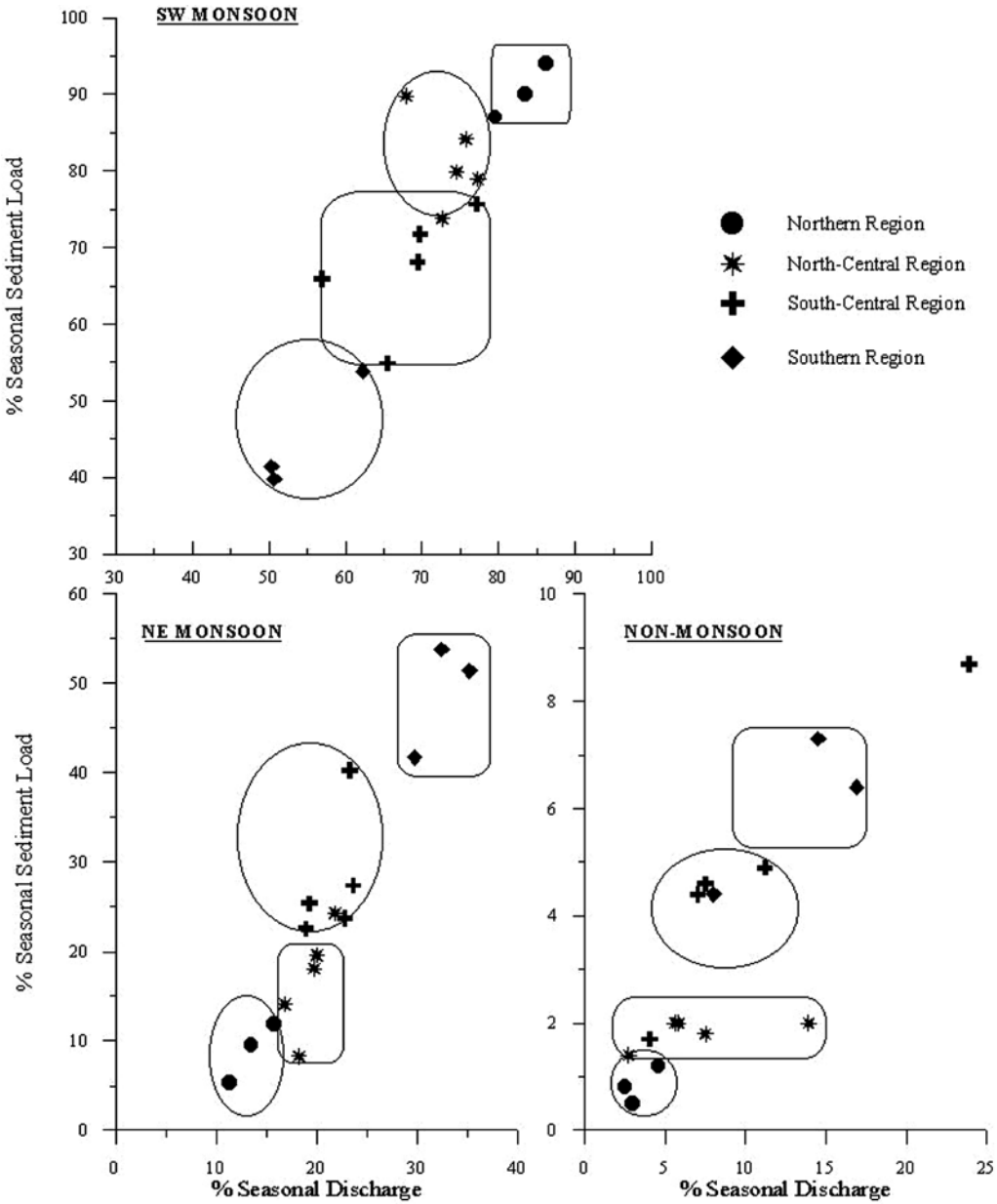
Figure 2. Seasonal % (Q Vs S) relationship showing the demarcation of zones

this is about 42-76 % for southern rivers (SZ + SCZ). During NE monsoon season, northern rivers (NZ + NCZ) yield 5-24 % of the total sediment load whereas it is 23-54 % for the southern rivers (SZ + SCZ). Sediment load for non-monsoon season is nominal for northern rivers while southern rivers register about 2-9 % of the annual sediment load.

The sediment yielding characteristics of these individual zones can be further illustrated as in Figure 3, where monthly variation of rainfall [P], discharge [Q] and sediment load [S] contributions of representative rivers from each of the above four zones is demonstrated. It can be seen that the discharge and sediment flow pattern closely follow the monthly rainfall distribution. Northern rivers (NZ + NCZ) showed an asymmetrical uni-mode distribution whereas south-central and SZ Rivers developed a bi-mode distribution. The dominance of NE monsoon rainfall on sediment transport over the southern zone (SZ + SCZ) can be clearly seen.

The spatial and seasonal variation of sediment yield [S/A] and average sediment concentration [S/Q] for the rivers are given in Table 3. The division of the State into different zones, as discussed in Figure 2 and Table 2, can be seen in this case also.

Average Sediment Concentration [S/Q]
This ratio is large for the northern rivers, shows a declining trend towards central rivers and again increases towards south. This denotes high erodibility of the northern and southern zones and indicates the availability of material for transport rather than the stream conditions. Slope of the terrain also

is a factor, which is more for the northern and southern Kerala where the land becomes narrow. The specific sediment yielding zones, as explained based on the % [Q-S] relationship is valid here also.

When season-wise yield is considered, the trend is similar for monsoon season. The ratio during SW monsoon is more for northern rivers while it is higher during NE monsoon for southern rivers. During the non-monsoon season, the ratio is almost constant except for the southern most rivers, where the summer rains are of appreciable quantity.

Sediment Yield [(S/A]
From Table 3, it can be seen that the sediment yield is maximum for the northern rivers. The rivers in the central and southern zones show highly unstable values, with a reducing trend towards central parts of the State and increasing towards southern zone. This factor also denotes the high erosion rates for the northern rivers, lesser for southern rivers and least for the central rivers.

The presence of four sediment-yielding zones is noticeable in this case also. However, the demarcation between south-central and north-central zones is not so well defined. The unstable values for the central zones (NCZ + SCZ) may be due to the fact that comparatively larger rivers drain this zones. Inter basin water transfer exists between Periyar and Muvattupuzha, which results in large yields even during non-monsoon season. Also, some extreme discharge and sediment load events were noticed for these rivers from the data set, which affects the [S/A] ratio. The effect of these outliers may not appear in [S/Q] ratio, since both discharge and sediment load varies simultaneously.
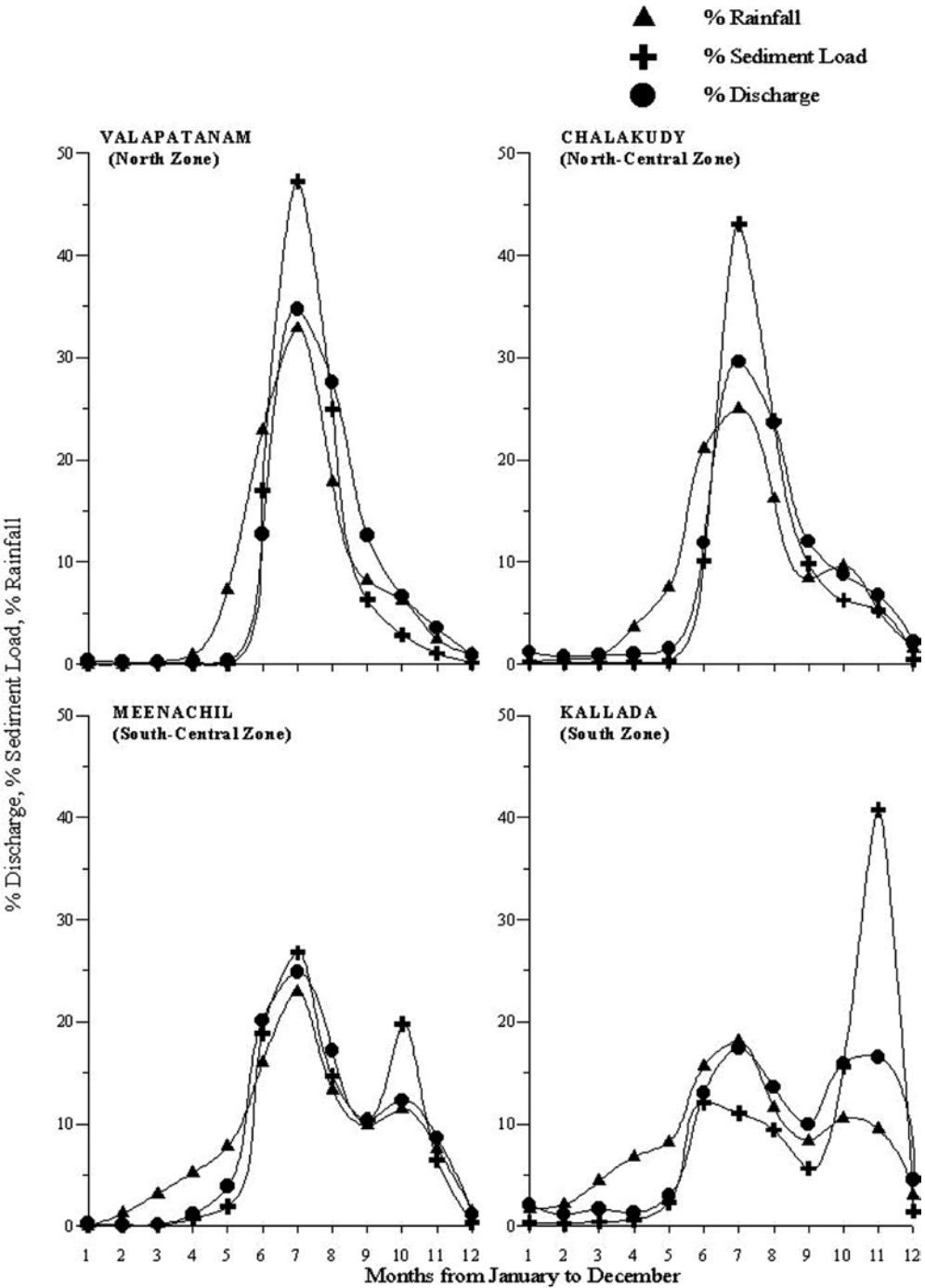
Figure 3. Monthly distribution of (%) rainfall, discharge and sediment load
for rivers from different zones

Table 3. Variation of the [S/Q] and [S/A] ratios for the rivers

Name of the River	Sediment Load/ Discharge (S/Q)					Sediment Load/ Catchment Area (S/A)				
	Year	M	NM	SW	NE	Year	M	NM	SW	NE
Payaswini	8.7	8.9	1.3	9.4	6.2	250.7	249.6	1.2	225.7	23.9
Valapatanam	6.2	6.3	1.9	6.7	2.9	235.7	233.8	1.8	221.4	12.4
Chaliyar	8.3	8.6	2.1	9.1	6.3	214.1	211.6	2.5	186.2	25.4
Kadalundi	5.7	5.7	3.0	5.8	5.5	113.6	112.0	1.6	89.7	22.3
Bharatapuzha	7.4	7.7	2.5	7.9	6.8	64.2	62.9	1.3	51.3	11.6
Pulanthode	5.0	5.2	1.7	5.1	5.6	108.3	106.2	2.1	79.9	26.3
Chalakudy	2.4	2.6	0.6	2.7	2.0	37.4	36.8	0.7	31.5	5.3
Periyar	4.0	4.6	0.6	5.3	1.8	75.6	74.1	1.5	67.9	6.2
Muvattupuzha	2.7	3.2	1.0	3.1	3.6	130.0	118.6	11.4	85.7	33.0
Kaliyar	3.2	3.3	1.4	3.2	3.9	110.3	108.4	1.9	83.5	25.0
Meenachil	1.8	1.9	1.1	1.9	1.9	59.5	56.8	2.7	42.7	14.1
Manimala	3.4	3.5	2.2	3.3	4.0	96.4	92.1	4.3	65.7	26.5
Pamba	3.4	3.6	1.5	2.8	5.8	91.6	87.1	4.5	50.3	36.9
Achankovil	5.4	5.6	3.0	4.6	7.5	95.2	91.0	4.2	51.3	39.7
Kallada	5.5	6.2	2.1	4.3	9.2	86.3	80.8	5.6	34.4	46.4
Vamnapuram	8.5	9.2	4.2	7.0	12.4	127.1	117.9	9.2	52.6	65.3

Regional Division

Based on the analyses of annual and seasonal water and sediment yield, the Kerala State can be roughly divided into four zones with similar sediment transport characteristics. These four zones namely; North Zone (NZ), North-Central Zone (NCZ), South-Central Zone (SCZ), and South Zone (SZ); can be delineated as shown in Figure 4. The difference in transport characteristics among the zones is mainly attributed to the spatial variation of rainfall and discharge, slope along the course of rivers, and physiography of the river basins. The seasonal distribution of discharge and sediment load and the variation in sediment yield, for these four zones, are given in Table 4. The average sediment yield for the northern rivers goes up to 240 ton/km², whereas for the rest of the state this ranges between 80 and 100. However, the difference in distribution of sediment load and to some extent the discharge, from north to south, during the two monsoon seasons is obvious as can be noticed from the Table 4.

CONCLUSIONS

Water and sediment yield data of 15 years (from 1986-87 to 2000-01) for 16 west flowing rivers of Kerala, India, were collected and analyzed to compare the discharge and suspended sediment carrying characteristics of these rivers. In general, the sediment yield pattern follows the seasonal distribution of rainfall and the topography of the river basin.

From the spatial and seasonal analyses of the data, it is found that a broad division of the state into four zones is possible. These are, high sediment yielding North Zone; North-Central Zone with low yield; South-Central Zone with low to medium yield, a sizeable share of which occurs during

northeast monsoon season; and South Zone with medium yield, where the yield is almost equal for both the monsoon seasons.

The reasons for the above sediment yielding zones for the State is basically due to the spatial distribution of rainfall during the two monsoons over various parts of the State. NE monsoon plays a major roll in the sediment yield characteristics of SZ rivers, whereas SW monsoon is responsible for supplying major share of sediment load for northern rivers (NZ + NCZ). The other factors affecting the variation in suspended sediment transport are slope of the river basin, geology, soil type and land use activities.
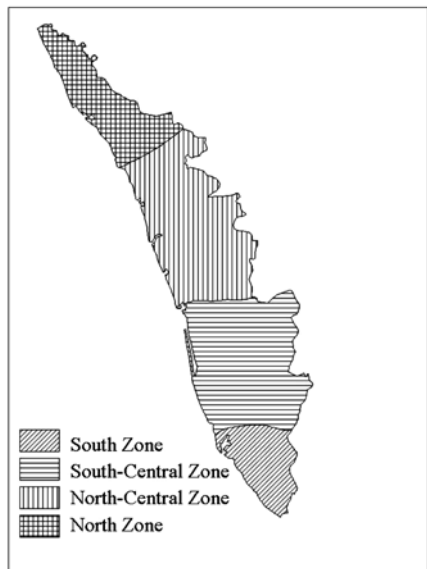
Figure 4. Sediment yielding zones of Kerala

Table 4. Seasonal distribution of discharge, sediment load and sediment yield for the four zones of the state

% Discharge				% Sediment Load				Sediment Yield (ton/km2)			
NZ	NCZ	SCZ	SZ	NZ	NCZ	SCZ	SZ	NZ	NCZ	SCZ	SZ
ANNUAL											
								233.5	79.8	89.4	102.9
MONSOON											
96.6	92.9	92.6	86.9	99.2	98.2	96.1	94.0	231.7	78.4	86.1	96.6
SW MONSOON											
83.1	73.6	70.4	54.4	90.3	81.3	67.6	45.0	211.1	64.1	60.6	46.1
NE MONSOON											
13.5	19.3	22.2	32.4	8.9	16.9	28.5	49.0	20.6	23.3	25.6	50.5
NON-MONSOON											
3.4	7.1	7.4	13.3	0.8	1.8	3.9	6.0	1.8	1.4	3.4	6.3

REFERENCES

ABBAS, N. & SUBRANAIAN, V. (1984): Erosion and Sediment Transport in the Ganges River Basin (India). *Journal of Hydrology*.; Vol. 69, pp. 173-182.

BASAK, P. (1998): Water Resources of Kerala - Myths and Realities. *Water Scenario of Kerala, STEC Technical Report*. Government of Kerala.

BIKSHAM, G. & SUBRAMANIAN, V. (1988): Sediment Transport of the Godavari River Basin and its Controlling Factors. *J. Hydrolo*.; Vol. 101, pp. 275-290.

CHAKRAPANI, G.J. & SUBRAMANIAN, V. (1993): Rates of Erosion and Sedimentation in the Mahanadi River Basin, India. *J. Hydrolo*.; Vol. 149, pp. 39-48.

CWRDM (1995): *Water atlas of Kerala*. Centre for Water Resources Development and Management (CWRDM) Publication, Kozhikode, Kerala.

GOSWAMI, D.C. (1985): Brahmaputra River, Assam, India: Physiography, Basin Denudation, and Channel Aggradation. *Wat. Resour. Res*.; Vol. 21, No. 7, pp. 959-978.

GRIFFITHS, G.A. (1982): Spatial and Temporal Variability in Suspended Yields of North Island Basins, New Zealand. *Wat. Resour. Bull*.; Vol.18, No. 4, pp. 575-584.

HOLEMAN, J.N. (1968): Sediment Yield of World Rivers. *Wat. Resour. Res*.; Vol. 4, pp. 737-742.

KEOWN, M.P., DARDEAU, E.A. & CAUSEY, E.M. (1986): Historic Trends in the Sediment Flow Regime of the Mississippi River. *Wat. Resour. Res*.; Vol.22, No. 11, pp. 1555-1564.

LAJCZAK, A. & JANSSON, M.B. (1993): Suspended Sediment Yield in the Baltic Drainage Basin. *Nordic Hydrolo*.; Vol. 24, pp. 31-52.

NAIR, K. S. (1987): *Hydrometeorological Studies of Kerala State in Relation to the Western Ghats: Ph.D. Thesis*. Cochin University of Science & Technology 1987, Kerala, pp. 34-45.

RAMESH, R. & SUBRAMANIAN, V. (1988): Temporal, Spatial and Size Variation in the Sediment Transport in the Krishna Basin, India. *J. Hydrolo*.; Vol. 98, pp. 53-65.

RAO, S.V.N., RAO, M.V. & RAMASASTRI, K.S. (1997): A study of Sedimentation in Chenab Basin in Western Himalayas. *Nordic Hydrolo*.; Vol. 28, No. 3, pp. 201-216.

VAITHIYANATHAN, P., RAMANATHAN, A. & SUBRAMANIAN, V. (1992): Sediment Transport in the Cauvery River Basin: Sediment Characteristics and Controlling Factors. *J. Hydrolo*.; Vol. 139, pp. 197-210.

WILSON, L. (1972): Seasonal Sediment Pattern of U.S. Rivers. *Wat. Resour. Res*.; Vol. 8, No. 6, pp. 1470-1478.

YANG, S., ZHAO, Q. & BELKIN, I.M. (2002): Temporal Variation in the Sediment Load of the Yangtze River and the Influence of Human Activities. *J. Hydrolo*.; Vol. 263, pp. 56-71.

Technology of producing impressed filters to encompass two layers of aquifers

Tehnologija izdelave vtisnega filtra v dva paketa vodonosnikov

Željko Vukelič[1], Bojan Lajlar[2], Ivan Supovec[3], Goran Vižintin[1]

[1]University of Ljubljana, Faculty of Natural Sciences and Engineering, Aškerčeva cesta 12, SI-1000 Ljubljana, Slovenia; E-mail: zeljko.vukelic@ntf.uni-lj.si, goran.vizintin@ntf.uni-lj.si
[2]Velenje Lignite Mines, Partizanska cesta 78, 3320 Velenje, Slovenia;
E-mail: bojan.lajlar@rlv.si
[3]HGEM d.o.o., Zaloška cesta 143, SI-1000 Ljubljana, Slovenia; E-mail: supovec@hgem.si

Abstract: To ensure safe excavation under aquifers it is necessary to employ drainage in order to decrease water pressure in the aquifers above the coal layer. In calculating the permissible height values of excavation, water pressure is one of the most important input data. To obtain real data it is necessary to provide suitable monitoring of the water pressure, which is an indicator of water drainage efficiency. To improve the effects of drainage by using jetted dewatering boreholes, a possible solution was either to install more impressed filters on a shorter distance, or to encompass two aquifers simultaneously through one borehole. We have gradually developed a novel technology of constructing jetted dewatering boreholes also which could encompass two aquifers. This technology can significantly reduce the costs for mine water drainage.

Izvleček: Za zagotavljanje varnega odkopavanja pod vodonosnimi plastmi je potrebno v največji možni meri z odvodnjevalnimi procesi znižati tlake vode v vodonosnikih nad premogovim slojem. Tlak vode je tudi eden izmed glavnih vhodnih podatkov pri izračunu dovoljenih višin odkopavanja, zato je za pridobitev realnih podatkov potrebno izvajati tudi ustrezen monitoring gibanja tlakov vode, ki so kazalec učinkov odvodnjevanja. Za izboljšanje učinkov odvodnjevanja z vtisnimi filtri, vidimo rešitev predvsem v povečanju gostote izdelave vtisnih filtrov ali v zajemanju dveh vodonosnikov hkrati na eni vrtini. Tako smo razvili popolnoma novo tehnologijo izdelave vtisnih filtrov, ki omogočajo zajem dveh vodonosnikov. Tehnologija zajema dveh vodonosnikov, pomeni tudi občutno znižanje stroškov jamskih odvodnjevalnih objektov.

Scientific paper

Introduction

To ensure safe excavation under aquifers it is necessary to employ drainage in order to decrease water pressure in the aquifers above the coal layer. In calculating the permissible height values of excavation, water pressure is one of the most important input data. To obtain real data it is necessary to provide suitable monitoring of the water pressure, which is an indicator of water drainage efficiency. Due to the excavation in the north-western part of the Preloge coal field, the system of surface piezometers and drift filters has been damaged. Therefore, it was necessary to find a suitable replacement for the system. A good solution to overcome this problem was to install jetted dewatering boreholes, which would replace the drainage system. Since 1990, we have used the technology of vertical and inclined jetted dewatering boreholes by drilling with filter pipes into a single aquifer in the Velenje Coal Mines. In the Škale coal field, intensive drainage from the hanging wall aquifers with in-mine boreholes has been practiced since 1960. To reduce drilling in the cave, the jetted dewatering boreholes, based on drilling technology using screens, is functionally less efficient than the object - a drift filter, which is made from the surface. To improve the effects of drainage by using jetted dewatering boreholes, a possible solution was either to install more impressed filters on a shorter distance, or to encompass two aquifers simultaneously through one borehole. Drilling with screens is possible if an inner tube is installed in the screen which will direct the flow of the drilling fluid directly through the drilling crown. During the activation procedure this part is removed.

To make the drainage processes more efficient, a suitable solution was to design an jetted dewatering boreholes, which would simultaneously encompasses two aquifers through one borehole, provided that the two aquifers have no hydraulic impact on one another. With this in mind, we have gradually developed a novel technology of constructing jetted dewatering boreholes also which could encompass two aquifers. This technology can significantly reduce the costs for mine water drainage.

Geological and hydrogeological conditions

Geological characteristics of the Velenje Coal Mines

The Velenje depression is of tectonic origin. It was formed already in the Helvet, however, the formation of sediments above the pre-pliocenic layers occurred during the period of late Miocene and at the beginning of Pliocene, during which, due to a series of neotectonic fractures, the whole territory of the Velenje-Dobrnik region sank. This resulted in a depression, which was formed between the Smrekovec and Šoštanj fracture, which is meshed with local fractures of different ages, going in all directions. The valley, as seen today, has been formed by sinking and simultaneous deposition of sediments, and the coal layer has been formed along its synclinal shape. This layer extends over an area which is approx. 8.3 km long and 1.5 to 2.5 km wide. The coal layer is closest to the surface on the edges of the valley, and deepest in the centre, where it reaches a thicknees of 168 m, yielding high quality coal.

The layers, which were accumulated by settling of sediments into the depression, represent a complete sedimentation cycle: from the land phase, to marsh land, and lake sedimentation, and back to marsh and land phase. This sequence is frequently broken by fluviatile sediments, sand, and gravel which had been drifted from the north and north-west.

Basically, the geological picture of the Velenje synclinal valley consists of Plio-quatenary hanging wall layers, a coal layer, Pliocene layers in the footwall, and a pre-Pliocenic basement.

Hanging wall strata
The Plioquaternary stratain the hanging wall of the Velenje synclinal valley consist of a series of layers of sand, sand with gravel, silt, arenaceous and clayey silts, arenaceous clays, clays, siltstone and claystone, intertwined in vertical and horizontal direction, thus forming a unique multilayer system, which on the vertical line consists of more than a hundred of layers of different thickness. This sedimentary sequence of the hanging wall is mainly in the central, northern and western part of the synclinal valley, while on the southern and eastern part, the hanging wall consists mainly of clays and claystones silts and silstones.

Coal layer
The coal layer needs to be considered as complex system, consisting of sequences of "Plioquatenary formations" (basement layer, direct footwall, coal layer, Pliocenie hanging wall and Pleistocene hanging wall strata), which are typical for orogenetic active zones. After a short transport period,

coarse-grained clastites were deposited from the north-west into the intramontane depression where a lake was formed.

On the eastern side, where the possibilities of open-pit mining and underground coal gasification have been considered, the coal layer is relatively poor in terms of quality. However, at the opposite end, on the west, the coal layer dips into depth, becomes thicker, and has better quality. The north-eastern edge is characterised by a steep Triassic slope, where the coal layer becomes thinner and turns upwards. At some places the coal directly contacts the Triassic strata. In the central part on the north, and north-west, numerous layers of clay and sand penetrate into the coal layer. Towards south, these layers become thinner and tail out. In this area too, sand layers can be found in the hanging wall.

In Topolšica (on the western side) the coal layer slightly turns up, becomes thinner and tails out. The southern edge of the depression lies directly on the Šoštanj fracture zone, which can be clearly seen from the shape of the coal layer in this area. We can observe sudden changes and interruptions of the layer. In the central part the layer of coal is deepest and of high quality, reaching maximum thickness of 168 metres.

The footwall Pliocene strata
The pre-Pliocene basement is directly covered by basal layers consisting of green arenaceous silts and sands, while above the triassic layers there is some red and grey clay, followed by direct footwall of a similar formation, with increased content of clay.

<u>Pre-Pliocene basement</u>

A great part of the pre-Pliocene basement of the Velenje synclinal valley, as well as the most of the eastern, northern and north-western edge of the valley is composed of Triassic strata of various ages and lythology. Triassic strata, particularly those from middle and upper Triassic period, are limestone and dolomites, which make up a system of aquifers. The system is useful for supplying water, however, it also represents a risk for the mine water inrushes due a close proximity of the mine workings and a thin protective layer.

The central and southern part of the synclinal valley is composed of Oligocene materials (andezite with tuff and breccia) and Miocene sediments (sandstone and litothamnian limestone). Oligocene sediments and Miocene sandstone are impervious and thus not a problem from the hydrogeological point of view. The Miocene litothamnian limestone is an aquifer, however, it covers only a limited area in this mine. In addition, it is not renewed with water, therefore it is irrelevant in this situation.

A brief description of hydrogeological problems in the Velenje Coal Mines

The geological description of the site shows that the Velenje coal mine consists of two main types of aquifers: the Pliocene gravely-sandy aquifers in the hanging wall, and Triassic (dolomites prevailing) in the footwall. There have been no problems with water during excavations in the southern region of the synclinal valley of the mine since there are no aquifers which could have impact on the excavations, neither in the hanging wall, nor in the footwall. However, the situation is dif-ferent in the central, western, northern and eastern parts: the Preloge coal field lies in the northern part, and the Leženj region is situated on the east. The layer of clay between the coal and the water-bearing sands is very thin, only a few metres thick. Due to high water-pessure in the water-bearing sands lying above the coal, these aquifers represent a potential danger for water and quicksand inrush during excavations, and consequently mean direct risk for safe mining. Since the hanging wall consists of a multi-layer system of aquifers, where individual layers are not necessarily connected, the distribution of pressure in these aquifers varies. This means that hydrodynamic properties of the layers are different too.

Because of the potential danger of water and quicksand inrushes, from sandy to silty aquifers close to the hanging wall, it was necessary to decrease water pressure in the lower part of the hanging wall aquifers system to ensure safe mining and to meet the criteria for safe mining (Kočar et al., 1989) to avoid the risk of water inrush. In the period from 1979 to 1988, 36 drift filters were installed in the Velenje coal mine to drain water from the Pliocene hanging wall aquifers. The filters were placed in the following mine dewatering roadways named barrage roadway: central barrage roadway (drift filters V-9o to VO-9), north-western barrage roadway (drift filters BV-2 to BV-13), northern barrage roadway (drift filter BV-20), the barrage roadway running along the synclinal valley (drift filters V-11n to V-12z), and southern barrage roadway, or southern barrage upraise roadway (drift filters BV-22 to BV-31). The central barrage roadway was

constructed as an experimental roadway already in the period from 1979 to 1981, while other drift filters were constructed later and finished in 1988. Since 1984, the central barrage roadway has been connected with the drainage pipeline system in the PV coal mine. These drift filters are still operating on this roadway, draining the water coming from complex Pliocene hanging wall aquifers. Other drift filters were gradually connected to the drainage system in the mine, and since 1996 they have been serving in this purpose.

The design of the drainage system was made based on the experience and knowledge, gained during the experimental drainage in the period 1964-1972. During this period numerous wells for gravitational drainage of water from the hanging wall aquifers into the mine, were made in the Ležcnj area, together with installation of a series of dewatering boreholes (105 objects), which additionally contributed to decrease the water pressure in the sands above the coal, particularly in the areas where surface drainage system, could not be implemented due to excavation operations.

The drainage technology, which was used in the period from 1979 to 1988, was selected upon previous experience and the technology which was used 20 years before that, using submersible pumps to pump water from the wells to the surface (wells NV-1 to NV-4). At that time it was proved that the most efficient method of water drainage is gravitational drainage of water from the hanging wall aquifers via drift filters into the mine.

However, hydrogeological conditions above the Šoštanj coal field demanded a different approach to deal with the problem of water drainage. Thus, two wells for pumping water to the surface were constructed during 1998 and 1999 (BV-23 and BV-24), using the so called MOYNO pumps.

Considering that before any drainage operation, the levels of water throughout the Plioquternary formations are approximately the same, the drainage of water from the hanging wall aquifers would results in lowering the water level: in the sand layers directly above the coal (and the layers above sand) the level would decrease for more than 350 metres, in the upper layers from 100 m to 150 m, depending on whether the aquifer has been drained directly, or indirectly (by leakage from the superimposed layers). In the Quaternary layers the impact of drainage has not been noticed since these layers were not directly drained. Due to the intermediary sealing layers the connection with the underlying Pliocene layers, is too weak.

By simulation of the drainage processes using a mathematical model (1995, 1998) it was proved that, in order to maintain low water-pressure in the sands directly above the coal seam, a good drainage of several subsequent water bearing layers overlying these sands would be needed. Nowadays, in the Preloge coal field, a great part of the drainage system has been abandoned due to coal excavations (the whole central barrage roadway, some wells from the barrage roadway along the synclinal valley, and north-western and northern barrage

roadway). Consequently, the quality of the drainage system in the hanging wall layers has deteriorated: the drainage process has become relatively slow and the effects of the elimination of the drainage will only become evident in the near future.

In addition to this, there have been some problems with the drainage from both wells used for pumping water to the surface. This calls for the construction of substitutional mine drainage fascilities, which would partially replace the drainage by drift filters. For this purpose we developed a technology of a double screen jetted dewatering boreholes, which is presented further on.

Technological implementation of a double screened jetted dewatering boreholes

Conventional methods for constructing dewatering boreholes are frequently unreliable due to high pore pressure which occurs in the aquifers. Thus, already in constructing the jetted dewatering boreholes for a single aquifer we developed a technology which is based on cemented technical pipes and drilling with pipe-screen which is built in the aquifer (Veselič et al., 1991; Vukelić, 2005). Drilling with pipe-screen, can be made if an inner pipe is installed into the screen, which will direct the flow of the drilling fluid through the drilling crown. During the activation procedure this part is removed. To rationalise the drainage processes and to improve the effects of drainage it was necessary to consider the construction of a jetted dewatering borehole, which would use one borehole and simul-

taneously encompass two aquifers, provided that in terms of hydraulics the two aquifers would not interfere with one another (Vukelić, 2005). The technology was developed and tested in the Velenje coal mine in the borehole No. JV 3175–K/03, located on the transport roadway of the excavating plates G1/B in the north-western part of the Preloge cave. The location is presented in Figure 2. There are two factors which are crucial for a successful implementation of the technology: good understanding of hydrogeological conditions and good geological prognosis. The geological prognostic profile of the borehole JV 3175–K/03 is presented in Figure 1. The main feature of this new technology is that drilling is not interrupted after installing the first screen with a larger diameter into the first layer of sands above the coal: drilling can be continued by loosening the drilling crown and activating the screen in the first aquifer. After the screen has been activated, drilling is continued using the first screen and related pipes as liner to the subsequent aquifer. Drilling is performed with a filter with ϕ73 mm diameter through the pipe with ϕ128 mm diameter. After the filter has been installed in the second layer of sand, it is activated. Figure 3 presents the installation of the jetted dewatering borehole into two aquifer layers.

Installation procedure of the jetted dewatering borehole into two layers of aquifers

Construction of the conductor pipe

The conductor pipe is made in a standard way. A borehole for the conductor pipe is drilled with a drilling crown which is
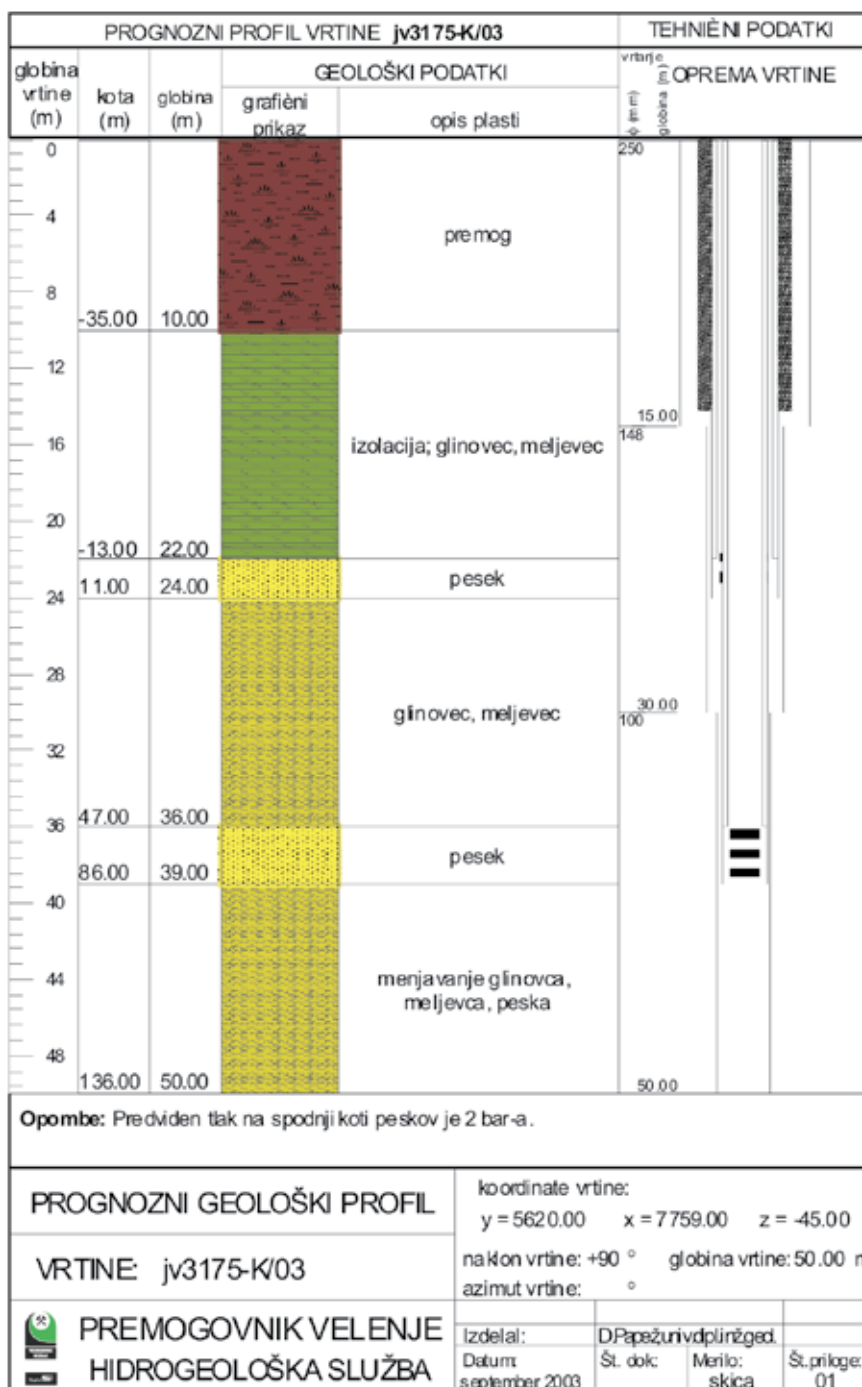
Figure 1. Geological prognostic profile of the borehole JV 3175–K/03
Slika 1. Prognozni geološki profil vrtine JV 3175–K/03

Figure 2. Location of the borehole JV 3175–K/03
Slika 2. Lokacija vrtine JV 3175–K/03

then cased with the conductor pipe. The length and the diameter of the conductor pipe will depend on the length of the jetted dewatering borehole and water pressure in the aquifers lying above the coal. Next, a tightness test of the conductor pipe needs to be carried out: water is pushed into the borehole via the liquidation flange with 50 % greater pressure than the maximum anticipated water pressure in the aquifers. If the borehole does not provide the desired tightness, cement slurry needs to be injected, or the edges of the borehole need to be sealed down with cement. After completing the tightness test, and before proceeding with drilling, it is necessary to fit the mouth of the borehole with tube brakes, and a valve, as shown in Figure 4.

Drilling and installation of the filter into the first aquifer
Drilling through the conductor pipes is carried out in a standard way, using drilling pipes with diameter of φ128 mm and a double-layer screen with φ128/113 mm diameter. The drilling crown of the screen is composed of two parts: a fixed crown

with cutting diameter of φ148 mm, which remains on the screen, and a removable crown fixed to the seal pipe. After fixing the swivel pipe behind the valve (the swivel needs to correspond with the diameter of
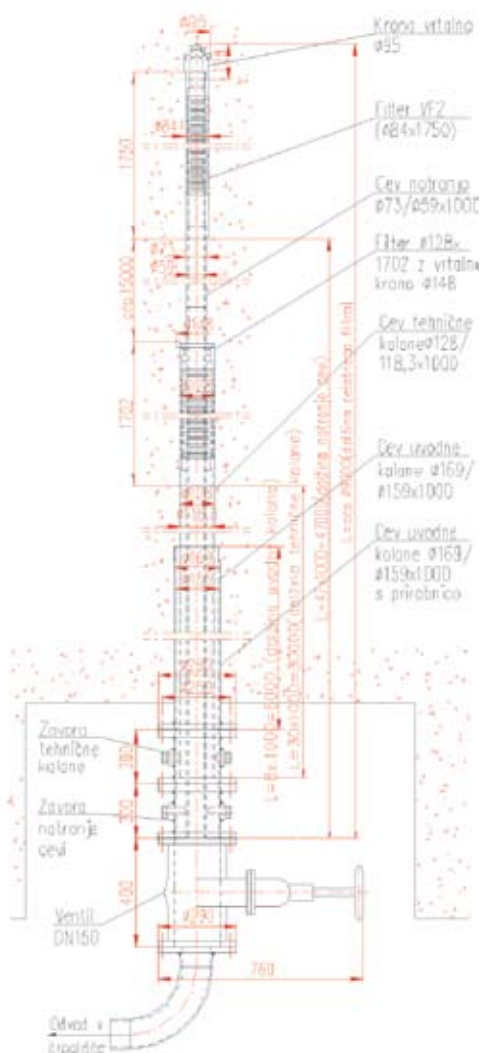
Figure 3. Installation of the jetted dewatering borehole into aquifers
Slika 3. Shematski prikaz vtisnega filtra v dveh paketih vodonosnikov

Figure 4. A flange of the conductor pipe, brakes, a valve, and a swivel pipe
Slika 4. Prirobnica uvodne kolone, zavore, zaporni zasun in izlivka

the pipe of ϕ128 mm), drilling can be continued to a desired depth using a suitable polymer drilling fluid. In the Velenje coal mine we used Modipol 600, a polymer additive (powder), or Argipol, which is a liquid polymer additive. The first layer of the aquifer is activated by loosening the seal head and the removable crown. Figure 5 shows an adapted transportable unit K1 for preparing the drilling fluid, while Figure 6 shows the first filter with diameter of 128 mm with the drilling crown (cutting diameter 148 mm), and the removable crown.

RMZ-M&G 2007, 54

Drilling and installation of the screen into the second aquifer

Further drilling to reach the second water-bearing sand layer, is made through the screen which has been installed and activated. Drilling is performed by using screen VF2, which consists of the filtering part with ϕ84 mm diameter and a cutting crown of ϕ95 mm. The screen is connected with the drilling pipes with ϕ73 mm diameter. In case the material between the first and the second aquifer is harder, it is possible to modify the technology so as to achieve faster drilling, using a pyramid drill. When the desired length of the borehole has been achieved it is necessary to remove the pyramid drill and reinsert jet-in screen, with ϕ84 mm / ϕ95 mm with drilling pipes ϕ73 mm. After that, the screen is activated using the general procedure.

Figure 5. Preparation of the drilling fluid
Slika 5. Priprava izplake

Figure 6. Filter with φ128 mm diameter, a drilling crown with cutting diameter of φ148 mm, fixed to the screen, and removable crown
Slika 6. Filter premera φ128 mm, vrtalna krona z rezalnim premerom φ148 mm, ki je fiksirana na filtru in izvlačljiva krona

EQUIPMENT FOR THE CONSTRUCTION OF JETTED DEWATERING BOREHOLE INTO TWO AQUIFER LAYERS

The following equipment is needed for the construction of jetted dewatering borehole:

• a RVS-Max drill	45 kW
• ČGZ 250 Pump, or TRIDO 220 pump	22 kW
• Submersible pump [3 m³/min]	37 kW
• Flygt Submersible pump	2.9 kW
• suitable pipe armature	
• telephone	
• illumination of the worksite	
• supply of technological water and wastewater drainage	

RVS-Maxdrill

The RVS-Max drill is used for drilling in mine workings and in methane conditions, and particularly for drilling of boreholes for the drainage from water-bearing layers. The RVS-Max drill is manufactured by HTZ Velenje.

Basic components of the RVS-Maxdrill

1. Hydraulic drive unit (Figure 7), which is an independent transportable unit, driven by a 45 kW (500 V) electric engine. Secondary drive is provided by two hydraulic pumps.

2. A mast with integrated extension and double clamping jaws (Figure 8). The mast facilitates the movement of the carriage with rotation head and provides movement of the drilling pipes forward and backward during drilling. The stroke-length of the head allows for the use of pipes with 1500 mm in length. The pull-down and the pullback force is transmitted to the pipes via a hydraulic cylinder and a stud-link chain Wipermann ¾''. The extension of the mast is integrated, with double clamping jaws attached to it.

3. A system for fixing or supporting the mast (hydraulic - mechanical support).

4. Control panel with driving and control tools (Figure 9).

5. The rotation head on the carriage is a multi-stage reduction gear, driven by two hydro engines, which can be started in three different modes.

Figure 7. Hydraulic drive unit
Slika 7. Pogonski hidravlični agregat

Figure 8. A mast with the rotation head, clamping jaws and the system for fixing the mast
Slika 8. Lafeta z rotacijsko glavo, vpenjalnimi čeljustmi ter sistemom za vpetje lafete

Figure 9. Control desk
Slika 9. Kontrolno krmilna plošča

Technical data

Rotating head stroke	1500 mm
Mast length	2500 mm
Max. speed	0.3 m/s
Operating oil-pressure	180 bar
Max. thrust force	4500 N
Machine weight	1700 kg

Level	Moment [Nm]	Rotation [rev/min]
I (M1+M2)	3150	100
II (M2)	1240	254
III (M1)	1930	163

Clamping jaws: technical data

	Clamping diameter [mm]	Clamping force [N]
Front jaws	42 - 73	6900
Rear jaws	89 - 163	6900

TIMEFRAME FOR THE CONSTRUCTION OF THE JETTED DEWATERING BOREHOLE

The construction procedure of the jetted dewatering borehole for working through two aquifers is an upgraded version of the standard construction procedure such a borehole for a single aquifer. Additional time is required for installation of an additional brake, and preparation of the second screen and for drilling, activation of the second screen, etc.

In our case, the total time needed for drilling was 691 min, for pushing down and removing the drill pipes 427 min, and for auxiliary works 353 min. The distribution of time needed for various work-phases in installing both screens is presented in Graph 1 below.

Legend:
- drilling
- pulling back the drilling pipes
- auxiliary works
- deadlocks
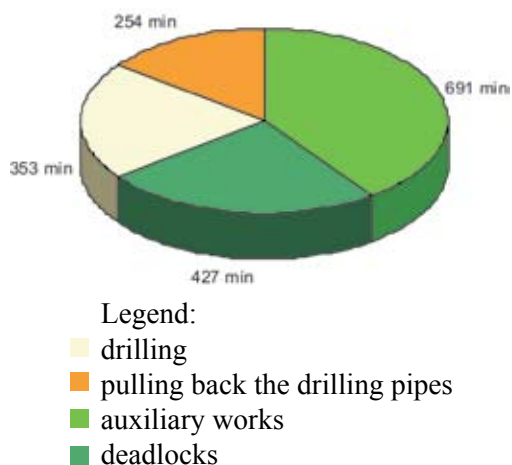
Graph 1. Time distribution of the operations for the installation of two jet-in screens
Diagram 1. Čas trajanja delovnih faz pri vgradnji dveh filtrov

A more detailed time-frame is presented below:
Screen one: drilling: 548 min, pushing the drill pipes: 58 min, and auxiliary works 263 min.
Screen two: drilling: 143 min, pushing and removal drill pipes: 369 min, and auxiliary works: 90 min.
The auxiliary works included: preparation works, assembling and dismantling of the pipe brakes, the swivel, the valve, the sealing head, fixing the pipe brakes, etc.

The histogram below (Graph 2) shows the comparison between the duration of work phases in the first and the second screen instalation. A significant difference can be observed in the duration of drilling, and the time needed for pushing down and pulling back the drill pipes.

Drilling through the first water-bearing layer took more time than drilling through the second layer. The average drilling speed used for the first screen was 2.1 cm/min, and 2.0 cm/min for the second screen (drilling was performed at the length of only 2.45 m), and 39.2 cm/min for drilling with the drilling pyramid (for the second filter). The difference in time was also due to the different length of the boreholes in the first and the second screen.

During the emplacement of second jet-in screen, more time was spent for pushing and pulling out the drill pipes. This is because the screen was equipped with the drilling crown, and because more drill pipes which had to be inserted into or removed from the borehole.

We saved no time for the preparations of the drilling set and the worksite, and for removing the drilling set and cleaning the worksite, and preparation of the drilling fluid and construction of the conductor pipe. The total time needed for these operations was similar to any other drilling operations.

CONCLUSIONS

To ensure safe mining under water-bearing layers it is necessary to provide drainage to minimise water pressure in the aquifers lying above the coal layer. Water pressure is one of the main entry data in calculating the permissible height of excavation. This means that it is necessary to introduce suitable monitoring methods to control changes in water pressure which is the indicator of the effects of drainage. Since by excavation works in the north-western part of the Preloge coal field the system of surface
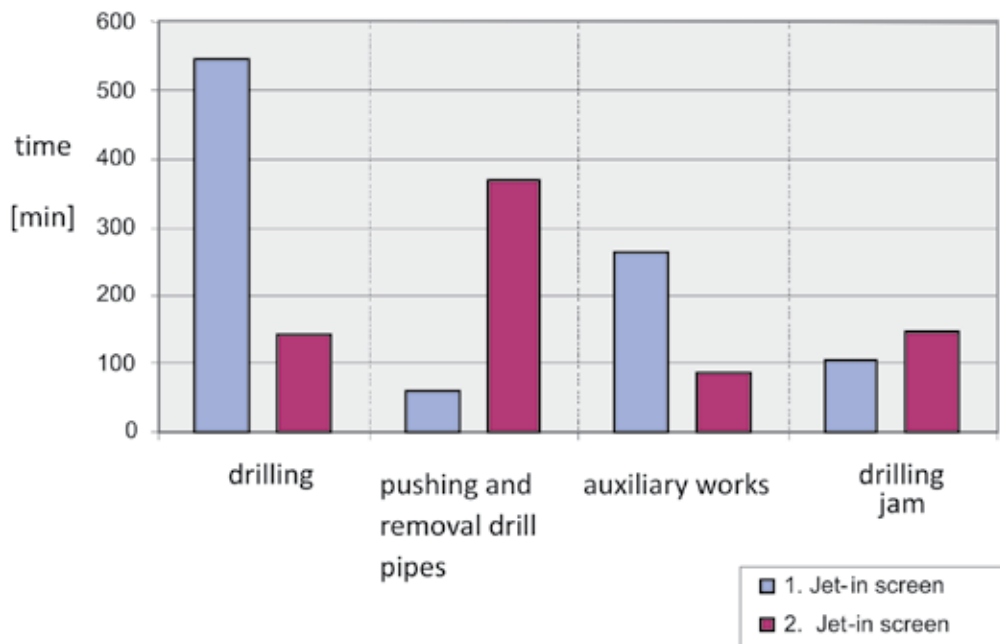
Graph 2. Duration of work operations in installing the impressed filter into
the aquifer 1 and 2
Diagram 2. Primerjava trajanja delovnih faz pri izdelavi vtisnega filtra v 1.
oziroma v 2. vodonosnik

observation wells and drift filters has been
damaged to a great extent, it was necessary
to find a suitable replacement. This was
done by installation of jetted dewatering
boreholes. From the existing jetted dewa-
tering boreholes, which dewater just one
aquifer, we have developed a completely
new technology for jetted dewatering
boreholes installation which would drain
two aquifers simultaneously, while each of
the aquifers is drained separately. In this
way we have significantly shortened the
time needed for the construction of a jet-
ted dewatering boreholes drainage system
and thus made the construction of drainage
facilities more cost-effective.

Povzetek

Tehnologija izdelave vtisnega filtra v dva
paketa vodonosnikov

Za zagotavljanje varnega odkopavanja
pod vodonosnimi plastmi je potrebno v
največji možni meri z odvodnjevalnimi
procesi znižati tlake vode v vodonosnikih
nad premogovim slojem. Tlak vode je tudi
eden izmed glavnih vhodnih podatkov pri
izračunu dovoljenih višin odkopavanja,
zato je za pridobitev realnih podatkov
potrebno izvajati tudi ustrezen monitoring
gibanja tlakov vode, ki so kazalec učinkov
odvodnjevanja. Ker si z odkopavanjem SZ

predela jame Preloge v veliki meri rušimo sistem površinskih piezometrov in visečih filtrov, je potrebno najti nadomestilo zanje. Rešitev se kaže v izdelavi nadomestnih jamskih objektov - vtisnih filtrov. Tehnologija izdelave vertikalnih in poševnih vtisnih filtrov z vrtanjem s cevmi filtra v en vodonosnik, je v jamah Premogovnika Velenje prisotna od leta 1990. Intenzivno odvodnjevanje krovninskih vodonosnikov z jamskimi vrtinami pa se je v jami Škale izvajalo že od leta 1960. Zaradi omejitev jamskega vrtanja, je vtisni filter izdelan po tehnologiji vrtanja s cevmi filtra funkcijsko slabši kot objekt - viseči filter, ki ga izdelamo iz površine. Za izboljšanje učinkov odvodnjevanja z vtisnimi filtri, vidimo rešitev predvsem v povečanju gostote izdelave vtisnih filtrov ali v zajemanju dveh vodonosnikov hkrati na eni vrtini. Vrtanje s cevmi filtra je možno, če v filtrski del vgradimo notranjo cev, ki usmerja tok izplake neposredno skozi vrtalno krono. Pri postopku aktivacije ta del izvlečemo. Zaradi racionalizacije odvodnjevalnih procesov in izboljšanja odvodnjevalnih učinkov, je bilo smiselno razmišljati o izvedbi vtisnega filtra, ki preko ene vrtine zajema dva vodonosnika hkrati, ob pogoju, da hidravlično ne vplivata drug na drugega. Tako smo razvili popolnoma novo tehnologijo izdelave vtisnih filtrov, ki omogočajo zajem dveh vodonosnikov. Tehnologija zajema dveh vodonosnikov, pomeni tudi občutno znižanje stroškov jamskih odvodnjevalnih objektov.

References

Bourgoyne, A.T., Chenevert, M.E., Miliheim, K.K., Young, F.S. (1991): *Applied Drilling Engineering*. Society of Petroleum Engineers, pp. 246-252.

Brnic, Z. (1989): *Prirucnik o isplaci*. INA-NAFTAPLIN, Zagreb, pp. 293-309.

Kočar, F., Veselič, M., Ribičič, M., Mramor, J. (1989): Kriterij varnega odkopavanja premoga pod vodonosnimi plastmi v Rudniku lignite Velenje. *Rudarsko metalurški zbornik.*; Vol. 36, No. 2, pp. 421-438.

Miharija, I., Galic, V. (1987): *Sprecavanje erupcije i kontrola dotoka*. INA-NAFTAPLIN, Zagreb, pp. 71-86.

Veselič, M., Enichlmayr, E., Vejvar, E., Popovič, M. (1991): Mine dewatering techniques and technology applied at SAKOG brown coal mine. *Proceeding of 4. IMWA Congress.*; Vol. 2, pp. 183-188, SP GZL IGGG & IMWA, Ljubljana.

Vukelić, Ž. (2005): *Tehnologija izdelave in vgradnja vtisnih filtrov*. Naravoslovnotehniška fakulteta, Oddelek za geotehnologijo in rudarstvo, Ljubljana.

A realistic estimate of the accuracy of position measurements of characteristic terrain points via the RTK-GPS method

Realna ocena natančnosti določanja karakterističnih točk terena po metodi RTK-GPS

MILIVOJ VULIĆ[1], ALEŠ LAMOT[2]

[1]University of Ljubljana, Faculty of Natural Sciences and Engineering, Department of Geotechnology and Mining Engineering, Aškerčeva cesta 12, SI-1000 Ljubljana, Slovenia;
E-mail: milivoj.vulic@ntf.uni-lj.si
[2]Ivan Potočnik s.p.-Drilling, Blasting and Fireworks, SI-3310 Žalec, Slovenia;
E-mail: potocnik.ognjemeti@siol.net

Abstract: Here at the Faculty of Natural Sciences and Engineering, we are developing our very own method for determining said volumes; a method that has thus far been lacking in an estimation of the accuracy of determining the position of characteristic points of the plane via the RTK-GPS method. With the aid of measurements of three different types of points, i.e. points with three different point placements, we have managed to engulf the measurements, which we then use to shape an estimation regarding the accuracy of characteristic terrain points' measurements when it comes to those points which are not materialised i.e. labelled - the third type. When measuring the positions of characteristic terrain points, what is encompassed in the procedure is both the accuracy of the GPS measuring aid as well as the accuracy regarding of the positioning of the characteristic points themselves with an average operator in mind. For the determination of the characteristic points of the plane, and with the aid of an overviewing computer programme (Microsoft Excel), a model intended for the levelling measurements of the positions of characteristic plane points and the determination of accuracy when it comes to the determination of said point positions has now been designed. The model represents an automatised process of point position measurements' levelling, and allows one to enter measuring data – the coordinates of a given point, the *a priori* standard deviation $\hat{\sigma}_0$ and the correlation matrix **Q** as the incoming data. The outgoing data is then obtained in the form of already levelled coordinates of characteristic points, the standard deviation of the weighted standard deviation $\hat{\sigma}_0$ *a posteriori*, deviations in the directions of coordinate axes $\hat{\sigma}_y$, $\hat{\sigma}_x$, $\hat{\sigma}_z$, the main standard deviations i.e. the attributed values of the tensor of deviations of point measurements and deviation pedaloid itself. In the computer programme MS Excel, a model aimed at the calculation of main deviations i.e. attributed

---

Scientific paper

values of the points' deviation tensor as well as the determination of pedalloid (ellipsoid) deviations is given.

Izvleček: Na Naravoslovnotehniški fakulteti se razvija lastna metoda za določanje prostornin, kateri je do sedaj manjkala ocena natančnosti določanja položaja karakterističnih točk ploskve po metodi RTK-GPS. Z meritvami točk s tremi različnimi postavitvami na točkah, in sicer s prisilnim centriranjem, s togim grezilom na znanih točkah in s togim grezilom s simuliranjem postavitve na karakt. točkah smo zajeli meritve, s katerimi smo podali oceno natančnosti merjenj karakt. točk terena, ki niso materializirane oziroma označene. Tako je zajeta natančnost GPS izmere kot tudi natančnost postavitve na karakt. točkah terena pri povprečnem operaterju. Za določitev natančnosti karakt. točk ploskve je sedaj, s pomočjo računalniškega programa za preglednice, izdelan model za izravnavo meritev položaja karakt. točk ploskve ter določitev natančnosti določanja položaja karakt. ploskve. Model predstavlja avtomatiziran proces izravnave merjenj položaja točke in omogoča, da se kot vhodni podatki vstavijo podatki merjenj, in sicer koordinate točke, *a priori* srednji pogrešek $\hat{\sigma}_0$ in korelacijska matrika **Q**. Izhodni podatki pa se dobijo kot izravnane koordinate karakt. točk, srednji pogrešek utežne enote $\hat{\sigma}_0$ *a posteriori*, pogreški v smereh koordinatnih osi $\hat{\sigma}_Y$, $\hat{\sigma}_X$, $\hat{\sigma}_Z$, glavni srednji pogreški oziroma lastne vrednosti tenzorja pogreškov merjenja točke in pedaloid pogreškov. V računalniškem programu MS Excel je podan tudi model za izračun glavnih pogreškov oziroma lastnih vrednosti tenzorja pogreškov točke in določitev pedaloidov (elipsoidov) pogreškov.

Key words: RTK-GPS, RTK-DGPS, main deviations, accuracy
Ključne besede: RTK-GPS, RTK-DGPS, glavni pogreški, natančnost

INTRODUCTION

Focusing on realistic, on-location measurements of characteristic terrain points and their belonging errors, rather than only those allotted by whatever programme we happen to be using to later on process said measured data, we are able to get a truer-to-life assessment of the accuracy of our measurements. The RTK-GPS (Real Time Kinematic - Global Positioning System) is one of the tools we may use to aid us in the accomplishment of this. It may actually be used for both determining the shape of our measured terrain as well as its belonging surface and volume, which proves useful in engulfing the measurements of points of three different point placements, further categorised as we elaborate on the procedure in pages to come. Thus, we are one step closer to shaping an estimation regarding the accuracy of characteristic terrain points' measurements.

What is important is that we keep in mind both the accuracy of the GPS measuring aid as well as the accuracy of an average human operator dealing with it when it comes to the positioning of the the characteristic points. As for the actual determination of

the latter, what has now been designed with the aid of Microsoft Excel, our chosen overwieving computer tool, is a model intended for the levelling measurements of the positions of characteristic plane points and the determination of accuracy when it comes to said point positions. Here at the Faculty of Natural Sciences and Engineering, the design of such a simple and financially undemanding model - oriented at the levelling that comes with characteristic points' accuracy measurements - has still managed to enhance the accuracy estimations associated with the measurements of characteristic terrain points, as we will now proceed to make evident.

THE LEVELLING MEASUREMENT OF POINTS AIMED AT DETERMINING THE ACCURACY OF THE CHARACTERISTIC POINTS OF A PLANE

When it comes to a derisive levelling of corellated measurements, it is necessary to determine the most probably value of the unknown vector $\mathbf{x}_{u \times 1}$ with the aid of the vector of measured quantities $\mathbf{l}_{nu \times 1}$ with the aid of *a priori* known corellations $\Sigma_{nu \times nu}$, and give an estimate i.e. evaluation of the accuracy of all these measuremants i.e. the sought-for quantities. When it comes to the latter, the number n is the number of measured quantities i.e. measurements, and u is the number of sought-for (unknown) quantities.

With one derisive levelling of corellated measurements, the sought-for (unknown) quantities are determined via a string of measurements, but all this under the condition that the sum of squares of their correlated residuals is smallest:

$$\underset{1 \times nu}{\mathbf{v}^{\mathrm{T}}} \underset{nu \times nu}{\Sigma_{ll}^{-1}} \underset{nu \times 1}{\mathbf{v}} = \min \tag{1}$$

where:

- $\underset{nu \times nu}{\Sigma_{ll}^{-1}}$, the correlation matrix of measured quantities is the matrix of cofactors of said measured quantities
- $\underset{nu \times 1}{\mathbf{v}}$ is the vector of residuals of the measured quantities.

When it comes to measuring sciences, the determination of a uniform solution is obtained through the least squares method (LS).

In the case of a derisive levelling procedure, what is determined first is the residuals' vector $\underset{u \times 1}{\xi}$ of approximate values of the unknown values $\underset{u \times 1}{\mathbf{x}}$, and then the residuals of measured quantities $\underset{nu \times 1}{\mathbf{v}}$ may be dealt with. For n derisive measurements, the vector of residuals is labelled as $\underset{nu \times 1}{\mathbf{v}}$, the matrix of coefficients of equations of the residuals – the design matrix - as $\underset{nu \times u}{\mathbf{A}}$, the vector of derivatives of unknowns as $\underset{u \times 1}{\xi}$, and the vector of free terms with $\underset{n \times 1}{\mathbf{f}}$, which would make it:

$$\underset{nu \times 1}{\mathbf{v}} = \begin{bmatrix} \mathbf{v}_1 \\ \mathbf{v}_2 \\ \mathbf{v}_3 \\ \vdots \\ \mathbf{v}_n \end{bmatrix}, \underset{nu \times u}{\mathbf{A}} = \begin{bmatrix} a_{11} & a_{12} & \cdots & a_{1u} \\ a_{21} & a_{22} & \cdots & a_{2u} \\ \vdots & \vdots & \ddots & \vdots \\ a_{n1} & a_{n2} & \cdots & a_{nu} \end{bmatrix}, \underset{u \times 1}{\xi} = \begin{bmatrix} \xi_1 \\ \xi_2 \\ \xi_3 \\ \vdots \\ \xi_u \end{bmatrix}, \underset{nu \times 1}{\mathbf{f}} = \begin{bmatrix} \mathbf{f}_1 \\ \mathbf{f}_2 \\ \mathbf{f}_3 \\ \vdots \\ \mathbf{f}_n \end{bmatrix} \tag{2}$$

That is how, for n derisive measurments, with the aid of with the u of unknowns is to be determined, the system of residual equations of measured quantities equals:

$$\underset{nu \times 1}{\mathbf{v}} = \underset{nu \times u}{\mathbf{A}} \cdot \underset{u \times 1}{\xi} + \underset{nu \times 1}{\mathbf{f}} \tag{3}$$

The vector of free terms $\mathbf{f}_{nux1}$ can symbolically be denoted as:

f = approximate value – measured value

$\mathbf{f} = \mathbf{f}_{pribl} - \mathbf{1}$
$\mathbf{f} = \mathbf{f}\,(\xi_1\xi_2\xi_3...\xi_u) - \mathbf{1}$ (4)

For u unknowns, equations of free terms for an n number of measurements may be written as:

$$\mathbf{f}_1 \atop {}_{ux1} = \mathbf{f}_1\,(\xi_1\xi_2\xi_3...\xi_u) - \mathbf{1}_1 \atop {}_{ux1}$$

$$\mathbf{f}_2 \atop {}_{ux1} = \mathbf{f}_2\,(\xi_1\xi_2\xi_3...\xi_u) - \mathbf{1}_2 \atop {}_{ux1}$$

$$\mathbf{f}_3 \atop {}_{ux1} = \mathbf{f}_3\,(\xi_1\xi_2\xi_3...\xi_u) - \mathbf{1}_3 \atop {}_{ux1}$$ (5)

$$\vdots$$

$$\mathbf{f}_n \atop {}_{ux1} = \mathbf{f}_n\,(\xi_1\xi_2\xi_3...\xi_u) - \mathbf{1}_n \atop {}_{ux1}$$

The determination of a vector of unknowns ξ [1], the calculation of a matrix of coefficients of normal equations $\mathbf{N}_{uxu}$ and the determination of the vector of free terms $\mathbf{n}_{ux1}$ (FEIL, 1990)

The vector of unknowns ξ_{ux1} is begotten:

$$\xi \atop {}_{ux1} = -\mathbf{N}^{-1}_{uxu}\,\mathbf{n}_{ux1}$$ (6)

where:

- $\mathbf{N}_{uxu}$ is the matrix of the coefficients of normal equations:

$$\mathbf{N}_{uxu} = \mathbf{A}^T_{uxnu}\,\boldsymbol{\Sigma}^{-1}_{ll \atop nuxnu}\,\mathbf{A}_{nuxu}$$ (7)

---

[1] In an ample amount of books pertaining to this area, the vector of unknowns is denoted also as **x**. Due to practical reasons, however, the vector of unknowns may also be denoted with the Greek letter ξ, thus making matters more concise when it is to be dealt with in actual equations.

- $\mathbf{n}_{ux1}$ is the vector of free terms:

$$\mathbf{n}_{ux1} = \mathbf{A}^T_{uxnu}\,\boldsymbol{\Sigma}^{-1}_{ll \atop nuxnu}\,\mathbf{A}_{unx1}$$ (8)

- $\mathbf{A}_{nuxu}$ is the matrix of coefficients of residual equations - the so-called design matrix

- $\boldsymbol{\Sigma}^{-1}_{ll \atop nuxnu}$ is the corellation matrix of measured quantities

Considering that:

$$\mathbf{Q}_{\xi\xi} = \mathbf{N}^{-1}_{uxu}$$ (9)

- $\mathbf{Q}_{\xi\xi \atop uxu}$ is the matrix of covariances and the vector of unknowns denoted as ξ_{ux1} may also be written down as:

$$\xi \atop {}_{ux1} = -\mathbf{Q}_{\xi\xi \atop uxu}\,\mathbf{n}_{ux1}$$ (10)

The correlation matrix of measured quantities $\boldsymbol{\Sigma}_{ll \atop nuxnu}$ (FEIL, 1990)

For each correlated measurement l_i there is a belonging – on the basis of calculated variances and covariances pertaining to prior variantly known measurements – covariance matrix i.e. correlation between measured quantities $\boldsymbol{\Sigma}_{uxu}$ and the *a priori* standard deviation of the (prior) levelling σ_0. For murtually dependent measurements ðf varying accuracies, the matrix of cofactors of each measurement by itself is a symmetrical matrix, as seen below:

$$\boldsymbol{\Sigma}_{ll \atop uxu} = \hat{\sigma}^2_{0i}\,\mathbf{Q}_{i \atop uxu}$$ (11)

$$\boldsymbol{\Sigma}_{ll_i \atop uxu} = \hat{\sigma}^2_{0i} \cdot \begin{bmatrix} q_{xx} & q_{xy} & q_{xz} & \cdots & q_{xu} \\ q_{xy} & q_{yy} & q_{yz} & \cdots & q_{yu} \\ q_{xz} & q_{yz} & q_{zz} & \cdots & q_{zu} \\ \vdots & \vdots & \vdots & \ddots & \vdots \\ q_{xu} & q_{yu} & q_{zu} & \cdots & q_{uu} \end{bmatrix}_{uxu}$$ (12)

$$\Sigma_{\hat{l}\hat{l}_i}_{u \times u} = \begin{bmatrix} q_{xx}\hat{\sigma}_{0i}^2 & q_{xy}\hat{\sigma}_{0i}^2 & q_{xz}\hat{\sigma}_{0i}^2 & \cdots & q_{xu}\hat{\sigma}_{0i}^2 \\ q_{xy}\hat{\sigma}_{0i}^2 & q_{yy}\hat{\sigma}_{0i}^2 & q_{yz}\hat{\sigma}_{0i}^2 & \cdots & q_{yu}\hat{\sigma}_{0i}^2 \\ q_{xz}\hat{\sigma}_{0i}^2 & q_{yz}\hat{\sigma}_{0i}^2 & q_{zz}\hat{\sigma}_{0i}^2 & \cdots & q_{zu}\hat{\sigma}_{0i}^2 \\ \vdots & \vdots & \vdots & \ddots & \vdots \\ q_{xu}\hat{\sigma}_{0i}^2 & q_{yu}\hat{\sigma}_{0i}^2 & q_{zu}\hat{\sigma}_{0i}^2 & \cdots & q_{uu}\hat{\sigma}_{0i}^2 \end{bmatrix}_{u \times u} = \hat{\sigma}_{0i}^2 \mathbf{Q}_{\hat{l}\hat{l}}_{u \times u} \quad (13)$$

The correlatory matrix of measured quantities $\Sigma_{\hat{l}\hat{l}}_{nu \times nu}$ for u unknowns and n measurements is made up of the following sub-matrices:

$$\Sigma_{\hat{l}\hat{l}_{ij}}_{nu \times nu} = \begin{bmatrix} \Sigma_{\hat{l}\hat{l}11}_{u \times u} & \Sigma_{\hat{l}\hat{l}12}_{u \times u} & \cdots & \Sigma_{\hat{l}\hat{l}1n}_{u \times u} \\ \Sigma_{\hat{l}\hat{l}12}_{u \times u} & \Sigma_{\hat{l}\hat{l}22}_{u \times u} & \cdots & \Sigma_{\hat{l}\hat{l}2n}_{u \times u} \\ \vdots & \vdots & \ddots & \vdots \\ \Sigma_{\hat{l}\hat{l}1n}_{u \times u} & \Sigma_{\hat{l}\hat{l}2n}_{u \times u} & \cdots & \Sigma_{\hat{l}\hat{l}nn}_{u \times u} \end{bmatrix}_{nu \times nu} \quad (14)$$

Sub-matrices are of the shape depicted below:

$$\Sigma_{\hat{l}\hat{l}_{ii}}_{u \times u} = \begin{bmatrix} \Sigma_{xxi} & \Sigma_{xyi} & \Sigma_{xzi} & \cdots & \Sigma_{xui} \\ \Sigma_{xyi} & \Sigma_{yyi} & \Sigma_{yzi} & \cdots & \Sigma_{yui} \\ \Sigma_{xzi} & \Sigma_{yzi} & \Sigma_{zzi} & \cdots & \Sigma_{zui} \\ \vdots & \vdots & \vdots & \ddots & \vdots \\ \Sigma_{xui} & \Sigma_{yui} & \Sigma_{zui} & \cdots & \Sigma_{uui} \end{bmatrix}_{u \times u} \quad (15)$$

$$\Sigma_{\hat{l}\hat{l}_{ij}}_{u \times u} = \begin{bmatrix} 0 & 0 & 0 & \cdots & 0 \\ 0 & 0 & 0 & \cdots & 0 \\ 0 & 0 & 0 & \cdots & 0 \\ \vdots & \vdots & \vdots & \ddots & \vdots \\ 0 & 0 & 0 & \cdots & 0 \end{bmatrix}_{u \times u} \quad (16)$$

That is how the correlation matrix of measured values is composed of the following sub-matrices:

$$\Sigma_{\hat{l}\hat{l}}_{nu \times nu} = \begin{bmatrix} \begin{bmatrix} \Sigma_{xx1} & \Sigma_{xy1} & \Sigma_{xz1} & \cdots & \Sigma_{xu1} \\ \Sigma_{xy1} & \Sigma_{yy1} & \Sigma_{yz1} & \cdots & \Sigma_{yu1} \\ \Sigma_{xz1} & \Sigma_{yz1} & \Sigma_{zz1} & \cdots & \Sigma_{zu1} \\ \vdots & \vdots & \vdots & \ddots & \vdots \\ \Sigma_{xu1} & \Sigma_{yu1} & \Sigma_{zu1} & \cdots & \Sigma_{uu1} \end{bmatrix} & \begin{bmatrix} 0 & 0 & 0 & \cdots & 0 \\ 0 & 0 & 0 & \cdots & 0 \\ 0 & 0 & 0 & \cdots & 0 \\ \vdots & \vdots & \vdots & \ddots & \vdots \\ 0 & 0 & 0 & \cdots & 0 \end{bmatrix} & \cdots & \begin{bmatrix} 0 & 0 & 0 & \cdots & 0 \\ 0 & 0 & 0 & \cdots & 0 \\ 0 & 0 & 0 & \cdots & 0 \\ \vdots & \vdots & \vdots & \ddots & \vdots \\ 0 & 0 & 0 & \cdots & 0 \end{bmatrix} \\ \begin{bmatrix} 0 & 0 & 0 & \cdots & 0 \\ 0 & 0 & 0 & \cdots & 0 \\ 0 & 0 & 0 & \cdots & 0 \\ \vdots & \vdots & \vdots & \ddots & \vdots \\ 0 & 0 & 0 & \cdots & 0 \end{bmatrix} & \begin{bmatrix} \Sigma_{xx2} & \Sigma_{xy2} & \Sigma_{xz2} & \cdots & \Sigma_{xu2} \\ \Sigma_{xy2} & \Sigma_{yy2} & \Sigma_{yz2} & \cdots & \Sigma_{yu2} \\ \Sigma_{xz2} & \Sigma_{yz2} & \Sigma_{zz2} & \cdots & \Sigma_{zu2} \\ \vdots & \vdots & \vdots & \ddots & \vdots \\ \Sigma_{xu2} & \Sigma_{yu2} & \Sigma_{zu2} & \cdots & \Sigma_{uu2} \end{bmatrix} \cdots & & \begin{bmatrix} 0 & 0 & 0 & \cdots & 0 \\ 0 & 0 & 0 & \cdots & 0 \\ 0 & 0 & 0 & \cdots & 0 \\ \vdots & \vdots & \vdots & \ddots & \vdots \\ 0 & 0 & 0 & \cdots & 0 \end{bmatrix} \\ & \vdots & \vdots \qquad \vdots & \vdots \\ \begin{bmatrix} 0 & 0 & 0 & \cdots & 0 \\ 0 & 0 & 0 & \cdots & 0 \\ 0 & 0 & 0 & \cdots & 0 \\ \vdots & \vdots & \vdots & \ddots & \vdots \\ 0 & 0 & 0 & \cdots & 0 \end{bmatrix} & \begin{bmatrix} 0 & 0 & 0 & \cdots & 0 \\ 0 & 0 & 0 & \cdots & 0 \\ 0 & 0 & 0 & \cdots & 0 \\ \vdots & \vdots & \vdots & \ddots & \vdots \\ 0 & 0 & 0 & \cdots & 0 \end{bmatrix}_{nu \times nu} \cdots & & \begin{bmatrix} \Sigma_{xxn} & \Sigma_{xyn} & \Sigma_{xzn} & \cdots & \Sigma_{xun} \\ \Sigma_{xyn} & \Sigma_{yyn} & \Sigma_{yzn} & \cdots & \Sigma_{yun} \\ \Sigma_{xzn} & \Sigma_{yzn} & \Sigma_{zzn} & \cdots & \Sigma_{zun} \\ \vdots & \vdots & \vdots & \ddots & \vdots \\ \Sigma_{xun} & \Sigma_{yun} & \Sigma_{zun} & \cdots & \Sigma_{uun} \end{bmatrix} \end{bmatrix} \quad (17)$$

which can, in short, be denoted as:

$$\Sigma_{\hat{l}\hat{l}} \atop {nu \times nu} = \begin{bmatrix} \Sigma_{\hat{l}\hat{l}11} & \mathbf{0} & \cdots & \mathbf{0} \\ {u \times u} & {u \times u} & & {u \times u} \\ \mathbf{0} & \Sigma_{\hat{l}\hat{l}22} & \cdots & \mathbf{0} \\ {u \times u} & {u \times u} & & {u \times u} \\ \vdots & \vdots & \ddots & \vdots \\ \mathbf{0} & \mathbf{0} & \cdots & \Sigma_{\hat{l}\hat{l}nn} \\ {u \times u} & {u \times u} & & {u \times u} \end{bmatrix}_{nu \times nu}$$ (18)

The inverse (matrix) of the matrix of measured quantities is thus denoted as:

$$\Sigma_{\hat{l}\hat{l}}^{-1} \atop {nu \times nu} = \begin{bmatrix} \Sigma_{\hat{l}\hat{l}11}^{-1} & \mathbf{0} & \cdots & \mathbf{0} \\ {u \times u} & {u \times u} & & {u \times u} \\ \mathbf{0} & \Sigma_{\hat{l}\hat{l}22}^{-1} & \cdots & \mathbf{0} \\ {u \times u} & {u \times u} & & {u \times u} \\ \vdots & \vdots & \vdots & \vdots \\ \mathbf{0} & \mathbf{0} & \cdots & \Sigma_{\hat{l}\hat{l}nn}^{-1} \\ {u \times u} & {u \times u} & & {u \times u} \end{bmatrix}_{nu \times nu}$$ (19)

which may, again, be shortened to:

$$\Sigma_{\hat{l}\hat{l}}^{-1} \atop {nu \times nu} = \text{diag} \begin{bmatrix} \Sigma_{\hat{l}\hat{l}11}^{-1} & \Sigma_{\hat{l}\hat{l}22}^{-1} & \cdots & \Sigma_{\hat{l}\hat{l}nn}^{-1} \\ {u \times u} & {u \times u} & & {u \times u} \end{bmatrix}$$ (20)

and is the row-specific matrix of the inverse correlation sub-matrices $\Sigma_{\hat{l}\hat{l}ii} \atop {u \times u}$ of individual measured unknowns ξ_1, ξ_2, ξ_3, ..., ξ_u .

When we are dealing with the measurements of point positions via the RTK-GPS method, each measurement in itself may beget its own varance-covariance matrix Σ_{ll}. The variance-covariance matrix $\Sigma_{ll} \atop {nu \times nu}$ is determined on the basis of different measurement influences of the time. Sad »influences« are, in fact, the disparations of the receiver's an the satellite's timers, the atmosphere's influence upon wave expansion, a mistake pertaining to the determination of the hight of the antennae etc.

For an individual point measurement, we are thus able to obtain the coordinates of the measured point, as well as the sub-matrix $\Sigma_{\hat{l}\hat{l}i} \atop {3 \times 3}$.

As has already been depicted in equations (14) to (17), for the determination of a variance-covariance matrix $\Sigma_{ll} \atop {nu \times nu}$, it is already enough when we are acquainted with the correlation matrices of an individual measurement $\Sigma_{\hat{l}\hat{l}i} \atop {3 \times 3}$. The sub-matrices $\Sigma_{\hat{l}\hat{l}i} \atop {3 \times 3}$ are symmetrical matrices, and can therefore be written as below for each of the individual measurements:

$$\Sigma_{\hat{l}\hat{l}i} \atop {3 \times 3} = \hat{\sigma}_0^2 \begin{bmatrix} Q11 & Q12 & Q13 \\ & Q22 & Q23 \\ & & Q33 \end{bmatrix} =$$

$$= \hat{\sigma}_0^2 \begin{bmatrix} Q11 & Q12 & Q13 \\ Q12 & Q22 & Q23 \\ Q13 & Q23 & Q33 \end{bmatrix} = \hat{\sigma}_0^2 \mathbf{Q}_{ll} \atop {3 \times 3}$$ (21)

- i , the number of the measurement

The evaluations of accuracy of the levelling of an individual quantity

The standard deviation of a given levelling procedure - $\hat{\sigma}_0$

$$\hat{\sigma} = \sqrt{\frac{\mathbf{v}^T \atop {1 \times un} \; \Sigma_{\hat{l}\hat{l}}^{-1} \atop {nu \times nu} \; \mathbf{v} \atop {un \times 1}}{nu - u}}$$ (22)

- $r = nu - u$, the number of meaurements above the required number
- nu, the number of measured quantities i.e .the number of measurements
- u, the number of sought-for (unknown) quantities

Σ_{lli}^{-1}, the correlation matrix of measured

- quantities, the matrix of cofactors of measured quantities
- $\underset{unx1}{\mathbf{v}}$, the vector of residuals of measured quantities

The standard deviation of unknown quantities - $\hat{\sigma}_\xi$

The medium residuals of unknowns are the functions of standard deviations of meaurements. Unknowns can thus be denoted as the functions of measurements bearing in mind that we must take into consideration the Law of Cofactor Increment. The matrix of covariances $\underset{uxu}{\mathbf{Q}_{\xi\xi}}$ is equal to the inverse matrix of coefficients of normal equations $\underset{uxu}{\mathbf{N}^{-1}}$.

For three unknowns, the matrix of covariances $\underset{3\times3}{\mathbf{Q}_{\xi\xi}}$ may be written in the form of:

$$\underset{3\times3}{\mathbf{Q}_{\xi\xi}} = \underset{3\times3}{\mathbf{N}^{-1}} = \begin{bmatrix} Q_{xx} & Q_{xy} & Q_{xz} \\ Q_{xy} & Q_{yy} & Q_{yz} \\ Q_{xz} & Q_{yz} & Q_{zz} \end{bmatrix}_{3\times3} \tag{23}$$

The necessary cofactors, intended for the estimation of the accuracy of the unknowns, are on the main diagonal of the covariance matrix (the matrix of the cofactors of the unknowns) $\underset{uxu}{\mathbf{Q}_{\xi\xi}}$. The standard deviations of the unknown quantities are therefore:

$$\hat{\sigma}_{\xi_1} = \hat{\sigma}_0 \sqrt{Q_{\xi_1\xi_1}}$$
$$\hat{\sigma}_{\xi_2} = \hat{\sigma}_0 \sqrt{Q_{\xi_2\xi_2}}$$
$$\hat{\sigma}_{\xi_3} = \hat{\sigma}_0 \sqrt{Q_{\xi_3\xi_3}} \tag{24}$$
$$\vdots$$
$$\hat{\sigma}_{\xi_u} = \hat{\sigma}_0 \sqrt{Q_{\xi_u\xi_u}}$$

or even:

$$\hat{\sigma}_\xi = \hat{\sigma}_0 \sqrt{Q_{\xi\xi}} \tag{25}$$

The standard deviation of levelled quantities - $\hat{\sigma}_{l'l'}$

$$\hat{\sigma}_{l'l'i} = \hat{\sigma}_0 \sqrt{K_{l'l'ii}} \tag{26}$$

The necessary cofactors for an evaluation of accuracy of said levelled quantities are on the main diagonal of the matrix of cofactors of levelled quantities, $\underset{nuxnu}{\Sigma_{l'l'}}$:

$$\underset{nuxnu}{\mathbf{Q}_{l'l'}} = \underset{nuxu}{\mathbf{A}} \; \underset{uxu}{\mathbf{Q}_{\xi\xi}} \; \underset{uxnu}{\mathbf{A}^T} \tag{27}$$

The standard deviation of residuals of measured quantities - $\hat{\sigma}_{vv}$

The standard deviation of residuals of measured quantities may be gotten through the following:

$$\hat{\sigma}_{vvi} = \sqrt{\Sigma_{vvii}} = \sqrt{\Sigma_{llii} - \Sigma_{l'l'ii}} \tag{28}$$

The cofactors necessary to obtain an evaluation of the accuracy of the residuals of our measured values Σ_{vvii}, can be obtained as the difference between the cofactors of measured quantities Σ_{llii} and the cofactors of levelled quantities $\Sigma_{l'l'ii}$.

Determination of the main standard deviations of unknowns:

During a given levelling of derisive measurements, the position of a point may be determined on the basis of certain previously measured quantities. That is how, besides levelled quantities of unknowns, ξ_1, ξ_2, ξ_3, ..., ξ_u $\underset{ux1}{\xi}$, one also obtains the covariance matrix, $\Sigma_{\xi\xi}$:

$$\underset{u\times 1}{\boldsymbol{\xi}} = \begin{bmatrix} \xi_1 \\ \xi_2 \\ \xi_3 \\ \vdots \\ \xi_u \end{bmatrix}_{u\times 1} \qquad (29)$$

$$\underset{u\times u}{\boldsymbol{\Sigma}_{\xi\xi}} = \begin{bmatrix} \hat{\sigma}_x^2 & \hat{\sigma}_{xy} & \hat{\sigma}_{xz} & \cdots & \hat{\sigma}_{xu} \\ \hat{\sigma}_{xy} & \hat{\sigma}_y^2 & \hat{\sigma}_{yz} & \cdots & \hat{\sigma}_{yu} \\ \hat{\sigma}_{xz} & \hat{\sigma}_{yz} & \hat{\sigma}_z^2 & \cdots & \hat{\sigma}_{zu} \\ \vdots & \vdots & \vdots & \ddots & \vdots \\ \hat{\sigma}_{xu} & \hat{\sigma}_{yu} & \hat{\sigma}_{zu} & \cdots & \hat{\sigma}_u^2 \end{bmatrix} =$$

$$= \hat{\sigma}_0^2 \begin{bmatrix} q_{xx} & q_{xy} & q_{xz} & \cdots & q_{xu} \\ q_{xy} & q_{yy} & q_{yz} & \cdots & q_{yu} \\ q_{xz} & q_{yz} & q_{zz} & \cdots & q_{zu} \\ \vdots & \vdots & \vdots & \ddots & \vdots \\ q_{xu} & q_{yu} & q_{zu} & \cdots & q_{uu} \end{bmatrix} = \hat{\sigma}_0^2 \underset{u\times u}{\mathbf{Q}_{\xi\xi}}$$

$$(30)$$

The elements on the main diagonal of the covariance matrix, $\underset{uxu}{\boldsymbol{\Sigma}_{\xi\xi}}$ are squares of standard deviations of the determination of the position of our given point in the direction of the coordinate axis. Many times, however, it is also necessary to determine the maximum - or minimum, depending on the case - values of said deviations.

The values of our main deviations (the maximum, minimum and binormal standard deviations) are determined with the aid of the selves' values of λ_i and their belonging selves' vectors $\mathbf{s}_i$ of the covariance matrix $\underset{uxu}{\mathbf{Q}_{\xi\xi}}$. The »self values« of the covariance matrix, $\underset{uxu}{\mathbf{Q}_{\xi\xi}}$ are obtained according to the equation:

$$\det(\underset{uxu}{\mathbf{Q}_{\xi\xi}} - \lambda\mathbf{I}) = 0 \qquad (31)$$

and the equation for the determination of self values λ_i of the covariance matrix $\underset{uxu}{\mathbf{Q}_{\xi\xi}}$

is obviously not much different:

$$\begin{vmatrix} q_{xx}-\lambda & q_{xy} & q_{xz} & \cdots & q_{xu} \\ q_{xy} & q_{yy}-\lambda & q_{yz} & \cdots & q_{yu} \\ q_{xz} & q_{yz} & q_{zz}-\lambda & \cdots & q_{zu} \\ \vdots & \vdots & \vdots & \ddots & \vdots \\ q_{xu} & q_{yu} & q_{zu} & \cdots & q_{uu}-\lambda \end{vmatrix} = 0 \quad (32)$$

The characteristic equation then goes like this:

$$P_u(\lambda) = (-1)^u \lambda^u + a_{u-1}\lambda^{u-1} + \ldots + a_1\lambda + a_0 \qquad (33)$$

- $P_u(\lambda)$ being the characteristic polynomial

The »zeroes« of the characteristic polynomial $P_u(\lambda)$ are the self values of the covariance matrix $\underset{uxu}{\mathbf{Q}_{\xi\xi}}$.

The self values λ_i, of course, have belonging self vectors denoted as $\mathbf{s}_i$, of the covariance matrix $\underset{uxu}{\mathbf{Q}_{\xi\xi}}$, and the latter are defined as:

$$\underset{uxu}{\mathbf{Q}_{\xi\xi}} \cdot \mathbf{s} = \lambda \cdot \mathbf{s} \qquad (34)$$

Each self value of λ_i provides one witha system of equations with the aid of which the afore-mentioned $\mathbf{s}_i$ vectors may be determined.

Determining the solutions of higher-degree polynomials is a very expansive and demanding practice, which is why various computer programmes have been enlisted with this very purpose in mind, aiding us in this quest to determine the previously mentioned self values and vectors.

The self values of λ_i and their belonging self vectors $\mathbf{s}_i$ of the covariance matrix $\underset{uxu}{\mathbf{Q}_{\xi\xi}}$ determine the quantitative values and

directions of our main deviations. The quantities of main standard deviations of unknowns are thus determined with the aid of the following equations:

$$\hat{\sigma}_{1\_eigen} = \hat{\sigma}_0 \sqrt{\lambda_1}$$
$$\hat{\sigma}_{2\_eigen} = \hat{\sigma}_0 \sqrt{\lambda_2}$$
$$\hat{\sigma}_{3\_eigen} = \hat{\sigma}_0 \sqrt{\lambda_3}$$
$$\vdots$$
$$\hat{\sigma}_{u\_eigen} = \hat{\sigma}_0 \sqrt{\lambda_u}$$

(35)

- $\hat{\sigma}_0$, the standard deviation of the levellin of the measured quantities
- λ_1, λ_2, λ_3, ..., λ_n the self values of the covariance matrix $\mathbf{Q}_{u x u \xi \xi}$
- $\hat{\sigma}_{u\_eigen}$, the main deviation of unknowns in the direction of itself's coordinate system plane (of a pedalloid as well as ellipoid)

The main standard deviations and the pedalloid (ellipsoid) of deviations

The directions of mai deviation unknowns $\hat{\sigma}_{1\_eigen}$, $\hat{\sigma}_{2\_eigen}$, $\hat{\sigma}_{3\_eigen}$, ..., $\hat{\sigma}_{u\_eigen}$ are determined by the self vectors $\mathbf{s}_i$. That is how the $s_{\hat{\sigma}i}$ vectors, which obviously determine the directions and quantities of main standard deviations, $\hat{\sigma}_{1\_eigen}$, $\hat{\sigma}_{2\_eigen}$, $\hat{\sigma}_{3\_eigen}$, ..., $\hat{\sigma}_{u\_eigen}$, of unknowns, may be written down as:

$$\mathbf{s}_{\hat{\sigma}1} = \hat{\sigma}_0 \sqrt{\lambda_1} \cdot \mathbf{s}_1$$
$$\mathbf{s}_{\hat{\sigma}2} = \hat{\sigma}_0 \sqrt{\lambda_2} \cdot \mathbf{s}_2$$
$$\mathbf{s}_{\hat{\sigma}3} = \hat{\sigma}_0 \sqrt{\lambda_3} \cdot \mathbf{s}_3$$
$$\vdots$$
$$\mathbf{s}_{\hat{\sigma}u} = \hat{\sigma}_0 \sqrt{\lambda_u} \cdot \mathbf{s}_u$$

(36)

If the main standard deviations are written down for three particular coordinates X, Y, Z, then:

$$\hat{\sigma}_{binor} = \hat{\sigma}_0 \sqrt{\lambda_1} = a$$
$$\hat{\sigma}_{minor} = \hat{\sigma}_0 \sqrt{\lambda_2} = b$$
$$\hat{\sigma}_{major} = \hat{\sigma}_0 \sqrt{\lambda_3} = c$$

(37)

are the equations for the determination of main deviations of the position of the point. The main standard deviations $\hat{\sigma}_{binor}$, $\hat{\sigma}_{minor}$, $\hat{\sigma}_{major}$ represent the values of the half-axes a, b, c of the deviations' ellipsoid. The directions and quantitative values of the half-axes a, b, c of the deviations' ellipsoid may be obtained with the aid of vectors $s_{\hat{\sigma}x}$, $s_{\hat{\sigma}y}$, $s_{\hat{\sigma}z}$, as in:

$$\mathbf{s}_{\hat{\sigma}x} = \hat{\sigma}_0 \sqrt{\lambda_1} \cdot \mathbf{s}_1$$
$$\mathbf{s}_{\hat{\sigma}y} = \hat{\sigma}_0 \sqrt{\lambda_2} \cdot \mathbf{s}_2$$
$$\mathbf{s}_{\hat{\sigma}z} = \hat{\sigma}_0 \sqrt{\lambda_3} \cdot \mathbf{s}_3$$

(38)

A REALISTIC EVALUATION OF THE ACCURACY OF THE MEASUREMENTS OF THE POSITION OF A PLANE'S CHARACTERISTIC POINTS

The characteristic points of a plane

The data in connection to the positions of characteristic points of a given plane have been obtained on-terrain, via the methods of RTK-GPS for three different types of point placement, namely via forced centering (type 01), a lame plumb line upon the known points (type 02), or a lame plumb line and a simulated placement upon the characteristic points (type 03). Even the levelling and evaluation of measurements according to the RTK-GPS (Real Time Kinematic - Global Positioning System) method has been developed in accordance with all three types of point placement, which enables a comparison of

the measurement results and their accuracy for all three types. The points are sorted as the figure directly below depicts.

For each type of point (type 01 – type 03), four points have been measured with 25 separate measurements, and four points with five measurements per point. That is how a number of measurements above the required number has been secured, and the procedure of levelling and accuracy evaluation may thus commence. The label of a given point represents its type and how many times exactly it has been measured. Points with an odd first digit have been measured 25 times, and those with an even first digit have had their positions measured five times. The second digit pertaining to the label on each individual point, on the other hand, denotes the type of positioning upon the point, i.e. the numbers 1, 2 and 3 inform us whether is is a (type 01), (type 02) or (type 03), respectively. The palcement upon a point which is labelled as belonging to (type 01) is a placement upon a known point on the ground, with forced centering via a tripod and antenna latched onto said tripod, whereas a (type 02) informs us that teh positioning has been done with a lame plumb line upon a known point on the ground and (type 03) with the same sort of lame plumb line upon a point, except that here it is on the ground within the area which has been labelled via circularly distributed spray paint with a circumference of approximately 1m. These circles have not been drawn with the utmost precision, but via free-hand, and
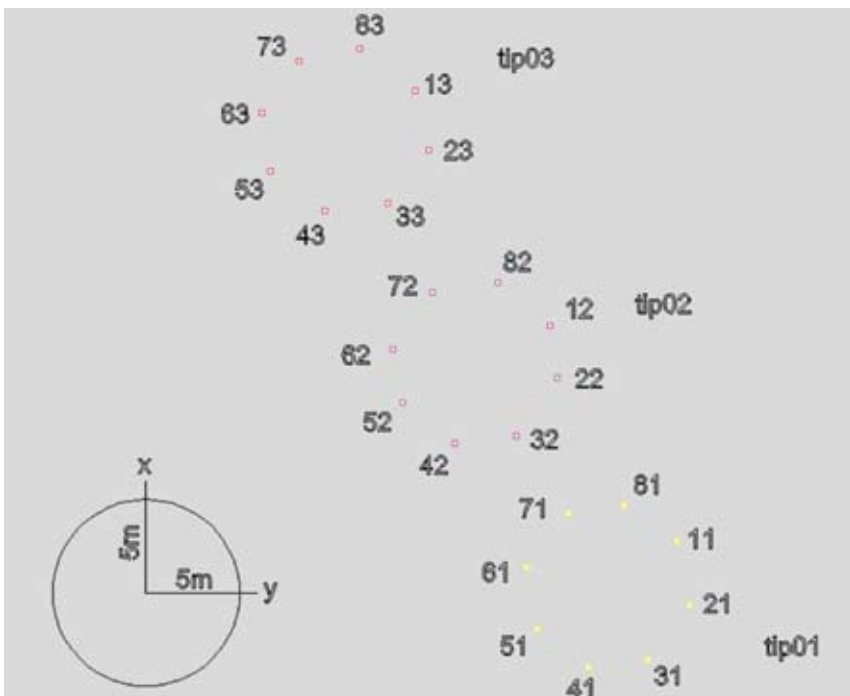
Figure 1. The point arrangement and labels
Slika 1. Razporeditev in oznake točk

Table 1. Maximum deviations in the direction of coordinate axes and main deviations (type 01)
Tabela 1. Maksimalni pogreški v smeri koordinatnih osi in glavni pogreški (tip 01)

Tripod points (type 01):

No. of measurements	Point	$\hat{\sigma}_{x1}$ Maximum deviation of the coordinate axes			Point	$\hat{\sigma}_{max1}$ Main deviations		
		Z	X	Y		ζ	ξ	ψ
25	11	0,0020	0,0010	0,0008	11	0,0020	0,0010	0,0008
25	31	0,0017	0,0008	0,0006	31	0,0017	0,0008	0,0006
25	51	0,0016	0,0007	0,0006	51	0,0016	0,0007	0,0006
25	71	0,0019	0,0009	0,0007	71	0,0019	0,0009	0,0007
5	21	0,0037	0,0018	0,0014	21	0,0037	0,0018	0,0014
5	41	0,0036	0,0017	0,0013	41	0,0036	0,0017	0,0013
5	61	0,0040	0,0019	0,0015	61	0,0041	0,0019	0,0015
5	81	0,0045	0,0021	0,0017	81	0,0045	0,0021	0,0017

were consequently less like circles than ellipses. The figurant had tried to place the plumb line on the same place every time, but only with the aid of a visual evaluation of where the pervieved centre of the circle is.

The results of the levelling of characteristic point measurements
In the comparative tables below, the results of said levelling of characteristic point measurements are presented.
The said results have shown that the folowing for point of forced centering (type 01):
- Deviations in the direction of coordinate axis Z do not exceed 5 mm (the largest one would be 4.5 mm), even for the smallest number of measurements (5).
- Deviations in the direction of coordinate axis Y do not surpass 2 mm (the largest one would be 1.7 mm).

- Deviations in the direction of coordinate axis X do not surpass 2.5 mm (the largest one would be 2.1 mm).

This is all depicted in the table 1.

Results of the levelling of characteristic point measurements with a lame plumb line upon known points show that:
- Deviations in the direction of coordinate axis Z do not exceed 8 mm (the largest one would be 7.4 mm), even when it comes to the smallest number of measurements (3).
- Deviations in the direction of coordinate axis Y do not exceed 3 mm (the largest one would be 2.5 mm).
- Deviations in the direction of coordinate axis X do not exceed 3 mm (the largest one would be 3.0 mm).

Again, this is all depicted in the table 2.

Table 2. Maximum deviations in the direction of coordinate axes and main deviations (type 02)
Tabela 2. Maksimalni pogreški v smeri koordinatnih osi in glavni pogreški (tip 02)

Lame plumb line points – determined in the ground (type 02):

		$\hat{\sigma}_{x2}$					$\hat{\sigma}_{max2}$		
		Maximum deviation of the coordinate axes				Main deviations		
No. of measurements	Point	Z	X	Y	Point	Z	X	Y
19	12	0,0026	0,0012	0,0010	12	0,0027	0,0012	0,0010
19	32	0,0027	0,0013	0,0010	32	0,0027	0,0013	0,0010
19	52	0,0025	0,0011	0,0009	52	0,0025	0,0011	0,0009
21	72	0,0022	0,0010	0,0008	72	0,0022	0,0010	0,0008
3	22	0,0037	0,0016	0,0013	22	0,0037	0,0016	0,0013
3	42	0,0074	0,0030	0,0025	42	0,0074	0,0030	0,0025
4	62	0,0053	0,0022	0,0018	62	0,0053	0,0023	0,0018
4	82	0,0049	0,0023	0,0018	82	0,0049	0,0023	0,0018

Table 3. Maximum deviations in the direction of coordinate axes and main deviations (type 03)
Tabela 3. Maksimalni pogreški v smeri koordinatnih osi in glavni pogreški (tip 03)

Lame plumb line points – not determined in the ground (type 03):

		$\hat{\sigma}_{x3}$					$\hat{\sigma}_{max3}$		
		Maximum deviation of the coordinate axes				Main deviations		
No. of measurements	Point	Z	X	Y	Point	Z	X	Y
20	13	0,0045	0,0022	0,0017	13	0,0045	0,0022	0,0017
20	33	0,0036	0,0017	0,0014	33	0,0036	0,0017	0,0014
20	53	0,0038	0,0018	0,0014	53	0,0038	0,0018	0,0014
20	73	0,0039	0,0018	0,0014	73	0,0039	0,0018	0,0014
5	23	0,0072	0,0035	0,0028	23	0,0072	0,0035	0,0027
5	43	0,0037	0,0020	0,0016	43	0,0038	0,0020	0,0015
5	63	0,0099	0,0047	0,0039	63	0,0099	0,0047	0,0038
5	83	0,0099	0,0045	0,0037	83	0,0099	0,0045	0,0037

Results of the levelling of characteristic point measurements with a lame plumb line via simulating the approximate positioning upon the characteristic points (type 03) have shown that:

- Deviations in the direction of coordinate axis Z do not exceed 1 cm (the largest one would be 9.9 mm), even when it comes to the smallest number of measurements (5).
- Deviations in the direction of coordinate axis Y do not exceed 4 mm (the largest one would be 3.9 mm).
- Deviations in the direction of coordinate axis X do not exceed 5 mm (the largest one would be 4.7 mm).

Once again, this is all depicted in the table 3.

On the following picture, a pedalloid and ellipsoid of deviations of measurement point 13 are shown:

CONCLUSIONS

With the on-terrain measurements, we have managed to obtain a realistic estimate i.e. evaluation of the accuracy of the characteristic point meaurements on our terrain. With the measurements of three different types of points, i.e. points with three different varieaties of on-point placement – namely with forced centering (type 01), a lame plumb line on known points (type 02) and a lame plumb line and simulated placement on characteristic points (type 03) – we have obtained the measurements necessary for us to provide an evaluation of the accuracy of said characteristic point measurements, which have not been materialised i.e. labelled (type 03). When measuring these characteristic point upon our terrain, the accuracy of GPS measurements has thus also been captured, as well as the accuracy of average operator placement of said characteristic terrain points.

With the measurements of said terrain points, the designing of a simple and financially undemanding model intended for the levelling of the afore-mentioned measurements, we have, at the Faculty of Natural Sciences and Engineering, managed to complement the accuracy estimations pertaining to the measurement of characteristic terrain points.

The characteristic points of the terrain which have not been materialised i.e. labelled (type 03) can be detected and measured with an accuracy where the standard deviation in the direction of coordinate axis Z does not, even with the smallest given number of measurements (5) surpass 1 cm (the largest having been 9.9 mm), the standard deviations in the direction of coordinate axis Y do not surpass 4 mm (the largest having been 3.9 mm), and the deviations in the direction of coordinate axis X do not surpass 5 mm (the largest having been 4.7 mm).

The comparison of measurements of all three types of points that have been measured has shown us that the designed model has provided us with realistic results. We are thus able to claim that the accuracy of the determination of characteristic terrain points via the RTK-GPS method is 1 cm or less.
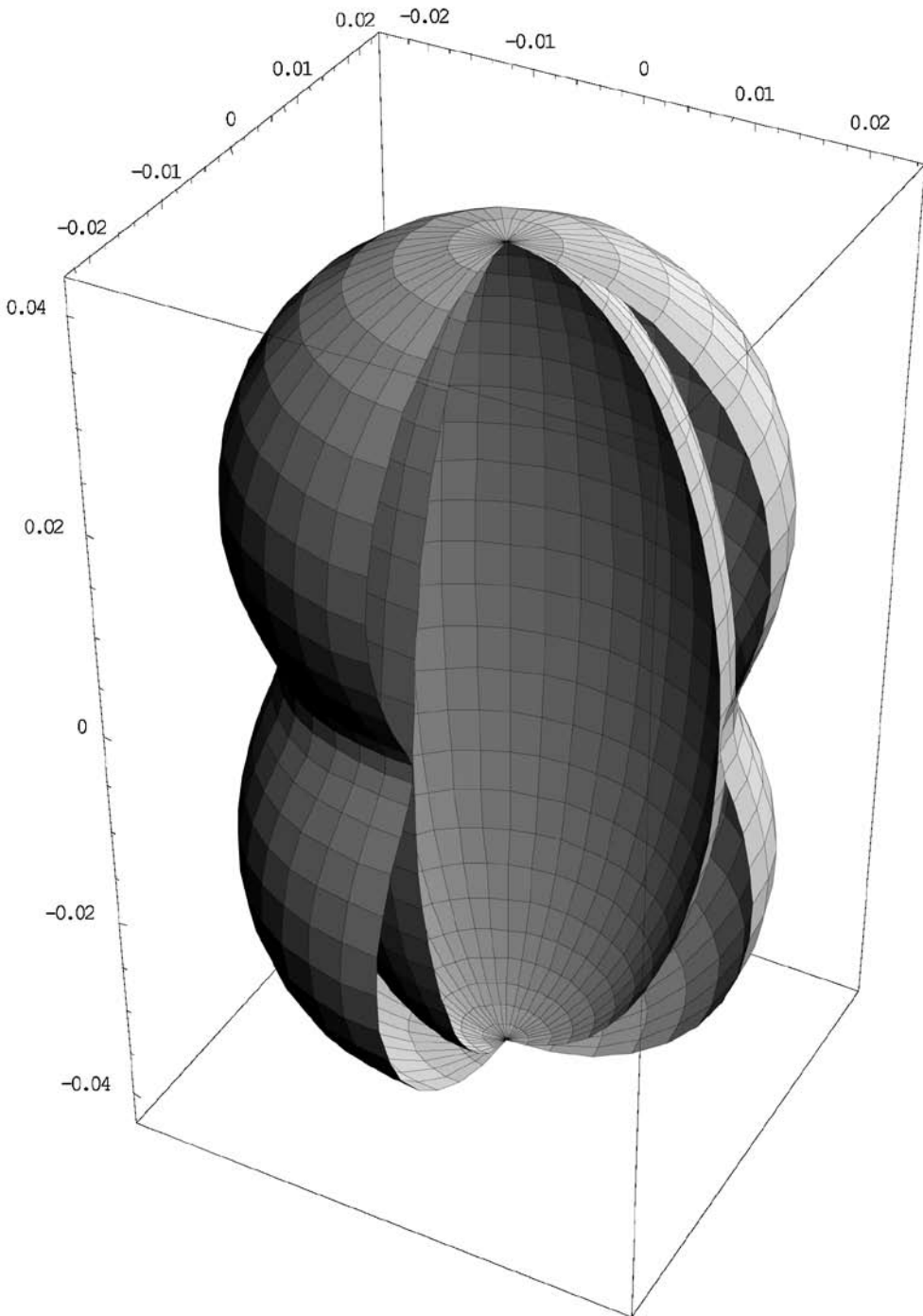
Figure 2. The pedalloid and ellipsoid of deviations of point 13
Slika 2. Pedaloid in elipsoid pogreškov točke 13

Povzetek

Realna ocena natančnosti določanja karakterističnih točk terena po metodi RTK-GPS

Z meritvami na terenu smo dobili realno oceno natančnosti meritev položaja karakterističnih točk terena. Z meritvami treh različnih tipov točk oz. točk s tremi različnimi postavitvami na točkah, in sicer s prisilnim centriranjem (tip01), s togim grezilom na znanih točkah (tip02) in s togim grezilom s simuliranjem postavitve na karakterističnih točkah (tip03) smo zajeli meritve, s katerimi smo podali oceno natančnosti merjenj karakterističnih točk terena, ki niso materializirane oziroma označene (tip03). Pri merjenju položaja karakterističnih točk terena je tako zajeta natančnost GPS izmere kot tudi natančnost postavitve na karakterističnih točkah terena pri povprečnem operaterju.

Z meritvami položaja karakterističnih točk terena, izdelavo enostavnega in cenovno ugodnega modela za izravnavo merjenj in podanimi ocenami natančnosti merjenj karakterističnih točk, pri povprečnem operaterju smo lastno metodo za določanje prostornin, ki se razvija na NTF, dopolnili z oceno natančnosti merjenj karakterističnih točk terena.

Karakteristične točke terena, ki niso materializirane oziroma označene (tip03) lahko zaznamo in izmerimo z natančnostjo kjer srednji pogreški v smeri koordinatne osi Z tudi pri manjšem številu merjenj (5) ne presegajo 1 cm (največji je 9,9 mm), pogreški v smeri koordinatne osi Y ne presegajo 4 mm (največji je 3,9 mm) in pogreški v smeri koordinatne osi X ne presegajo 5 mm (največji je 4,7 mm).

Primerjava meritev vseh treh omenjenih tipov točk je pokazala, da je izdelani model podal realne rezultate. Trdimo lahko, da je natančnost določitve karakterističnih točk terena po metodi RTK-GPS 1cm ali manjša.

References

Durgutović, A. (2005): *Izmera in določanje prostornin nepravilnih teles z uporabo metode 'RTK-GPS': diplomsko delo*. Naravoslovno-tehniška fakulteta, 51 p.

Feil, L. (1990): *Teorija pogrešaka i račun izjednačenja.* Part II, Sveučilište u Zagrebu, Zagreb, 202 p.

Lamot, A. (2007): *Priloga k določanju natančnosti karakterističnih točk terena za potrebe RTK-GPS metode: diplomsko delo*. Naravoslovnotehniška fakulteta, 84 p.

Strang, G. (1997): *Linear Algebra, Geodesy, and GPS*. Wellesley-Cambridge Press, 624 p.

Wolf, R.P., Ghilani D.C. (2005): *Elementary Surveying: An Introduction to Geomatics*. XI Edition, 916 p.

The use of Leica Geo Office in mine surveying

Uporaba programskega paketa Leica Geo Office v jamomerstvu

Gregor Bilban[1], Milivoj Vulić[2], Aleksandar Ganić[3]

[1]Geoservis d.o.o., Litijska cesta 45, SI-1000 Ljubljana, Slovenia;
E-mail: gregor.bilban@geoservis.si
[2]University of Ljubljana, Faculty of Natural Sciences and Engineering, Department of Geo-technology and Mining Engineering, Chair for Mine Surveying and Applied Geophysics, Aškerčeva cesta 12, SI-1000 Ljubljana, Slovenia; E-mail: milivoj.vulic@ntf.uni-lj.si
[3]University of Belgrade, Faculty of Mining and Geology, Chair for Mine Surveying, Đušina 7, 11000 Belgrade, Serbia: E-mail: aganic@rgf.bg.ac.yu

Abstract: Software forms an important part of a surveyor's product basket. Leica Geosystems offers a broad range of software solutions that seamlessly connect measurement sensors to provide maximum productivity from field data collection to final data processing presentation. Leica Geo Office is a powerful software package that offers complete office environment for a mine surveyor. Regardless of the surveying instrument and field technique used, a mine surveyor can easily transfer data to and from the instrument, create various reports, export data into most popular formats, process, adjust and present data. Due to its modular design, one can fully suit the package to one's needs. Different options support everything from regular daily measuring to specific and highly specialised surveying tasks, from network design to combined adjustment. The core of Leica Geo Office's options is of course GNSS processing and adjustment kernel. Leica Geo Office is a programme to be used by the mine surveyor in carrying out his most vital office operations**.**

Izvleček: Programska oprema je pomembno orodje vsakega geodeta. Leica Geosystems nudi širok nabor programskih rešitev, ki predstavljajo komplement merilnim inštrumentom in zagotavlja najvišjo produktivnost od zajema meritev na terenu do končne predstavitve podatkov. Leica Geo Office predstavlja zmogljivo in celovito pisarniško okolje tudi za potrebe v jamomerstvu. Ne glede na izbran inštrumentarij ali mersko tehniko jamomerec z njim prenaša podatke med inštrumentom in osebnim računalnikom, pripravlja terenske zapisnike in zapisnike obdelav, izvaža podatke v številne besedilne, GIS in CAD zapise, naknadno obdeluje in izravnava meritve ter nenazadnje predstavi rezultate. Zaradi modularne zasnove si lahko vsak uporabnik popolnoma prilagodi Leica Geo Office svojim potrebam. Posamezni standardni in opcijski moduli nudijo podporo tako vsakdanjim rutinskim kot tudi

Technical paper

specifičnim merskim nalogam, od tahimetrije do načrtovanja in izravnave geodetske mreže. Poglavitni del Leica Geo Offica sta nedvomno jedri za naknadno obdelavo opazovanj in izravnavo. S programom Leica Geo Office jamomerec lahko opravi ključna pisarniška opravila.

Keywords: Leica Geo Office, GPS, post-processing, adjustment, mine surveying
Ključne besede: Leica Geo Office, GPS, naknadna obdelava opazovanj, izravnava, jamomerstvo

Iɴᴛʀᴏᴅᴜᴄᴛɪᴏɴ

Leica Geo Office is a single software package that supports all sensors and surveying techniques. Based on its predecessors – Leica Survey Office, Leica Ski-Pro and Leica LevelPack Pro, Geo Office allows handling GPS (or wider Global Navigation Satellite Systems), TPS (Terrestrial Positioning System) and levelling data in a similar way with standardized tools and data flow, either individually or in an integrated way.

It is based on an intuitive, graphical interface within a Windows™ multitasking environment, rendering it easy to learn and operate.

A consistent operating concept, a common Windows™ look and feel, common tools and data flows for all different survey instruments and the possibility of customising and configuring the customer's needs all ensure a shorter learning curve, and thus less effort is needed regardless whether one uses it for a highly specific, or regular and day-to-day tasks.

This common concept also avoids the duplication of effort connected with maintenance, training and support.

Lᴇɪᴄᴀ Gᴇᴏ Oꜰꜰɪᴄᴇ ᴍᴏᴅᴜʟᴇꜱ

Leica Geo Office is modularly designed. It includes the following standard functionality:

- Data Management,
- View and Edit,
- TPS processing,
- Flexible Reporting,
- Flexible Import and Export,
- Tools for GNSS, TPS and levels.

The *Data Management* module is responsible for data transfer between Leica Geo Office and all kinds of sensors – GPS families 500, 900 and 1200, TPS families Builder, 300, 400, 700, 800, 1100, 1200 and electronic levels Sprinter and DNA. One can transfer not only measurements, but also format files, codelists, coordinate systems, stakeout points etc.

View and Edit allows the user to visualise and edit observations – the reflector or prism height and type, plot error ellipses, verify setups, create, edit and visualise lines and areas, check coordinates etc.

The *Import end Export* functionality allows creating customisable ASCII files, ESRI Shapefiles, DXF/DWG files and even preparing DXF files to be used as an active map in the field.
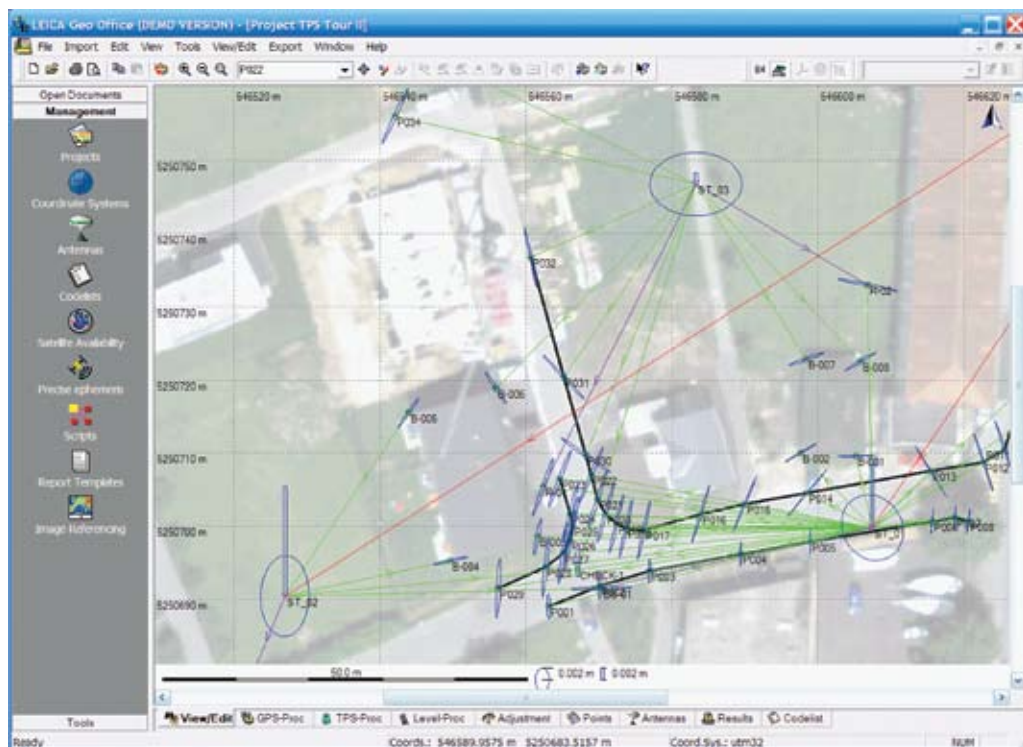
Figure 1. Leica Geo Office main view. In the View/Edit tab one can visualise, check and edit objects collected as well as observations, error ellipses and background.
Slika 1. Glavno okno programa Leica Geo Office. V zavihku View/Edit uporabnik grafično pregleduje opazovanja, elipse pogreškov, zajete objekte, v pomoč pa mu je tudi rastrska podlaga.

Reports (fieldbook, GNSS processing, traverse processing, adjustment, loop misclosure, mean coordinates and differences, satellite availability, datum and map transformation) are based on XML/HTML and fully customizable using XSL.

TPS Processing is another module in a Standard Leica Geo Office package. It allows one to edit and update existing TPS setups, recalculate TPS and/or SmartStation stations and orientations and even create new TPS setups and TPS traverse.

Since the introduction of Leica SmartStation – the first total station with an integrated GPS receiver, it is also important that Leica Geo Office allows an exchanging coordinate system for the whole or part of the project and recalculating TPS station with only one mouse click.

The standard functionality can be extended with additional powerful options:
- Coordinate Transformations,
- GNSS post processing,
- Level data processing,
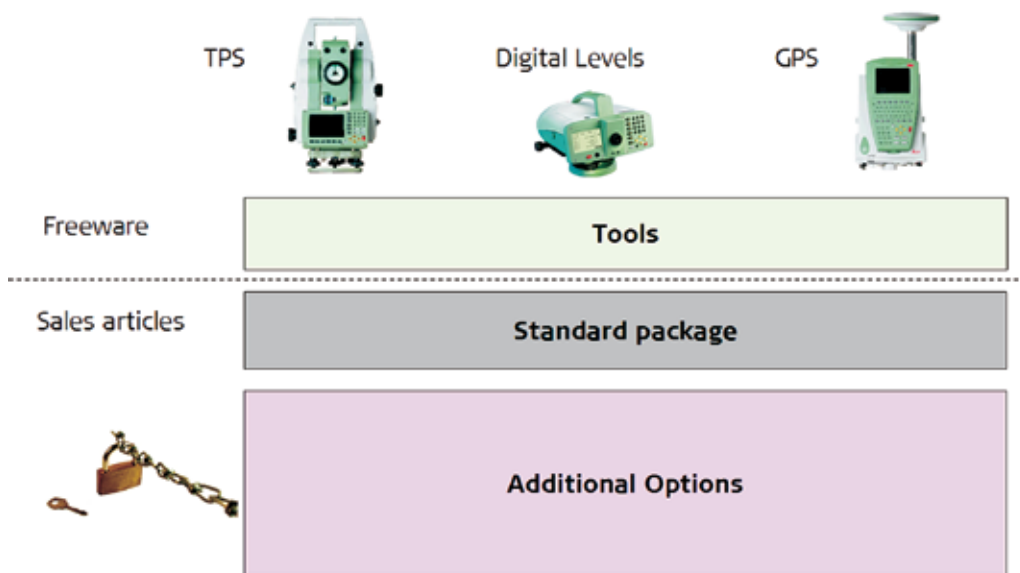
Figure 2. Different Leica Geo Office Packages from free of charge Geo Office Tools, to the standard package suitable for RTK GPS and TPS users, up to the most complete and flexible options for specific tasks
Slika 2. Leica Geo Office je na voljo v različnih paketih kot brezplačni Leica Geo Office Tools, kot standardni paket, ki je najbolj primeren za RTK GPS in TPS uporabnike, do najbolj celovitih in fleksibilnih možnosti, ki jih nudijo dodatni moduli
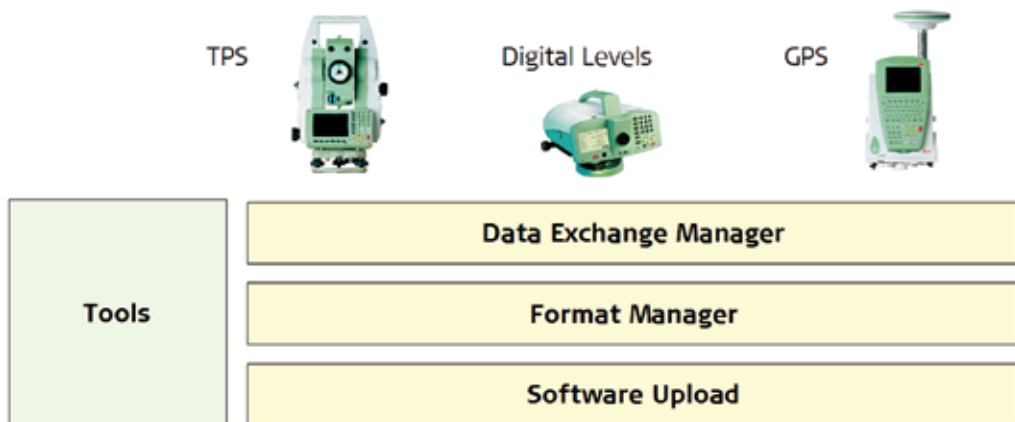
Figure 3. Leica Geo Office Tools components mainly consist of tools for data transfer between the instrument and personal computer
Slika 3. Leica Geo Office Tools v prvi vrsti sestavljajo orodja za prenos podatkov med inštrumentom in osebnim računalnikom
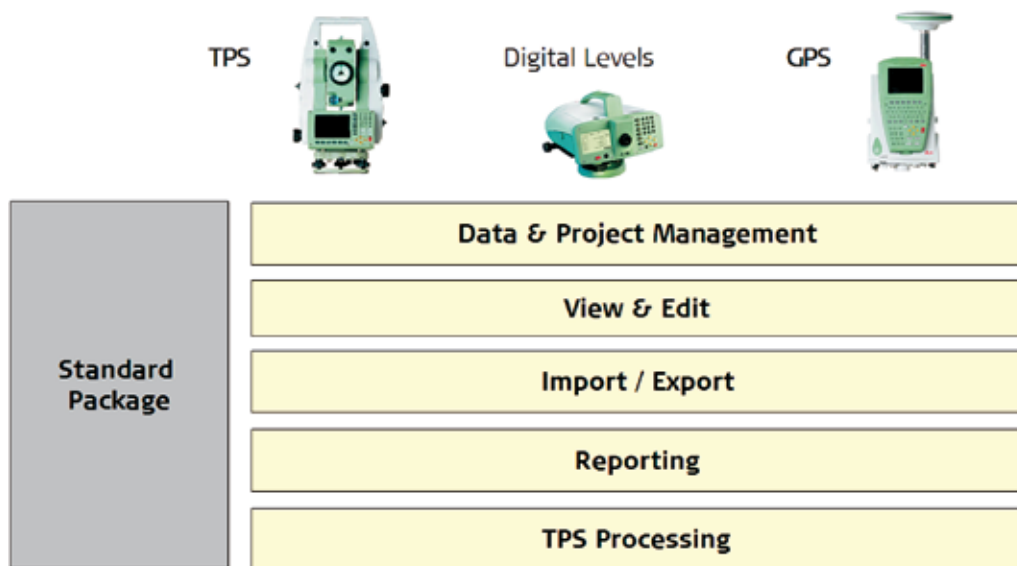
Figure 4. The standard package is expanded to viewing and editing, powerful export and import possibilities including a Design to Field module for creating backgrounds from AutoCAD DXF, flexible reporting and TPS processing e.g. the recalculation of station and orientation, traverse etc.

Slika 4. Standardni paket je razširjen z možnostmi pregledovanja in urejanja, zmogljivimi možnostmi za uvoz in izvoz podatkov, vključno s pripravo vektorskih podlag, fleksibilnimi možnostmi za pripravo zapisnikov in obdelavo tahimetričnih opazovanj

- Network Adjustment,
- GIS/CAD Export,
- Surfaces & Volumes.

POST-PROCESSING MODULE

GNSS processing and the adjustment kernel are the most important and powerful components of Leica Geo Office. The GNSS processing kernel - since PSI-Pro offers GPS+GLONASS post-processing since version 2.0 with the same processing algorithms found in RTK, namely SmartCheck. It is the only processing kernel which is able to handle all different processing scenarios; static, rapid static, stop-and-go, kinematic, kinematic on-the-fly etc. PSI-Pro is used in the office software as well as on the field.

The continuous ambiguity check algorithm SmartCheck increases the reliability, in the way that the ambiguity is permanently and independently determined, approximately every ten seconds, and checked for consistency during the whole kinematic chain. In addition to that, the processing kernel also includes backwards processing, which ensures an unprecedented reliability of the results provided.

Of paramount importance for both the first-time user and a professional one, is
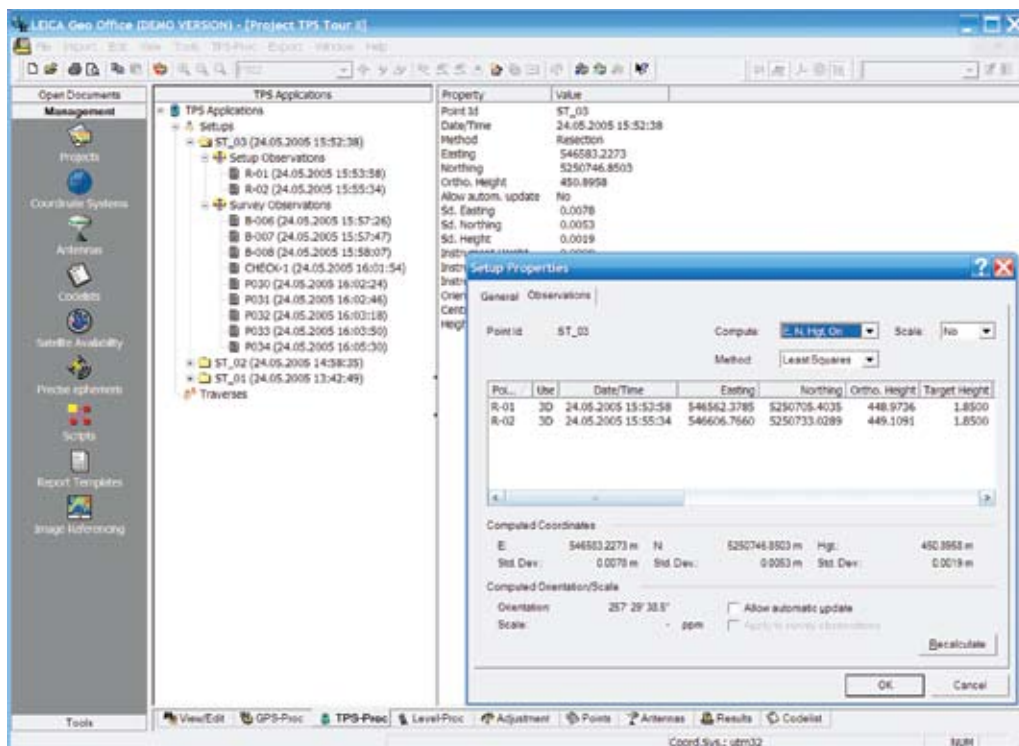
Figure 5. In the TPS Processing tab, one can check and edit station and orientation coordinates, instrument and reflector height, prism type, and use theses to recalculate station and orientation

Slika 5. V zavihku TPS Processing lahko uporabnik preverja in ureja koordinate stojišč in orientacij, višine inštrumenta, višine in tipe reflektorjev in preračunava tahimetrična opazovanja

the selection of processing parameters. With the built-in intelligence Leica Geo Office selects the best possible parameters by default. This is due to the analysis just before post-processing. On the other hand, skilled users have the full option to select appropriate settings. To illustrate the power of Leica's GNSS processing kernel, one would notice the baseline length for ambiguity fixing, which is by default set to 80 km.

Of course, RINEX and precise ephemeris files including GLONASS can be imported for post-processing.

Post-processing results are presented in XML/HTML reports with an extensive amount of information: project information, point information (receiver, antenna, initial coordinates, time frame), processing parameters (selected and used), satellite selection, computed iono model, antenna information (type, horizontal and vertical offset, phase centre offsets and phase centre variations based on either elevation/azimuth or spherical harmonics), observation statistics (common epochs, used observations, rejected observations, tracking sta-
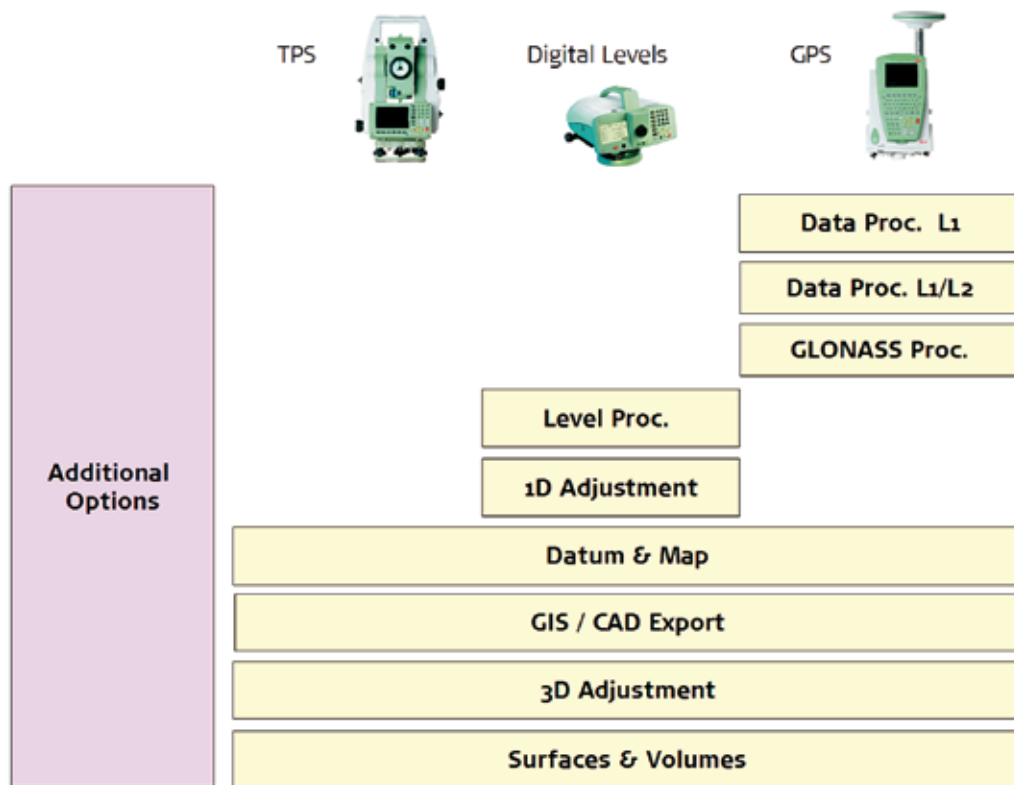
Figure 6. Leica Geo Office options give additional power to more specific tasks in surveying
Slika 6. Opcijski moduli Leica Geo Offica nudijo podporo tudi najzahtevnejšim specifičnim merskim nalogam

tus), ambiguity statistics (the total number of ambiguities, the number of fixed ambiguities, the number of independent fixes, the average time between independent fixes, as well as the percentage of fixed epochs and overall statistical data), cycle slips statistics and final coordinates. The graphical part of results displays residuals which allow the user to quickly detect poor satellites or to give general statements about ionospheric influence. The user will per default get the DOP values, azimuth information and the elevation of the used satellites. An advanced user has the option to plot all different kind of residuals for single, double and triple differences, code and phase residuals.

THE DESIGN AND ADJUSTMENT MODULE

The adjustment kernel in Leica Geo Office is based on Grontmij's MOVE3. MOVE3 is a software package for design, adjustment and quality control of 3D, 2D and 1D geodetic networks in compliance with the procedures of the "Delft School" of geodesy. MOVE3 allows fully integrated processing of GPS and terrestrial (TPS and level) observations.
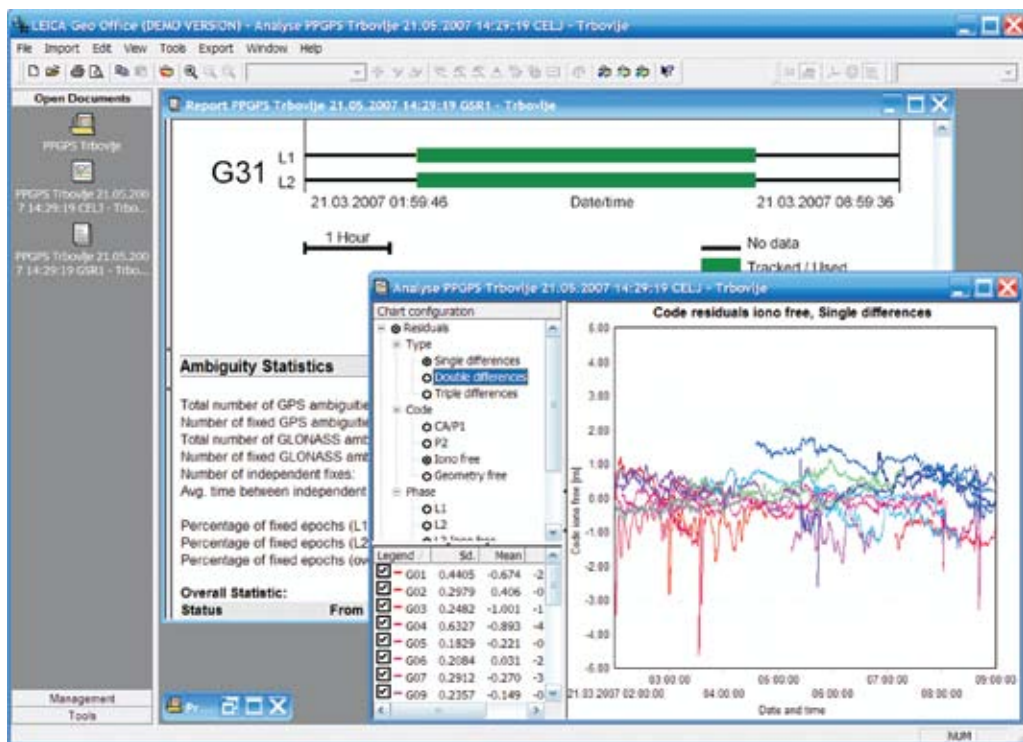
Figure 7. An important part of Geo Office's processing kernel is a complete and powerful reporting including tools for in-depth analyses of the processed data
Slika 7. Pomemben del jedra za naknadno obdelavo opazovanj je zmogljivo orodje za pripravo celovitih zapisnikov ter analizo obdelanih opazovanj

More than that – the Design & Adjustment option was even customised to our needs. In cooperation between Leica Geosystems Technical Support Team, Geoservis d.o.o. a Leica Geosystems representative for Slovenia and University of Ljubljana, Faculty of Natural Sciences and Engineering, Chair of Mine Surveying and Applied Geophysics this option was extended to create a full co-variance matrix of the adjusted system as a separate ASCII file, which is needed for additional quality control and analysis.

The Surfaces and Volumes module

The Surfaces & Volumes option allows one to calculate digital terrain models from points being stored in his project. Surfaces can either be imported from System 1200 jobs using the application onboard a TPS or GPS1200 instrument, or can be created manually from any set of points that is stored in the project. Single points can be de-activated or activated, or complete triangles can be excluded or included from the calculation. In addition to that, the cre-
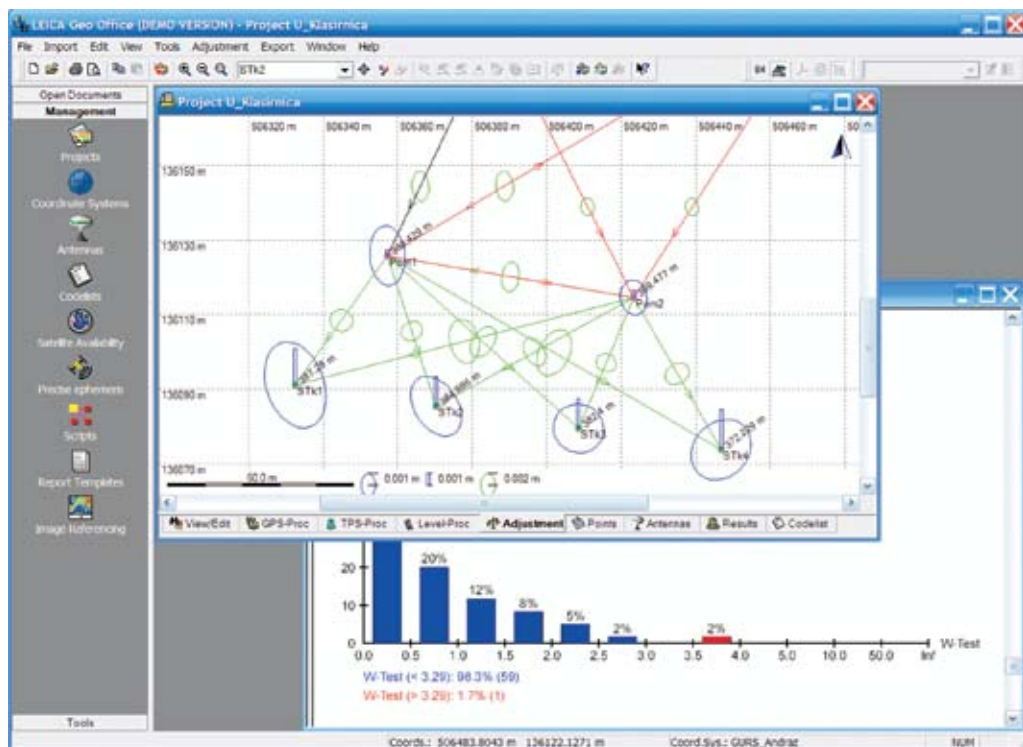
Figure 8. The Design and Adjustment kernel offers one total control of all crucial parameters, as well as extensive reporting with the result of the adjustment including various statistical testing

Slika 8. Jedro za načrtovanje geodetske mreže in izravnavo nudi uporabniku popoln nadzor nad pomembnimi parametri ter podrobnen zapisnik z rezultati izravnave vključno s statističnim testiranjem

ated digital terrain model can be modified by introducing break-lines or boundary lines. Computed results such as volumes, areas and additional statistical information are presented in a property view underneath the Surface View. It is possible to choose between a calculation Above Level and Against Surface (e.g. to control excavations). Surfaces stored in the project can be exported to either a System 1200 DTM job or to a DXF file.

UTILITIES

Last but not least, two standard options are Format Manager and Codelist Manager.

Format Manager is used to create format files. A format file is quite simply a "mask" or "filter" which allows surveyed data collected in the field to be exported in any format as an ASCII text file (e.g. DXF, report, coordinate list).
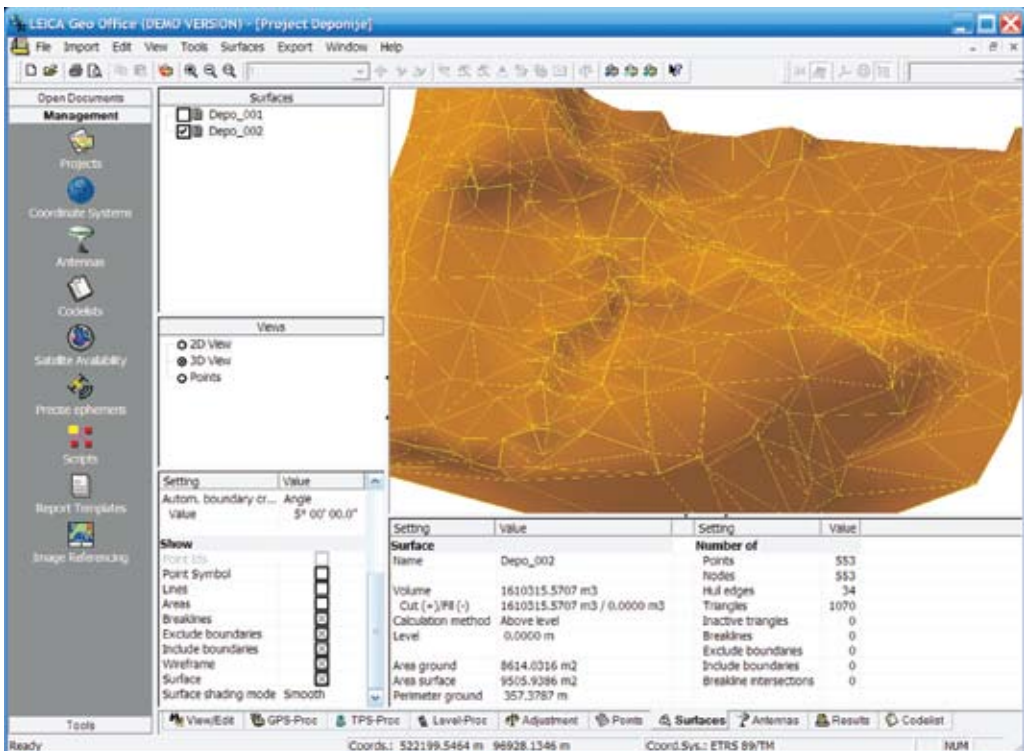
Figure 9. The surfaces in Leica Geo Office can be easily created from GPS, TPS, imported or entered points. One can create break-lines and boundaries. Volume can be calculated against reference height or another surface.
Slika 9. Površine v Leica Geo Officu uporabnik pripravi neposredno iz GPS ali tahimetričnih opazovanj, iz uvoženih ali ročno vnešenih točk, vnese lome in meje. Prostornina se lahko izračuna glede na referenčno višino ali med dvema površinama.

A Codelist contains a list of predefined descriptions and information (codes) that can be used to describe the surveyed features in the field. Thematical codes are point-related, and contain non-spatial information (e.g. Code: tree, Attributes: species, diameter etc.). Codes can later be interpreted by the office software to create symbols, lines and areas and speed up the whole process from field to finish.

CONCLUSIONS

Leica Geo Office is a programme with the aid of which the mine surveyor is able to carry out the most vital office operations (for surface and underground surveying) such as:

- Optimal design of standard daily survey procedures in underground and open pit (quarry) mining including ex-

tended networks for underground and surface control, subsidence observations, engineering constructions survey and control, etc.

- Assessing the quality and cost of any survey activities.
- Processing the observations made by staff mine surveyors.
- Assessing the quality of the processed observations.
- Obtaining a "terrain model" that for the time being can be created exclusively for surfaces (topographic survey of surface installations, quarry operations: drilling, blasting, production control, disposal and waste management).

Povzetek

Uporaba programskega paketa Leica Geo Office v jamomerstvu

Programska oprema je pomembeno orodje vsakega geodeta. Leica Geosystems nudi širok nabor programskih rešitev, ki predstavljajo komplement merilnim inštrumentom in zagotavlja najvišjo produktivnost od zajema meritev na terenu do končne predstavitve podatkov.

Ne glede na izbran inštrumentarij ali mersko tehniko jamomerec z njim prenaša podatke med inštrumentom in osebnim računalnikom, pripravlja terenske zapisnike in zapisnike obdelav, izvaža podatke v številne besedilne, GIS in CAD zapise, naknadno obdeluje in izravnava meritve ter nenazadnje predstavi rezultate. Zaradi modularne zasnove si lahko vsak uporabnik popolnoma prilagodi Leica Geo Office svojim potrebam. Posamezni standardni in opcijski moduli nudijo podporo tako vsakdanjim rutinskim kot tudi specifičnim merskim nalogam.

Leica Geo Office predstavlja zmogljivo in celovito pisarniško okolje tudi za potrebe v jamomerstvu. Podprte so standardne vsakodnevne merske naloge tako rudnikih kot pri odprtih kopih (topografska merjenja, kontrolna merjenja, izračuni volumnov, obdelava tahimetričnih opazovanj...), vse do najzahtevnejših nalog, vključno s projektiranjem, merjenjem in obdelavo geodetskih mrež. Prav jedri za naknadno obdelavo opazovanj in 3D izravnavo sta najpomembnejša in zelo zmogljiva modula v programskem paketu. Modul PSI-Pro omogoča naknadno obdelavo GPS in GLONASS opazovanj s SmartCheck algoritmi, ki omogočajo najvišjo zanesljivost zaradi stalne neodvisne kontrole integritete inicializacije. Algoritmi omogočajo samodejno izbiro parametrov naknadne obdelave, izkušenemu uporabniku pa so na voljo številne napredne možnosti, popoln nadzor nad obdelavo ter zmogljiva orodja za predstavitev in analizo rezultatov. MOVE3 jedro za izravnavo omogoča kombinirano GPS in terestrično izravnavo opazovanj. V sodelovanju z Leico Geosystems, podjetjem Geoservis, ki je njihov avtoriziran distributer in serviser, ter Naravoslovno tehniško fakulteto, Katedro za rudarsko merjenje in geofizikalno raziskovanje je bil modul celo nadgrajen z možnostjo izpisa celotne variančno-kovariančne matrike, ki je potrebna za dodatne analize in kontrolo kvalite.

REFERENCES

[1]   *Guidelines to Data Processing in Ski-Pro v3*. Leica Geosystems, 2003.

[2]   *Leica Geo Office v3 Release Notes*. 2005.

[3]   *Leica Geo Office v4 Release Notes*. 2006.

[4]   Leica Geo Office v5 online help.

[5]   *Leica Geo Office v5 Release Notes. 2006*.

[6]   Leica Geosystems homepage, www.leica-geosystems.com, 2007.

[7]   *Ski-Pro v3 – GPS Data Processing, What's New*. Leica Geosystems, 2003.

Author`s Index

Author`s Index, Vol. 54

RMZ MATERIALS AND GEOENVIRONMENT

Contents
Volume 54, 2007/1, 2, 3, 4

54/3

54/4

RMZ MATERIALS AND GEOENVIRONMENT

Subject Index
Volume 54, 2007/1, 2, 3, 4

Geology

Geotechnology and Mining

INSTRUCTIONS TO AUTHORS

RMZ-MATERIALS & GEOENVIRONMENT (RMZ- Materiali in geookolje) is a periodical publication with four issues per year (established 1952 and renamed to RMZ-M&G in 1998). The main topics of contents are Mining and Geotechnology, Metallurgy and Materials, Geology and Geoenvironment.

RMZ-M&G publishes original Scientific articles, Review papers, Technical and Expert contributions (also as short papers or letters) **in English**. In addition, evaluations of other publications (books, monographs,...), short letters and comments are welcome. A short summary of the contents in Slovene will be included at the end of each paper. It can be included by the author(s) or will be provided by the referee or the Editorial Office.

* Additional information and remarks for Slovenian authors:

*English version with extended »Povzetek«, and additional roles (in Template for Slovenian authors) **can** be written. Only exceptionally the articles in the Slovenian language with summary in English will be published. The contributions in English will be considered with priority over those in the Slovenian language in the review process.*

Authorship and originality of the contributions. Authors are responsible for originality of presented data, ideas and conclusions as well as for correct citation of data adopted from other sources. The publication in RMZ-M&G obligate authors that the article will not be published anywhere else in the same form.

Specification of Contributions

Optimal number of pages of full papers is 7 to 15, longer articles should be discussed with Editor, but 20 pages is limit.

Scientific papers represent unpublished results of original research.

Review papers summarize previously published scientific, research and/or expertise articles on the new scientific level and can contain also other cited sources, which are not mainly result of author(s).

Technical and Expert papers are the result of technological research achievements, application research results and information about achievements in practice and industry.

Short papers (Letters) are the contributions that contain mostly very new short reports of advanced investigation. They should be approximately 2 pages long but should not exceed 4 pages.

Evaluations or critics contain author's opinion on new published books, monographs,

textbooks, exhibitions...(up to 2 pages, figure of cover page is expected).
In memoriam (up to 2 pages, a photo is expected).
Professional remarks (Comments) cannot exceed 1 page, and only professional disagreements can be discussed. Normally the source author(s) reply the remarks in the same issue.

Supervision and review of manuscripts. All manuscripts will be supervised. The referees evaluate manuscripts and can ask authors to change particular segments, and propose to the Editor the acceptability of submitted articles. Authors can suggest the referee but Editor has a right to choose another. **The name of the referee remains anonymous.** The technical corrections will be done too and authors can be asked to correct missing items. The final decision whether the manuscript will be published is made by the Editor in Chief.

The Form of the Manuscript

The manuscript should be submitted as a complete hard copy including figures and tables. The figures should also be enclosed separately, both charts and photos in the original version. In addition, all material should also be provided in electronic form on a diskette or a CD. The necessary information can conveniently also be delivered by E-mail.

Composition of manuscript is defined in the attached Template

The original file of Template is temporarily available on E-mail addresses:
peter.fajfar@ntf.uni-lj.si,
barbara.bohar@ntf.uni-lj.si

References - can be arranged in two ways:
- first possibility: alphabetic arrangement of first authors - in text: (Borgne, 1955), or
- second possibility: [1] numerated in the same order as cited in the text: example[1]

Format of papers in journals:
      Le Borgne, E. (1955): Susceptibilite magnetic anomale du sol superficiel. *Annales de Geophysique*, 11, pp. 399-419.

Format of books:
      Roberts, J. L. (1989): Geological structures, *MacMillan*, *London*, 250 p.

Text on the hard print copy can be prepared with any text-processor. The electronic version on the diskette, CD or E-mail transfer should be in MS Word or ASCII format. **Captions of figures and tables** should be enclosed separately. **Figures (graphs and photos)** and tables should be original and sent separately in addition to text. They can be prepared on paper or computer designed (MSExcel, Corel, Acad).
Format. Electronic figures are recommended to be in CDR, Al, EPS, TIF or JPG formats. Resolution of bitmap graphics (TIF, JPG) should be at least 300 dpi. Text in vector graphics (CDR, Al, EPS) must be in MSWord Times typography or converted in curves.
Color prints. Authors will be charged for color prints of figures and photos.
Labeling of the additionally provided material for the manuscript should be very clear and must contain at least the lead author's name, address, the beginning of the title and the date of delivery of the manuscript. In case of an E-mail transfer the exact message with above asked data must accompany the attachment with the file containing the manuscript.
Information about RMZ-M&G:
Editor in Chief prof. dr. Peter Fajfar (tel. ++386 1 4250-316) or
Secretary Barbara Bohar Bobnar, un. dipl. ing. geol. (++386 1 4704-630),
Aškerčeva 12, Ljubljana, Slovenia

or at E-mail addresses:
peter.fajfar@ntf.uni-lj.si,
barbara.bohar@ntfgeo.uni-lj.si

Sending of manuscripts. Manuscripts can be sent by mail to the **Editorial Office** address:
- RMZ-Materials & Geoenvironment
  Aškerčeva 12,
  1000 Ljubljana, Slovenia
or delivered to:
- **Reception** of the Faculty of Natural Science and Engineering (for RMZ-M&G)
  Aškerčeva 12,
  1000 Ljubljana, Slovenia
- E-mail - addresses of Editor and Secretary
- You can also contact them on their phone numbers.

TEMPLATE

The title of the manuscript should be written in bold letters (Times New Roman, 14, Center)

Name Surname[1], …. , & Name Surname[X]
(Times New Roman, 12, Center)

[x]Faculty of ... , University of ... , Address…, Country, e-mail: ...
(Times New Roman, 11, Center)

THE LENGTH OF FULL PAPER SHOULD NOT EXCEED TWENTY (20, INCLUDING FIGURES AND TABLES) PAGES (OPTIMAL 7 TO 15), SHORT PAPER FOUR (4) AND OTHER TWO (2) WITHOUT TEXT FLOWING BY GRAPHICS AND TABLES.

Abstract (Times New Roman, Normal, 11): The text of the abstract is placed here. The abstract should be concise and should present the aim of the work, essential results and conclusion. It should be typed in font size 11, single-spaced. Except for the first line, the text should be indented from the left margin by 10 mm. The length should not exceed fifteen (15) lines (10 are recommended).

Key words: a list of up to 5 key words (3 to 5) that will be useful for indexing or searching. Use the same styling as for abstract.

Introduction (Times New Roman, Bold, 12)

Two lines below the keywords begin the introduction. Use Times New Roman, font size 12, Justify alignment.

There are two (2) admissible methods of citing references in text:

1. by stating the first author and the year of publication of the reference in the parenthesis at the appropriate place in the text and arranging the reference list in the alphabetic order of first authors; e.g.:

   "Detailed information about geohistorical development of this zone can be found in: Antonijević (1957), Grubić (1962), ..."

   "… the method was described previously (Hoefs, 1996)"

2. by consecutive Arabic numerals in square brackets, superscripted at the appropriate place in the text and arranging the reference list at the end of the text in the like manner; e.g.:

   "... while the portal was made in Zope[3] environment."

MATERIALS AND METHODS (TIMES NEW ROMAN, BOLD, 12)

This section describes the available data and procedure of work and therefore provides enough information to allow the interpretation of the results, obtained by the used methods.

RESULTS AND DISCUSSION (TIMES NEW ROMAN, BOLD, 12)

Tables, figures, pictures, and schemes should be incorporated in the text at the appropriate place and should fit on one page. Break larger schemes and tables into smaller parts to prevent extending over more than one page.

CONCLUSIONS (TIMES NEW ROMAN, BOLD, 12)

This paragraph summarizes the results and draws conclusions.

Acknowledgements (Times New Roman, Bold, 12, Center - optional)

This work was supported by the ****.

REFERENCES (TIMES NEW ROMAN, BOLD, 12)

In regard to the method used in the text, the styling, punctuation and capitalization should conform to the following:

FIRST OPTION - in alphabetical order
Casati, P., Jadoul, F., Nicora, A., Marinelli, M., Fantini-Sestini, N. & Fois, E. (1981): Geologia della Valle del'Anisici e dei gruppi M. Popera - Tre

Cime di Lavaredo (Dolomiti Orientali). *Riv. Ital. Paleont.*; Vol. 87, No. 3, pp. 391-400, Milano.

Folk, R. L. (1959): Practical petrographic classification of limestones. *Amer. Ass. Petrol. Geol. Bull.;* Vol. 43, No. 1, pp. 1-38, Tulsa.

SECOND OPTION - in numerical order

[1] Trček, B. (2001): *Solute transport monitoring in the unsaturated zone of the karst aquifer by natural tracers.* Ph.D. Thesis. Ljubljana: University of Ljubljana 2001; 125 p.

[2] Higashitani, K., Iseri, H., Okuhara, K., Hatade, S. (1995): Magnetic Effects on Zeta Potential and Diffusivity of Nonmagnetic Particles. *Journal of Colloid and Interface Science 172*, pp. 383-388.

Citing the Internet site:

CASREACT-Chemical reactions database [online]. Chemical Abstracts Service, 2000, updated 2.2.2000 [cited 3.2.2000]. Accessible on Internet: http://www.cas.org/CASFILES/casreact.html.

POVZETEK (TIMES NEW ROMAN, 12)

A short summary of the contents in Slovene (up to 400 characters) can be written by the author(s) or will be provided by the referee or by the Editorial Board.

TEMPLATE for Slovenian Authors

The title of the manuscript should be written in bold letters (Times New Roman, 14, Center)

Naslov članka (Times New Roman, 14, Center)

NAME SURNAME[1],…. , & NAME SURNAME[X] (TIMES NEW ROMAN, 12, CENTER)
IME PRIIMEK[1], …, IME PRIIMEK[X] (TIMES NEW ROMAN, 12, CENTER)

[X]Faculty of ... , University of ... , Address…, Country; e-mail: ...
(Times New Roman, 11, Center)
[X]Fakulteta…, Univerza…, Naslov…, Država; e-mail: …
(Times New Roman, 11, Center)

THE LENGTH OF ORIGINAL SCIENTIFIC PAPER SHOULD NOT EXCEED TWENTY (20, INCLUDING FIGURES AND TABLES) PAGES (OPTIMAL 7 TO 15), SHORT PAPER FOUR (4) AND OTHER TWO (2) WITHOUT TEXT FLOWING BY GRAPHICS AND TABLES.
DOLŽINA IZVIRNEGA ZNANSTVENEGA ČLANKA NE SME PRESEGATI DVAJSET (20, VKLJUČNO S SLIKAMI IN TABELAMI), KRATKEGA ČLANKA ŠTIRI (4) IN OSTALIH PRISPEVKOV DVE (2) STRANI.

Abstract (Times New Roman, Normal, 11): The text of the abstract is placed here. The abstract should be concise and should present the aim of the work, essential results and conclusion. It should be typed in font size 11, single-spaced. Except for the first line, the text should be indented from the left margin by 10 mm. The length should not exceed fifteen (15) lines (10 are recommended).

Izvleček (TNR, N, 11): Kratek izvleček namena članka ter ključnih rezultatov in ugotovitev. Razen prve vrstice naj bo tekst zamaknjen z levega roba za 10 mm. Dolžina naj ne presega petnajst (15) vrstic (10 je priporočeno).

Key words: a list of up to 5 key words (3 to 5) that will be useful for indexing or searching. Use the same styling as for abstract.
Ključne besede: seznam največ 5 ključnih besed (3-5) za pomoč pri indeksiranju ali iskanju. Uporabite enako obliko kot za izvleček.

INTRODUCTION – UVOD (TIMES NEW ROMAN, BOLD, 12)

Two lines below the keywords begin the introduction. Use Times New Roman, font size 12, Justify alignment. All captions of text and tables as well as the text in graphics must be prepared in English and Slovenian language.

Dve vrstici pod ključnimi besedami se začne Uvod. Uporabite pisavo TNR, velikost črk 12, z obojestransko poravnavo. Naslovi slik in tabel (vključno z besedilom v slikah) morajo biti pripravljeni v slovenskem in angleškem jeziku.

> **Figure (Table) X.** Text belonging to figure (table)
> **Slika (Tabela) X.** Pripadajoče besedilo k sliki (tabeli)

There are two (2) admissible methods of citing references – obstajata dve sprejemljivi metodi navajanja referenc:

1. by stating the first author and the year of publication of the reference in the parenthesis at the appropriate place in the text and arranging the reference list in the alphabetic order of first authors; e.g.:
1. z navedbo prvega avtorja in letnice objave reference v oklepaju na ustreznem mestu v tekstu in z ureditvijo seznama referenc po abecednem zaporedju prvih avtorjev; npr.:
   "Detailed information about geohistorical development of this zone can be found in: Antonijević (1957), Grubić (1962), ..."
   "… the method was described previously (Hoefs, 1996)"

or/ali

2. by consecutive Arabic numerals in square brackets, superscripted at the appropriate place in the text and arranging the reference list at the end of the text in the like manner; e.g.:
2. z zaporednimi arabskimi številkami v oglatih oklepajih na ustreznem mestu v tekstu in z ureditvijo seznama referenc v številčnem zaporedju navajanja; npr.;
   "... while the portal was made in Zope[3] environment."

MATERIALS AND METHODS (TIMES NEW ROMAN, BOLD, 12)

This section describes the available data and procedure of work and therefore provides enough information to allow the interpretation of the results, obtained by the used methods.
Ta del opisuje razpoložljive podatke, metode in način dela ter omogoča zadostno količino informacij, da lahko z opisanimi metodami delo ponovimo.

RESULTS AND DISCUSSION – REZULTATI IN RAZPRAVA (TIMES NEW ROMAN, BOLD, 12)

Tables, figures, pictures, and schemes should be incorporated (inserted, not pasted) in the text at the appropriate place and should fit on one page. Break larger schemes and tables into smaller parts to prevent extending over more than one page.
Tabele, sheme in slike je potrebno vnesti (z ukazom Insert, ne Paste) v tekst na ustreznem mestu. Večje sheme in tabele je potrebno ločiti na manjše dele, da ne presegajo ene strani.

CONCLUSIONS – SKLEPI (TIMES NEW ROMAN, BOLD, 12)

This paragraph summarizes the results and draws conclusions.
Povzetek rezultatov in zaključki.

Acknowledgements – Zahvale (Times New Roman, Bold, 12, Center - optional)

This work was supported by the ………..
Izvedbo tega dela je omogočilo ………

REFERENCES - VIRI (TIMES NEW ROMAN, BOLD, 12)

With regard to the method used in the text, the styling, punctuation and capitalization should conform to the following:

Glede na uporabljeno metodo citiranja referenc v tekstu upoštevajte eno od naslednjih oblik:

FIRST OPTION (recommended) – PRVA MOŽNOST (priporočena) – in alphabetical order (v abecednem zaporedju)

Casati, P., Jadoul, F., Nicora, A., Marinelli, M., Fantini-Sestini, N. & Fois, E. (1981): Geologia della Valle del'Anisici e dei gruppi M. Popera – Tre Cime di Lavaredo (Dolomiti Orientali). *Riv. Ital. Paleont.*; Vol. 87, No. 3, pp. 391-400, Milano.

Folk, R. L. (1959): Practical petrographic classification of limestones. *Amer. Ass. Petrol. Geol. Bull.;* Vol. 43, No. 1, pp. 1-38, Tulsa.

SECOND OPTION – DRUGA MOŽNOST - in numerical order (v numeričnem zaporedju)

[1] Trček, B. (2001): *Solute transport monitoring in the unsaturated zone of the karst aquifer by natural tracers.* Ph.D. Thesis. Ljubljana: University of Ljubljana 2001; 125 p.

[2] Higashitani, K., Iseri, H., Okuhara, K., Hatade, S. (1995): Magnetic Effects on Zeta Potential and Diffusivity of Nonmagnetic Particles. *Journal of Colloid and Interface Science 172*, pp. 383-388.

Citing the Internet site:
CASREACT-Chemical reactions database [online]. Chemical Abstracts Service, 2000, updated 2.2.2000 [cited 3.2.2000]. Accessible on Internet: http://www.cas.org/CASFILES/casreact.html.

Citiranje Internetne strani:
CASREACT-Chemical reactions database [online]. Chemical Abstracts Service, 2000, obnovljeno 2.2.2000 [citirano 3.2.2000]. Dostopno na svetovnem spletu: http://www.cas.org/CASFILES/casreact.html.

Povzetek – Summary (Times New Roman, 12)

An extended summary of the contents in Slovene (from one page to approximately 1/3 of the original article length).
Razširjeni povzetek vsebine prispevka v Angleščini (od ene strani do približno 1/3 dolžine izvirnega članka).

No. of indexing of RMZ-M&G in singular Databases (Število indeksiranih člankov iz RMZ-M&G v posameznih bazah)

(prepared by Fajfar, P. – from search done by Šercelj, M., CTK Ljubljana, 15.2.2007)

	DATABASE NAME	HITS
1:	Civil Engineering Abstracts	773
2:	CA SEARCH® - Chemical Abstracts® (1967- present)	760
3:	Inside Conferences	313
4:	Materials Business File	253
5:	METADEX®	164
6:	ANTE: Abstracts in New Technologies and Engineering	158
7:	GeoRef	154
8:	Aluminium Industry Abstracts	36
9:	PASCAL	30
10:	Energy Science and Technology	27
11:	TEME - Technology and Management	27
12:	Ei Compendex®	13
13:	CSA Aerospace & High Technology Database	12
14:	Computer and Information Systems	10
15:	Mechanical & Transportation Engineering Abstracts	8
16:	Engineered Materials Abstracts®	3
17:	Corrosion Abstracts	3
18:	Analytical Abstracts	1
19:	FLUIDEX	1
20:	Solid State and Superconductivity Abstracts	1
21:	Electronics and Communications Abstracts	1

2748

ŠTOREQSTEEL
155 let

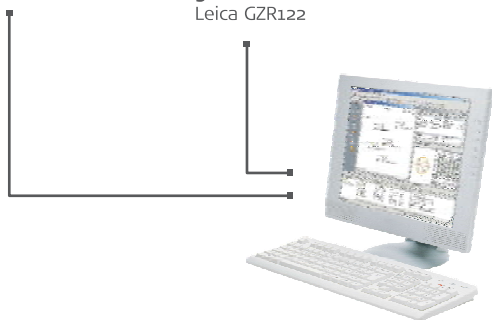# Rešitve za opazovanje premikov in deformacij
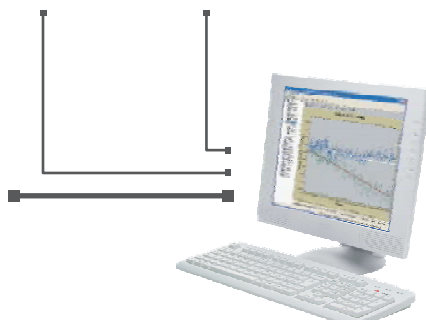

GNSS senzor
Leica GMX902 GG

GPS senzor
Leica GMX901
in 360° reflektor
Leica GZR122

Nagibni senzor
Leica NIVEL200

Samodejni tahimeter
Leica TCA1201 M

Programska oprema
Leica GNSS Spider

Programska oprema
Leica GeoMoS

- when it has to be **right**

Leica
Geosystems

geoservis

Geoservis, d.o.o.
Litijska cesta 45, 1000 Ljubljana
t. (01) 586 38 30, i. www.geoservis.si

prof. dr. Andrej Paulin

Tehniški metalurški slovar *(CD-ROM za WINDOWS)*
slovensko - angleško - nemški

Technical metallurgical dictionary *(CD-ROM for WINDOWS)*
Slovenian - English - German

Več kot 10.000 gesel s področij:
- metalurgije,
- tehniških materialov,
- tehnike površin,
- analiznih metod,
- strojništva,
- kemije,
- elektrotehnike,
- ekologije,
- standardizacije,
- predpisov,
- ekonomike in
- uporabe računalništva pri tehnoloških postopkih.

Osnovne značilnosti oz. prednosti elektronske različice slovarja so preprost in izjemno hiter dostop do iskanega gesla, besede ali zveze, tudi pri zahtevnejših pogojih, ter velika prilagodljivost vmesnika uporabnikovim potrebam in željam. Slovar uporablja pregledovalnik ASP32 in je združljiv s številnimi drugimi slovarji v tem sistemu.

Cenik elektronskega slovarja:
Enouporabniška lokalna verzija - 58,00 EUR
5 licenc mrežna verzija - 390,00 EUR
10 licenc mrežna verzija - 535,00 EUR
20 licenc mrežna verzija - 680,00 EUR
30 licenc mrežna verzija - 825,00 EUR
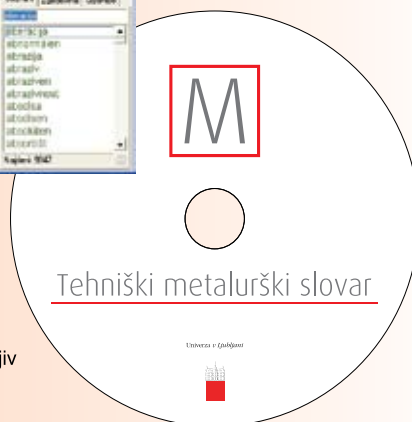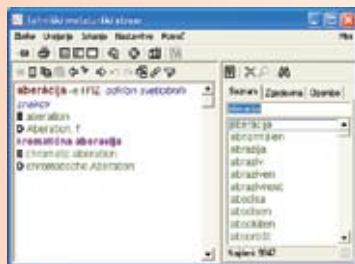40 licenc mrežna verzija - 970,00 EUR
50 licenc mrežna verzija - 1.115,00 EUR

Prices for the electronic dictionary:
Single user local version - 58,00 EUR
5 users network version - 390,00 EUR
10 users network version - 535,00 EUR
20 users network version - 680,00 EUR
30 users network version - 825,00 EUR
40 users network version - 970,00 EUR
50 users network version - 1.115,00 EUR

Tehniški metalurški slovar

Univerza v Ljubljani

Leto izdaje: 2007
Issued in 2007

More than 10 000 technical terms on:
-metallurgy
-technical materials
-surface engineering
-analytical methods
-mechanical engineering
-chemical engineering
-electrical engineering
-environmental engineering
-standardization
-technical regulations
-economics, and
-computer engineering in technological processes

Basic characteristics or advantages, respectively, of electronic version of the dictionary is simple and very fast access to sought term, word or to complex term, also in more demanding conditions, and a great adaptability of the interface to user's needs and wishes. The dictionary uses ASP32 search system that is compatible to numerous other dictionaries in this system.

Za naročila in dodatne informacijenas kontaktirajte preko e-pošte:
For orders and additional information please contact us by e-mail: ***omm@ntf.uni-lj.si***